Minimization of Interchannel Interference Effects in Nyquist-WDM Systems

Jhon James Granada Torres

Faculty of Engineering

Universidad de Antioquia

A thesis submitted for the degree of

PhilosophiæDoctor (PhD) in Electronic Engineering

November, 2017

1. Advisor: Ana María Cárdenas Soto

2. Advisor: Neil Guerrero González

3. Reviewer: Gustavo Adolfo Puerto Leguizamón

4. Reviewer: Moisés R. N. Ribeiro

5. Reviewer: Luis Fernando Díaz Cadavid

Day of the defense: November 8, 2017

Signature from head of PhD committee:

Abstract

The need of increasing the capacity of current deployed optical networks to perform terabits transmissions has been driven to the development of superchannel systems, (principally based on Nyquist-WDM) to be carried out in flexible grid or gridless scenarios. Nevertheless, one of the main issues to be mitigated in these systems is the interchannel interference (ICI), whose effect is intensified when the spectral channel spacing is reduced (for further spectral efficiency increment). In this thesis, we present a study of the ICI effects in Nyquist-WDM systems by means of BER calculation as a function of several system parameters such as: frequency channel spacing, roll-off factor of the digital pulse-shaping filter, laser's linewidth, transmission distance, mark probability of the pseudo-random bit sequence, optical-to-signal noise ratio, among others. Besides, two methods enabling ICI mitigation are proposed: on one hand, a method based on FEC-coded sequence distribution among optical carriers for applications of multiple carriers (superchannels) as a single entity, and on the other hand, a method to perform nonsymmetrical demodulation (NSD) based on the k-means algorithm enabling time-varying distortions mitigation. In contradiction of techniques for ICI mitigation in recent art, these proposals avoid the use of multiple-input multiple-output equalizers or training sequences. Specifically for NSD approach, information of adjacent channels is not required.

" All is well "

Acknowledgements

Contents

CONTENTS

List of Figures

List of Tables

List of Acronyms

ICI   Interchannel Interference or Inter-carrier Interference

CMA   Constant Modulus Algorithm

FEC   Forward Error Correcting

LMS   Least Mean Square

BER   Bit Error Rate

NSD   Nonsymmetrical Demodulation

DSP   Digital Signal Processing

MIMO   Multiple-input Multiput-output

QPSK   Quadrature Phase Shift Keying

QAM   Quadrature Amplitude Modulation

OFDM   Orthogonal Frequency Division Multiplexing

WDM   Wavelength Division Multiplexing

ROADM   Reconfigurable Optical Add-drop Multiplexer

RRC   Root Raised Cosine

SPM   Self-Phase Modulation

XPM   Cross-Phase Modulation

MP   Mark Probability

PRBS   Pseudo-Random Bit Sequence

NDA   Non-Data Aided

OSNR   Optical Signal-to-Noise Ratio

EDFA   Erbium Doped Fibre Amplifier

ASE   Amplified Spontaneous Emission

TW   Time Windows

BP   Back-Propagation

ADC   Analog-to-Digital Converter

DAC   Digital-to-Analog Converter

Psh   Pulse-Shaping

MZM   Mach-Zehnder Modulators

CD   Chromatic Dispersion

CW   Continuous Wave

IQ   In-phase and Quadrature

1

Introduction

1.1 Introductory Remarks and Motivation

In the last years, traffic on data optical networks has had an exponential growth due to the increasing demand of new telecommunication services, such as video on demand, full-high definition video transmission, cloud, and grid computing, among others. It leads to saturation of the current deployed networks in terms of capacity. Figure 1.1 shows a trend of traffic growth until the year 2021, where it continues growing exponentially. Thus, an upgrade in access, metro, and long-haul optical networks is expected to optimize the use of the "almost unlimited" bandwidth offered by the optical fiber.
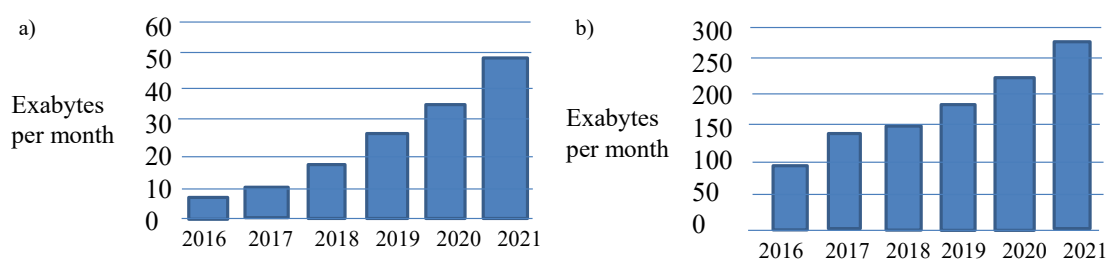
Figure 1.1: Traffic Growth based on CISCO's statistics a) Mobile b) IP.

Experimental reports show the generation, transmission and detection of bit rates up to 100 Gbps over the current optical transport network [1], [2]. At the beginning, 400-G solutions were envisioned to continue working in single channel but with a wider granularity (see Figure 1.2). Nevertheless, experimental tests for 400-G, 1-T and beyond, have shown new technological concepts related to the commercial 100-G systems

1. INTRODUCTION

100 G	200 G
DP-QPSK 28 Gbaud 50 GHz	DP-16QAM 28 Gbaud 50 GHz

First Proposals for 400 G			
DP-QPSK 112 Gbaud 200 GHz	DP-16QAM 56 Gbaud 100 GHz	DP-64QAM 42 Gbaud 75 GHz	DP-256QAM 28 Gbaud 50 GHz

Terabit Transmission and beyond	
Proposals	Limitation
Increase Symbol Rate per Carrier	Electrical Switching
Multi-core fibers	Deployed of new fibers
Higher order modulation formats	OSNR limitation
Multiple carriers per channel	Flexible grid required

Figure 1.2: Solutions to face the traffic demand.

such as: designing of multichannel transmitters, digital coherent receivers, advanced modulation formats and hybrid modulations [3].

Planning the optical transmission systems of long-reach to work with capacities above 400 Gbps, it will not possible to keep the spectral fixed-grid of 50 GHz in Wavelength Division Multiplexing (WDM) networks [4], [5]. Thereby, a new concept known as elastic optical networks emerges, proposing a gridless or flexible grid spectrum, where the spectral width changes according to bandwidth demand.

In elastic optical networks, multiple carriers can be part of a single channel (known as superchannels [6], [7], [8], [9], or can be different channels traveling through the optical fiber very close with the aim of increasing the spectral efficiency. In both cases, channels or superchannels may be added or dropped in transit nodes and their

wavelength might switched to avoid free slots in the spectrum. In these high-data rate networks, linear and nonlinear impairments increase their effects seen as distortions in the received signals, due to a lot of factors such as: dynamic wavelength assignment, randomness of the bit information, switching at high frequency of electronic devices, among others. Thus, several challenges in digital signal processing has to be faced, mainly, because in these scenarios would be very difficult to model the whole set of possible impairments in a transmission, besides, taking into a account the time-varying effects. Hence, new coding and Machine Learning techniques have came out as strong alternatives to be implemented in future terabit optical systems.

This thesis is focused on in one of the main issues of these networks, the interchannel interference. Exploring alternative techniques to the well-known multiple-input multiple-output equalizer, such as bit-coding and nonsymmetrical demodulation techniques, as further will be explained.

1.2   Multicarrier Optical Networks

The use of multiple optical carriers has been widely discussed in the last years as a solution to upgrade currently deployed optical systems to speeds beyond 100-G [10] [11] [12]. The foreseeing scenario of "Superchannels" composed of several tightly spaced optical carriers has further motivated the review of the following paradigms in the design of optical communication system: *i)* 50 GHz fixed vs. flexible channel grid in the context of wavelength division multiplexing (WDM) systems [11] (see Figure 1.3), *ii)* single vs. simultaneous coherent detection of optical carriers to effectively achieve data capacities beyond 100G per Superchannel [13] and *iii)* static routing vs multicarrier routing at the networking level [11] [14].

Initially, optical orthogonal frequency division multiplexing (OFDM) systems were proposed as a multicarrier solution for long-haul because of its efficient use of the spectrum. Furthermore, due to its flexibility, OFDM can be seen as a solution to face high data rates [15]. This technology has been widely adopted by wired and wireless standards such as 802.11a/g Wi-Fi, 802.16 WiMAX, LTE (Long-Term Evolution), DAB y DVB (Digital Audio and Video Broadcasting), and DSL (Digital Subscriber Loop). OFDM is a multicarrier modulation scheme which distributes the information in a fixed

1. INTRODUCTION
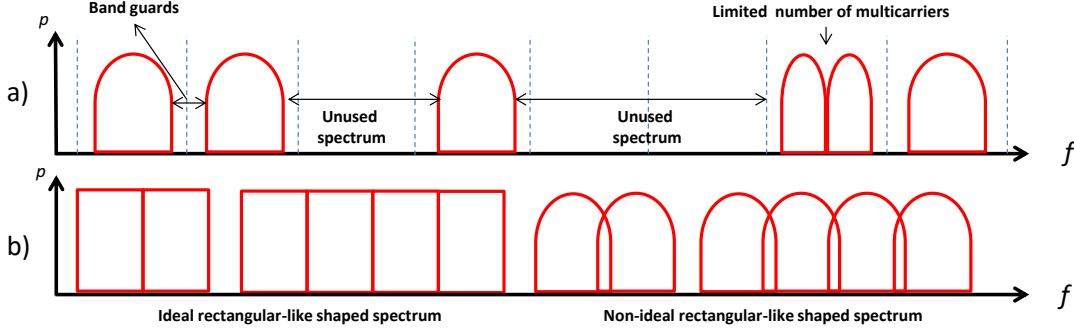
Figure 1.3: WDM a) Fixed-grid and b) Gridless.

number of subcarrriers generated with a orthogonality rule. Hence, in the spectrum each subcarrier does not interfere with its adjacent ones.

In optical appplications, OFDM has been generated with subcarriers separated 12.5 GHz for transmission over 4000 km, 2500 km, 1200 km, 800 km and 400 km for 1, 2, 4, 5 and 6 bits per symbol, respectively [9]. However, OFDM requires a high computational cost and complexity to generate the inverse Fourier transform at high data rates, for example receivers with a higher bandwidth and analog-to-digital converters of fast response. Hence, coherent optical OFDM may turned out in a non-viable solution to be standardized [16].

As an alternative for multicarrier transmission, wavelength division multiplexing (WDM) with flexible frequency carrier spacing or gridless WDM technology (removing 50 GHz fixed-grid of ITU-T standard) has emerged as a strong candidate to overcome the current need for network capacity upgrading [12]. Nyquist-WDM is a technology with the characteristic of having a rectangular spectrum with a bandwidth equal to the baud rate in hertz, which is an advantage for increasing the spectral efficiency [17], [18]. Hence, Nyquist-WDM is a technology more robust than OFDM according to the receiver's constraints and equipment's complexity. Figure 1.4 shows a comparison summarized between Nyquist-WDM and O-OFDM.

In recent art, Nyquist-WDM system has been reported working at $6\times$ 64-QAM with polarization multiplexing over 80 km of transmission distance, having a spectral efficiency of 10/bits/s/Hz by means of pre-equalization at the transmitter side and equalization at the receiver [19]. Besides, over deployed links of 1750 km, PDM-QPSK

8×216.8 Gbps Nyquist-WDM has been reported [20], and over 3300 km was achieved in quasi-Nyquist spacing (1.2 times the baud rate in Hz) using 16QAM [21].

Multicarrier Solution	Maximum Spectral Efficiency	All-Optical Reach	Cost and Complexity Tx	Cost and Complexity Rx
Nyquist-WDM	Dependent on the modulation format; channel spacing ≥ symbol rate: e.g., 4 b/s/Hz for PMQPSK and 8 b/s/Hz for PM-16-QAM	Dependent on the modulation format (several thousands km for PM-QPSK and PM-16-QAM, less for higher formats)	Mainly driven by DAC (e.g., electronic bandwidth ≥ 0.5 × symbol rate)	Mainly driven by ADC and DSP (e.g., electronic bandwidth ≥ 0.5 × symbol rate). Sampling rate ≥ symbol rate
O-OFDM	Dependent on the modulation format (for > 64 subcarriers); channel spacing is at least equal to the symbol rate: e.g., 4 b/s/Hz in case of PM-4-QAM and 8 b/s/Hz in case of PM-16-QAM	Dependent on the modulation format and detection scheme (several thousands km for PM-4-QAM and PM-16-QAM and CO-OFDM, less for higher formats or cost-effective metro solutions)	Mainly driven by DAC and DSP (e.g., inverse Fourier transform processing, Oversampling sampling rate > symbol rate)	Mainly driven by ADC and DSP (e.g., electronic bandwidth = 0.5 × symbol rate). Sample rate: one sample per symbol

Figure 1.4: Nyquist-WDM and O-OFDM Comparison [10].

Thanks to the advantages of scalability of current deployed networks for a future standardization, this thesis will be focus on Nyquist-WDM scenarios. In Chapter 2, a description of Nyquist-WDM concept is extended.

1.3   Challenges in Flexible and Gridless Scenarios

Technical dimensions to scale channel capacity from current 100-G to 400-G and beyond can be listed as follows: i) increase of baud rate by incorporating to optical transport systems higher-speed electro-optical components than commercially available 32 GHz, ii) implementation of higher spectrally efficient modulation formats than current dual-polarization quadrature phase shift keying (DP-QPSK) such as quadrature amplitude modulation (QAM) formats [22], [23], and iii) implementation of multi-carrier approaches over the current single-carrier solution, with advanced spectral shaping and multiplexing technologies [24].

Thereby, next commercial 400-G systems are envisioned as a Nyquist 2 x 200 Gb/s DP-16QAM carriers for transmissions below 400 km, and a Nyquist 4 x 100 Gb/s DP-QPSK carriers for long haul optical links, offering higher degree of parallelism and higher spectral efficiency when compared to DP-QPSK 100 Gb/s systems [25]. For further capacity increasing, high order modulation formats, such as 32QAM and

1. INTRODUCTION

64QAM, have been proposed. However, these modulation formats would not allow long reach transmission due to OSNR penalty [19], [6].

Besides, due to current bandwidth limitation above 32 GHz of opto-electronic components, multicarrier approaches seem to be the more realistic solution to the need of infrastructure upgrading. Thus, multicarrier based transmission systems, distributing the data traffic across several closely separated optical subcarriers, emerge as the solution to respond to the exponential traffic growth [26], [27]. Thence, carrier capacity of 32 Gbaud seems to be the right trade-off to increase the spectral efficiency without stressing too much electronics and transmission performance for the next multi-carrier transport systems beyond 100 Gb/s [28], [29].

One of the key factors to carry out the elasticity (flexibility) in optical networks will be the development of flexible transponders, due to these devices will allow the adaptation of transmitter's and receiver's parameters according to the channel conditions and demand requirements. Currently, transponders works at fixed data rate in fixed grids. It is foreseen, flexible transponder's parameters may allow the variation of number of carriers, pulse-shaping type, modulation format per carrier, baud rate per carrier and type of codification. Flexibility in joint with the ability to estimate system's characteristics, would enable that flexible transponders are the central devices in networks with dynamic topology such as Software Define Networks [9].

Another enabling technology, which has not been developed for commercializing yet, is the reconfigurable optical add drop multiplexer (ROADM). Currently, ROADMs have been tested to perform with a granularity of 12.5 GHz [30], which is the granularity standardized by the ITU-T as a flexible grid [31]. In this fleixble grid, lasers with a tunable granularity of 6.25 GHz should be developed. Nevertheless, due to the ever increasing demand, the standard of 12.5 GHz might not be a long term solution. Therefore, the flexibility in the enabling devices under research should be understood in the context of gridless scenarios. As it is mentioned in [32], "the goal of a truly flexible optical transport infrastructure is to remove fixed wavelengths per port (colorless), to allow any wavelength being added/dropped to/from any direction (directionless), and to enable multiple copies of the same wavelength on a single add/drop structure (contentionless)".

Hence, adding and dropping carriers in transit nodes without guard bands, and the dynamic changes of wavelengths, would generate interchannel interference (ICI). For

further increase of spectral efficiency, the channels might be overlapped increasing the ICI effects.

Moreover, nonlinear effects of the optical fiber are significant limitations that must be researched in detail in gridless scenarios. The nonlinear index significatively affects the transmission due to the power increasing required by long-haul transmission and high data rates. Furthermore, high order modulation formats such as m-QAM exhibit a higher sensitivity to linear as well as non-linear impairments throughout the optical link [33], [34]. Thence, digital signal processing techniques will play an important role to get high capacity in elastic and reconfigurable networks.

On the other hand, some impairments may be time-varying in nature arising from mechanical disturbance in optical fibers, temperature variations in the components and small variations of the bias control of the IQ optical modulators for example, which would have a higher impact in future terabit optical systems. As nonlinear impairments, also time-varying effects can induce nonsymmetrical distortion of the received symbols observed in a constellation diagram. Unlike optical gaussian noise, these degradations may have a probability density function (PDF) that is non-Gaussian and therefore may shift the centroids (mean value) of the received symbols from their ideal constellation positions by different extents. Thus, employing non-symmetrical decision boundaries in these terabits systems, would support the mitigation of time-varying and nonlinear impairments. Hence, Machine Learning techniques has started in the last years to be applied in optical coherent receivers with successful results for improving the overall system performance.

1.4 Interchannel Interference

In addition to the possibility of enlarging the amount of carriers by tightly spacing them in gridless multicarrier scenarios, ideal rectangular-like shaped spectrum per carrier with bandwidth equal to the baud rate has been proposed to improve even more the spectral efficiency of multicarrier based transmission [6]. Rectangular-like shaped spectrum can be obtained by Nyquist pulse implementations in the electronic domain by using finite-impulse-response (FIR) digital structures to perform root-raised-cosine (RRC) filtering. Theoretically, perfect rectangular spectrum is attained by a RRC digital filter with infinite length (or number of taps) under the assumption of unlimited

1. INTRODUCTION

hardware resources [35]. The implementation of optical Nyquist-WDM systems is restricted due to the limited resources offered by DSPs and FPGAs to generate electrical Nyquist pulses of infinite duration. This fact does not allow the proper rectangular-like shaped spectrum in the optical domain. Thus, the unavoidable non-ideal rectangular spectra lies on a bandwidth occupancy broader than the baud rate in Hz, causing interference between adjacent optical carriers for a frequency channel spacing near or equal to baud rate. This effect is known as inter-channel or inter-carrier interference (ICI) [36]. The finite RRC filter length and the subsequent extra-bandwidth occupied by optical carriers are characterized by the roll-off factor of the RRC function in the electrical pulse-shaping. The roll-off factor can have values between zero and one in the RCC function. There is a proportional relation between the roll-off factor and the ICI reflected as an optical signal to noise ratio (OSNR) degradation when frequency channel spacing is attempted to be lower than the baud-rate or the roll-off factor is greater than zero. In gridless scenarios where the optical carrier spacing may be user-defined is desired a carrier allocation as near as possible between adjacent channels to increase the spectral efficiency. Therefore, due to the overlapping increment, the signal degradation increases causing system performance limitations in terms of BER.

Additionally, in standardized WDM grids, ICI has been comprehended as a non-linear effect of the optical fiber due to the high launch power and its variation in adjacent channels. Principal nonlinearities produced by the Kerr effect in multichannel transmission are: self-phase modulation (SPM), cross-phase modulation (XPM) and four-wave mixing (FWM). These nonlinearities depend on chromatic dispersion directly or indirectly as well as the power intensity [37].

SPM and XPM produced a modification of signal's phase, which induces an alteration in its spectrum. SPM determines a pulse broadening seen in the spectrum, due to the intensity variation. In combination with material dispersion, the spectral broadening can drive to alterations in the pulse's temporal wide. the pulse's wide is expanded or compressed according to the group velocity dispersion [38]. Whilst, XPM generates alterations in signal phase due to the intensity of other signals transmitted at the same time in different wavelengths. Phase signal in a specific channel is affected by the average power and random bit of the whole set of carriers which is completely aleatory. Thus, complete cancelation of XPM is impossible in practice [39].

Summarizing, the causes of the interchannel interference can be enummeratted according to network's devices: laser, digital filter of the pulse-shaping and the nonlinearities of the optical fiber (see Figure 1.5).

Interchannel Interference			
Network's Devices/components	*Laser*	*Transmitter's Digital Filter*	*Optical Fiber*
Parameters	Central Wavelength	Number of taps	Power of signal transmitted
Issue	Closeness of adjacent channels	Roll-off factor of the RRC greater than zero	Kerr Effect
Consequences	Overlapping among channels	Channel Broadening	SPM, XPM, FWM

Figure 1.5: Causes of the interchannel interference.

Additionally, the randomness of bit-sequences and variations in channel's power can induce a higher interaction between the overlapped channels during the transmission in sub-Nyquist cases, increasing the impact of the nonlinear impairments of the optical fiber. Furthermore, even if in superchannel scenarios the information is distributed among several carriers, the demodulation may be carried out individually per carrier due to a simultaneous multicarrier demodulation for joint ICI cancelation may be excessively complex. Thus, in the individual channel demodulation, the interference between channels has been regularly interpreted as noise in the context of detection, processing and demodulation, becoming in an OSNR-like degradation in the carrier under evaluation, usually called as nonlinear interference noise (NLIN) [40] [41] [42].

Nevertheless, due to temporal correlations of data-symbols belonging to overlapped carriers in the frequency domain, the ICI (usually called as nonlinear interference noise -NLIN) can be modeled as a linear channel with time-varying intersymbol interference (ISI) [42] [43] [44]. Since ISI has been successfully compensated by linear equalization techniques [45] [46], ISI mitigation approaches may be extended for ICI mitigation. Reported techniques to mitigate ICI include: joint digital signal processing based on Chromatic Dispersion compensation algorithms with the incorporation of training sequences and of the least-mean square (LMS) algorithm for data-aided linear equalization [47], implementation of maximum likelihood sequence detection (MLSD) [48]

and Kobayashi coding [49] for processing at the bit-data level, and frequency-diversity multiple-input multiple-output (MIMO) equalization based on the Constant Modulus Algorithm (CMA) [50] in a non-Nyquist channel scenario, which separates dual polarization signals by also demultiplexing different carrier frequencies. In addition, the time-frequency packing method has also been proposed to increase the SE [51] [52] by reducing both the symbol period and the carrier spacing to lower levels than the Nyquist rate, and compensating using detectors that are able to cope with the interference intentionally introduced in the system. A comparison of some of the ICI mitigation techniques can be seen in Figure 1.6

ICI Mitigation Technique	Ref/year	Level of Processing	Info of Adjacent Channels is Requiered?	MIMO Equalizer	Modulation Format Tested	Max. Data Rate Tested	Scenario Tested
Joint DSP Architecure	2012 [a]	Electrical Signal	Yes, electrical signal	Yes	QPSK	32 Gbaud	Simulation
decision-aided CP recovery + ML approach + SD-FEC	2014 [b]	Electrical signal	Yes, electrical signal	Yes	QPSK 8QAM 16QAM	32 Gbaud	Simulation
Frequency Diversity MIMO Detection	2015 [c]	Electrical Signal	Yes, electrical signal	Yes	QPSK	10 Gbaud	Experimental
Han–Kobayashi and Dirty-Paper Coding	2015 [d]	Bits	Yes, bits	No	-----	32 Gbaud	Theoretical
Wave Mixing of Delayed Copies	2017 [e]	Optical Signal	Yes, Optical Signal	No	QPSK 16QAM	25 Gbaud	Experimental
FEC-distributed	2016 [Our proposal]	Electrical and Bits	Yes, bits	No	QPSK	32 Gbaud	Simulation
Nonsymmetrical Demodulation	2017 [Our proposal]	Symbols	No	No	16QAM	32 Gbaud	Experimental

Figure 1.6: Comparison of different techniques which enable the mitigation/minimization of interchannel interference effects a.[47]; b.[48]; c.[49]; d.[50]; e.[53].

1.5 Thesis Contribution

In this research, a deep evaluation about the impact of ICI effects in gridless Nyquist-WDM systems is systematically presented through the BER estimation as function of several system parameters, such as: frequency channel spacing, roll-off factor of the digital pulse-shaping filter, laser's linewidth, transmission distance, mark probabil-

ity of the pseudo-random bit sequence, launch power and optical-to-signal noise ratio (OSNR), in simulation as well as in experimental scenarios. Furthermore, two methods enabling the ICI mitigation are proposed. On one hand, one method is designed for superchannels applications, where the information is recovered using the enterily set of subcarriers. On the other hand, the second method is applied in each subcarrier, regardless if it belongs to a set of carriers or not. Figure 1.7 shows the modules where the methods are proposed. In the following subsections, highlights of each method are presented.
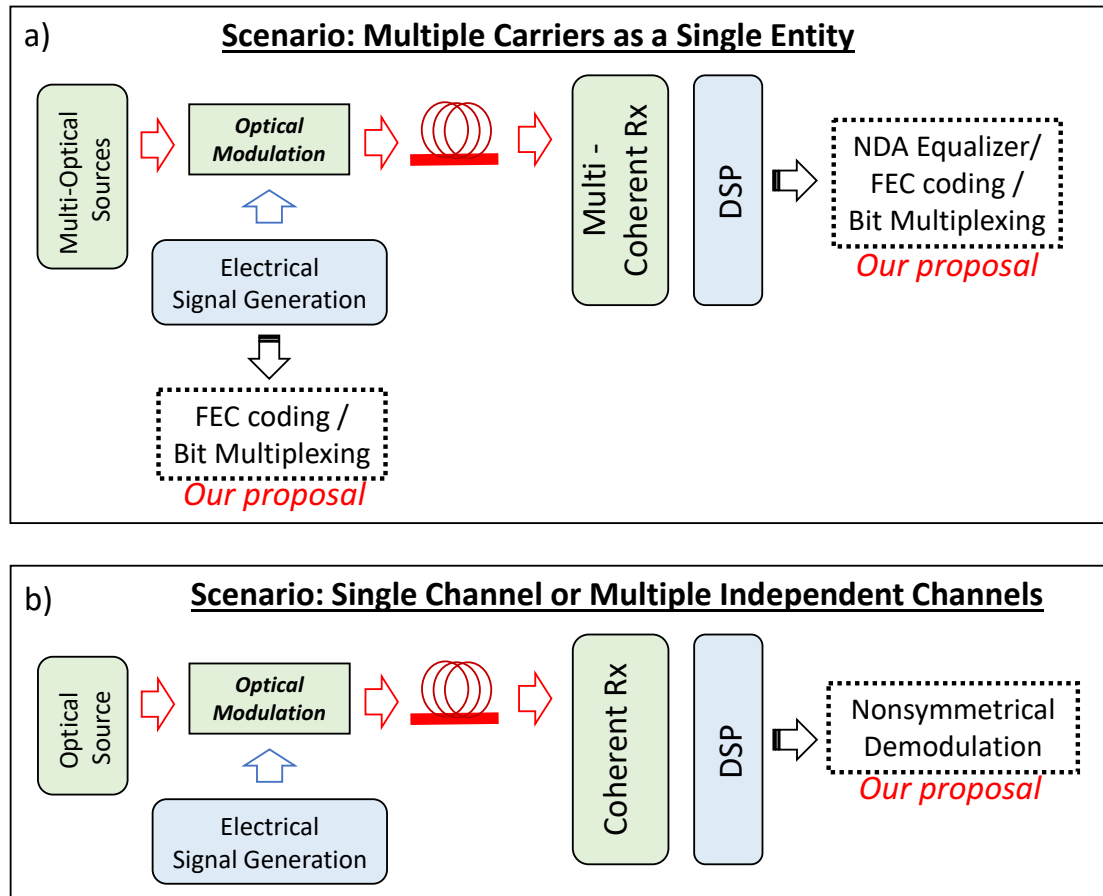
Figure 1.7: Block diagram of the scenarios where the proposed methods are implemented.

1.5.1 Contribution of Method 1: FEC distributed among carriers

The implementation of the following two sub-modules for ICI mitigation are proposed: i) an adapted non-data aided (NDA) equalization to improve the optical signal to noise ratio of single carriers avoiding complex joint multicarrier processing, and ii) the implementation of a hard-decision Forward-Error-Correction (FEC) technique based on Reed-Solomon coding, by means of a distribution of encoded bit-sequences among optical carriers, considering the entire set of carriers as a single entity at the bit-data level. From the one hand, the Constant Modulus Algorithm (CMA) makes a NDA equalization of the ICI degradation without previous knowledge of the channel statistics, performing error function minimization on the constant modulus of phase modulated signals in the constellation diagram. The equalization process is carried out on QPSK optical carriers to prove the linear ICI mitigation for WDM sub-Nyquist scenarios with non-strict close to zero roll-off factors in the pulse-shaping filter. On the other hand, a hard-decision FEC coding is proposed as second stage previous bit-to-bit distribution of the encoded sequences performed by a bit-multiplexer. The bit-multiplexer works as a frequency-interleaver with the aim of preventing that burst errors per carrier affect the FEC-overhead for the proper bit decoding at the receiver side. Furthermore, the FEC distribution allows information recovery even if a specific channel is more affected than the adjacent channels. We also show how CMA equalization as a first ICI mitigation stage improves the hard-decision FEC performance by increasing the OSNR of all carriers composing the superchannel. BER curves as functions of carrier spacing and roll-off factor reaffirm the improvement of the spectral efficiency allowing the carrier overlapping lower than the baud rate. Most of the reported investigations described above were tested in scenarios of 2 or 3 carriers up to 28 Gbaud under linear and non-linear fiber impairment considerations, including 11 x 80 km of optical transmission amplified by EDFAs. For this research purposes of ICI mitigation, it is simulated in VPITransmissionMaker and Matlab, a 3×32 Gbaud single-polarization QPSK multi-carrier system, from back-to-back up to 130 km without optical amplification.

1.5.2 Contribution of Method 2: Nonsymmetrical Demodulation

Nonsymmetrical demodulation (NSD) technique based on machine learning, relying on clustering techniques to mitigate the ICI as well as time-varying distortions, is proposed.

This NSD is experimentally verified in a 16QAM Nyquist system at 16 Gbaud and 32 Gbaud for back-to-back and up to $N \times 90 \ km$, in function of OSNR. Besides, the proposed demodulation technique allows temporal tracking of the centroids variations and symbols' variance of the received symbols represented in a constellation diagram, which also provides a measure of link stability. This NSD approach can be considered as a blind technique in two terms: $i)$ no feedback or channel information is provided, and $ii)$ information from the adjacent channels is not required. This technique may improve the performance of any QAM transmission system, where the symbols can be affected by distortions seen in the constellation diagram.

1.5.3 List of Publications

The research work has resulted in the following publications:

Journals

- **J.J. Granada Torres**, Siddharth Varughese, Varghese A. Thomas, Andrea Chiuchiarelli, Stephen E. Ralph, A. M. Cardenas, and N. Guerrero Gonzalez, "Mitigation of Time-varying Distortions in Nyquist-WDM systems using Machine Learning,"Optical Fiber Technology Journal (ELSEVIER), Vol. 38, pp: 130-135, 2017.

- **J.J. Granada Torres**, A. M. Cárdenas, and N. Guerrero González, "Enhanced intercarrier interference mitigation based on encoded bit-sequence distribution inside optical superchannels," SPIE Optical Enginnering Journal, 55(10), 106124, Oct. 27, 2016.

- **J.J. Granada Torres**, A.M. Cárdenas Soto, N. Guerrero González,"Redes Ópticas Elásticas: un Nuevo Paradigma en las Futuras Redes de Telecomunicaciones", Revista Respuestas vol.20 N. 2, 2015. ISSN: 1794-9831 (print), ISSN: 2322-7028 (web).

International Conferences

- **J.J. Granada Torres**,Siddharth Varughese, Stephen E. Ralph, A. M. Cardenas, and N. Guerrero Gonzalez, "Clustering in Short Time Windows for Nonsymmetrical Demodulation in 16QAM Overlapped WDM Channels," in Advanced

Photonics 2017 (SPPCom), OSA Technical Digest (online) (Optical Society of America, 2017), paper SpM3F.2.

- **J.J. Granada Torres**, Andrea Chiuchiarelli, Varghese A. Thomas, Stephen E. Ralph, A. M. Cárdenas, and N. Guerrero González, "Adaptive Nonsymmetrical Demodulation based on Machine Learning to Mitigate Time-varying Impairments," IEEE Avionics and Vehicle Fiber-Optics and Photonics Conference, Long Beach, CA, Nov. 2016, ThA2.3.

- **J.J. Granada Torres**, A. M. Cárdenas, and N. Guerrero González, "Inter-Carrier Interference Mitigation based on FEC-encoded sequence distribution," in Latin America Optics and Photonics Conference, (Optical Society of America, 2016), paper LTu2C.2.

- J. P. López, **J.J. Granada Torres**, A. M. Cárdenas, and N. Guerrero González, "Inter-Channel Interference Characterization in a Nyquist-WDM gridless scenario with Nonlinear Impairments Compensation by using Digital Backpropagation," Latin America Optics and Photonics Conference, (Optical Society of America, 2016), paper LTu2C.4.

- **J.J. Granada Torres**, A.M. Cárdenas Soto, N. Guerrero González, "Mitigation of Linear Inter-Channel Interference for Sub-Nyquist Spacing in Optical Multicarrier Systems," IEEE Latin-America Communications Conference (LATINCOM), Nov. 2015.

- **J.J. Granada Torres**, A.M. Cárdenas Soto, N. Guerrero González, "Evaluation and compensation of interchannel interference effects in a 16-QAM Nyquist-WDM system with LMS equalization," IEEE Latin-America Communications Conference (LATINCOM), pp.1,6, 5-7 Nov. 2014.

National Conferences

- **J.J. Granada Torres**, N. Guerrero González, F.C.G. Gunning, A.M. Cárdenas Soto, "Hybrid Time-Frequency Bit-multiplexing enabling Interchannel Interference Mitigation," in Photonics Ireland 2015 Conference, Cork, Ireland, Sep. 2015.

- **J.J. Granada Torres**, A.M. Cardenas Soto, N. Guerrero González, "Characterization of interchannel interference effects in multicarrier 32-Gbaud QPSK/16QAM Nyquist systems," IEEE Communications and Computing Conference (COL-COM), pp.1-6, 13-15, Popayán, Colombia, May. 2015.

Bachelor Thesis

- *Student*: J.P. López. *Advisor*: **J. J. Granada Torres**.
  "Interchannel Interference Characterization in Nyquist-WDM systems including linear and nonlinear mitigation of optical fiber impairments", Universidad de Antioquia, Faculty of Engineering, Department of telecommunications engineering, October 2016.

1.6   Thesis Organization

This Ph.D. Thesis comprises six chapters. In this first chapter, the context in which this work has been carried out is presented. Moreover, an introduction and the state-of-art about optical multicarrier systems is exposed. Furthermore, the main challenges to be faced for future deployment are discussed, highlighting the Interchannel Interference. In Chapter 2, an introductory and theoretical description about Nyquist-WDM is presented. Besides, the three setups in which this work is based on are depicted: *i)* a Nyquist-WDM system modeled in VPITransmissionMaker in co-simulation with Matlab, *ii)* an experimental 3 x 16 Gbaud Nyquist-WDM system implemented in the lab of CPqD (*Centro de pesquisa e desenvolvimento em telecomunicaões*, in Campinas - Brasil), and *iii)* a 3 x 32 Gbaud Nyquist-WDM system implemented in the Terabit Optical Networking Group of the Georgia Institute of Technology (in Atlanta - USA). In Chapter 3, a systematic characterization of the ICI effects in Nyquist-WDM systems is shown as function of system parameters such as: frequency carrier spacing, OSNR, transmission distance, laser linewidth, roll-off factor of the electrical pulse-shaping filter and the mark probability of the PRBS. Subsequently, in the Chapter 4, the proposed FEC distribution among optical carriers for ICI mitigation is described, including its verification by simulation results. The nonsymmetrical demodulation techniques based on adaptive k-means is exposed in Chapter 5, validating its effectiveness by means of

experimental results. Finally, the main conclusion of this work and outline possible futures lines of work are exposed in Chapter 6.

2

Theoretical Background

This Chapter presents a literature review of the main concepts used in our research. It was carried out in three big items: Nyquist-WDM systems, Equalization and Coding and Clustering.

2.1 Nyquist-WDM Systems

Wavelength-division-multiplexing (WDM) technology was born many years ago as a solution to increase the capacity by the use of multiple carriers transmitted at the same time through the optical fiber [54], [55]. This technology started to work with frequency separation between adjacent channels of 50 GHz and 100 GHz [56]. Each optical carrier is modulated independently and multiplexed through the optical fiber. At the receiver side, the optical signals are demultiplexed to be demodulated. WDM can work in direct detection as well as coherent detection. Coherent detection surged as the solution to increase the capacity per channel up to 100 Gbps for standardization, and in this technology, a demultiplexer might not be necessary thanks to the local oscillator tunes the desired frequency. Every channel of a classic WDM system works independently. However, in last years, some experimental results proposed the use of two carriers modulated in 16-QAM inside the fixed-grid to increase the capacity to 200-G [57]. Likewise, experimental results showed effectiveness by using 16-QAM modulation formats in two carriers for a possible 400-G standard.

With the aim of increasing the spectral efficiency, granularities of 25 GHz and 12.5 GHz were standardized by the ITU in the norm G.694.1, also known as ultradense

(UD) WDM. However, for the spectral efficiency increasing, (as it was mentioned in the previous Chapter) other steps should be applied, increment the m-ary modulation format, by using dual-polarization modulation, as well as the band guards reduction between channels and the pulse shaping.

Nyquist pulses based on *sinc* function were proposed to increase the spectral efficiency in UD-WDM networks, becoming in a established technology called Nyquist-WDM [58]. This technology is also attempted to be used not only in flexible grids (granularity of 12.5 GHz) but in gridless technologies when colorless transceivers are commercialized. In this chapter a brief theoretical description of Nyquist concept is shown. Besides, the Nyquist-WDM systems implemented by simulation and experimentally, are exposed in the following sections.

2.1.1 Nyquist Concept

The Nyquist concept defines that electrical pulses shaped by a root-raised cosine digital filter have an optical rectangular-like shaped spectrum, which occupy a bandwidth equal to the baud rate (see Figure 2.1.a). The square-root raised cosine pulse shape is given by [59]:

$$p(t) = \frac{2\mathrm{R}_{\mathrm{off}}}{\pi\sqrt{T_s}} \frac{\cos\left[(1 + \mathrm{R}_{\mathrm{off}})\,\pi\frac{t}{T_s}\right] + \frac{\sin\left[(1-\mathrm{R}_{\mathrm{off}})\pi\frac{t}{T_s}\right]}{4\mathrm{R}_{\mathrm{off}}\frac{t}{T_s}}}{\left[1 - \left(4\mathrm{R}_{\mathrm{off}}\frac{t}{T_s}\right)^2\right]} \tag{2.1}$$

Where $p(t)$ is the impulse response, R_{off} is the Roll-Off factor and the baud rate (BR) is $1/Ts$. Theoretically, ideal rectangular-like shaped spectrum allows frequency channel separation as small as the baud rate for all the wavelength multiplexed carriers. To get an ideal rectangular like-shaped spectrum is necessary Nyquist pulses with a Roll-Off value of zero of infinite duration (see Figure 2.1). However, in practice, it is difficult to get a perfect rectangle-like shape in the spectrum, due to the limited available number of taps of the digital filter at the transmitter. In spite of smaller roll-off gives narrower bandwidth in the spectrum, attenuation in spectrum stop band is reduced generating a side lobes increases.

The occupied bandwidth (Ch_{BW}) can be expressed in terms of the roll-off factor of the RRC digital filter, as follows:
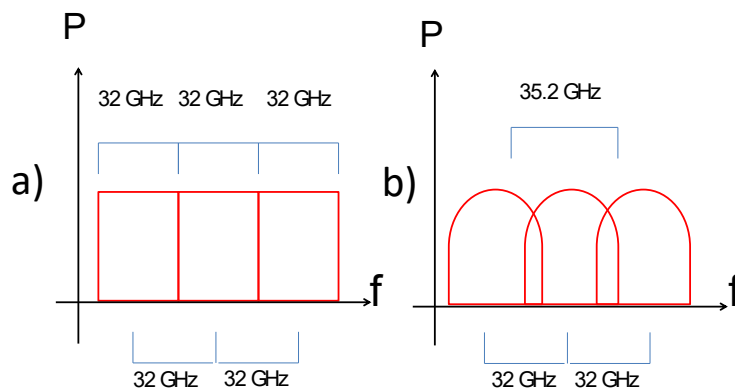
Figure 2.1: Ideal spectrums at 32 Gbaud for a) Roll-off of 0 and b) Roll-off = 0.1, with Nyquist channel spacing.

$$Ch_{BW} = B_R + (B_R)(R_{off}) \tag{2.2}$$

With a $R_{off} = 0.1$, Ch_{BW} is equal to 35.2 GHz, for a 32 Gbaud per carrier transmission (see Figure 2.1.b), according to the equation 2.2. Thus, if the frequency channel spacing is lower than channel bandwidth, overlap between adjacent channels is induced. Square-root is instead of raised-cosine function to minimize the Intersymbol Interference (ISI). Nevertheless, for different roll-off values, it is shown in figure 2.2 how the periodical lobes are unavoidable due to sinc-function in electrical temporal domain, with values are around -40 or -50 dB lower than the main lobe. This limitation induces a truncation of the pulse duration, seen in the optical spectrum as quasi-rectangular spectrum with an attenuation reduction of the lobes in the frequency stop band. Optical spectrums of three channels are observed in 2.3. Bandwidth broadening increases according to the roll-off value increases, as it can be detailed in the zoomed region.

2.1.2 Simulation Setup

A 3 x 32 Gbaud Nyquist-WDM system working with QPSK and 16-QAM modulation format is simulated using VPItransmissionMaker software (see Figure 2.4), in back-to-back (B2B) and for transmission distances up to 130 km without loops of optical amplifiers. A digital-to-analog-conversor (DAC) with 3 pairs of outputs is used to drive the IQ modulator. In the digital-to-analog converter (DAC), a pseudo-random binary sequence (PRBS) is generated. Besides, the pulse-shaping (PSh) is performed
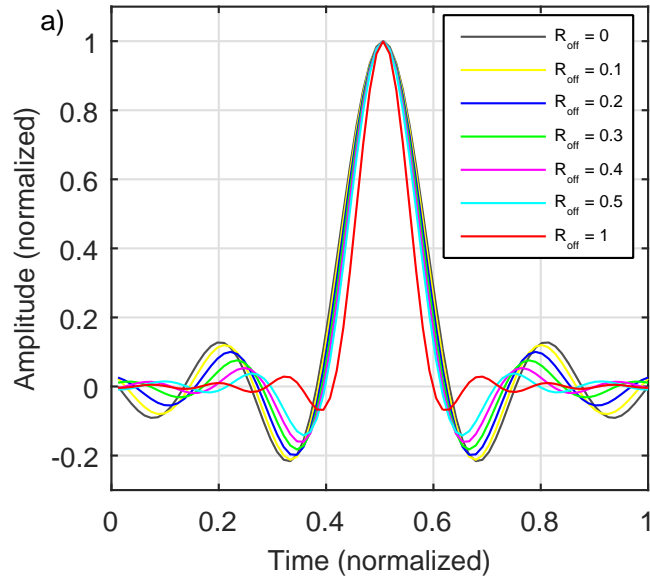
Figure 2.2: Electrical Nyquist pulses.
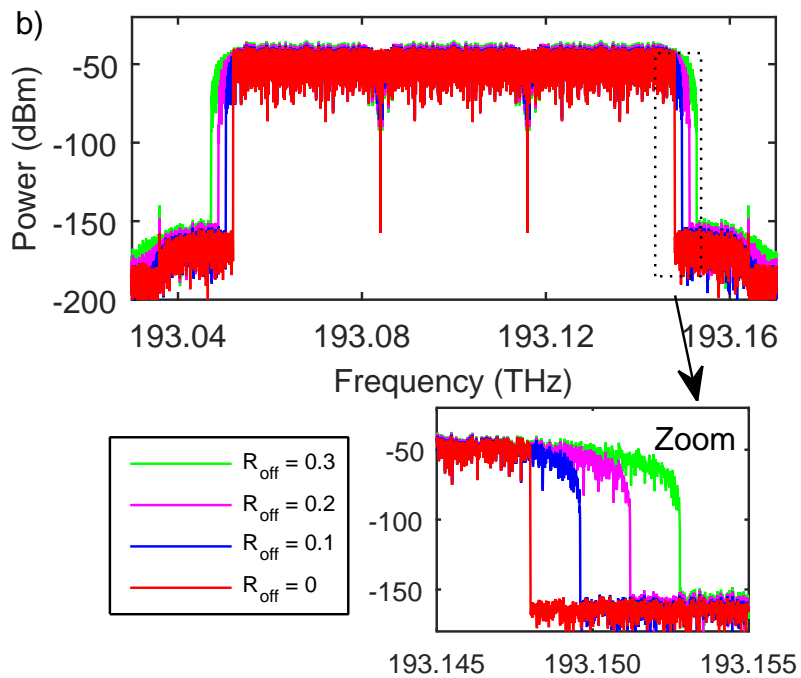
Figure 2.3: Optical spectrum generated by electrical Nyquist pulses.

by a root-raised-cosine (RRC) digital filter with a roll-off factor typical of 0.1, but for some evaluation, it is switched from 0 to 0.5. The optical source of each transmitter is a continuous wave (CW) laser with < 1 kHz linewidth at 1550 nm and a launched optical power of 0 dBm. Nevertheless, in some scenarios, the linewidth is tested up to 100 kHz. The light with polarization controller (PolC) is modulated with a pair of single drive Mach-Zehnder Modulators (MZM) for an In-phase and Quadrature (IQ) configuration to obtain QPSK and 16QAM formats. The signals are transmitted into standard single-mode fiber. Ideal coupler is used as flexible multiplexer. At the receiver side, demultiplexer with flexible grid is used. Optical demodulation is carried out with 3 independent coherent detectors. The coherent receiver is based on a 90° Hybrid coupler and two balanced photodiodes with a responsivity of 1. The local oscillator (LO) of the coherent receiver is a laser with the same characteristics than the one used as optical source in the transmitter side. Analog-to-Digital Conversion (ADC) is carried out after coherent detection. Match filter (MF) is used to separate electrically each channel by also using RRC function. The digital signal processor (DSP) is implemented by co-simulation with Matlab. At first, the chromatic dispersion is compensated (CDC) by means of a transversal filter by using the Fourier transform of the inverse fiber dispersion function. Moreover, the clock recovery (ClkR) module performs the signal synchronization before the phase correction (PhC).

2.1.3   Experimental Setup

2.1.3.1   Scenario A

The experimental setup depicted in Figure 2.5 is a 3 x 16 Gbaud Nyquist-WDM system with a DSP-enabled coherent receiver. In the back-to-back scenario, optical noise is added to yield an OSNR ranging from 16 to 32 dB. A multi-span link was also studied comprised of 5 spans of 50 km of standard single-mode fiber with a launch power of 0 dBm. The WDM transmitter is comprised of three tunable lasers with a linewidth of 100 kHz. The I and Q components in the X/Y polarizations are randomly generated by a digital-to-analog converter (DAC) operating at 64 GSa/s (5 ENoB bit resolution), with an electrical bandwidth of 14 GHz. The four DAC outputs are amplified by four RF drivers with 32 GHz bandwidth before being sent to the IQ modulator. A random PRBS source is used to generate 16-QAM symbols at 16 Gbaud in Matlab, where a
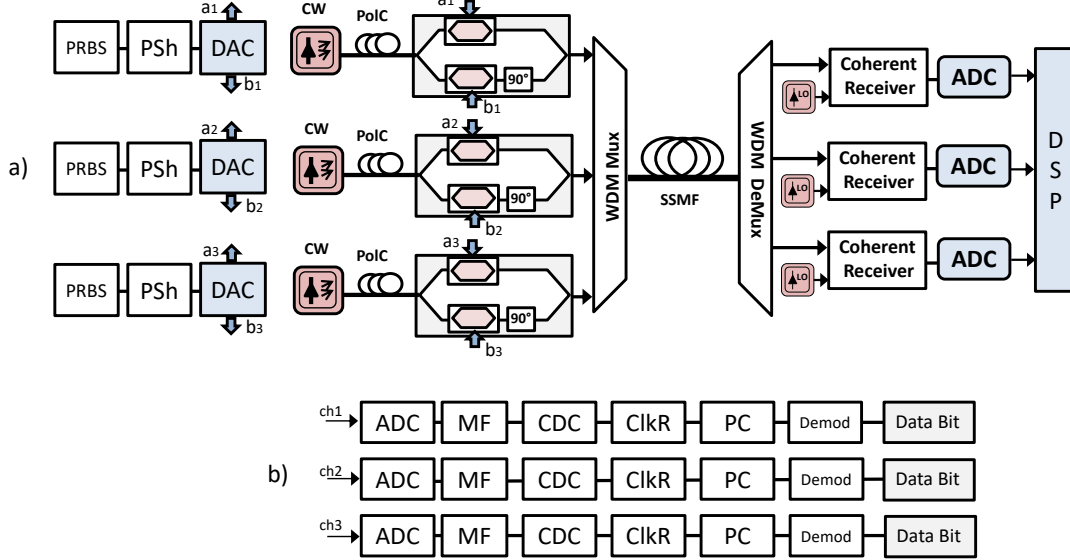
Figure 2.4: Simulation setup of a Nyquist-WDM system modeled in VPITransmission-Maker.

root raised cosine filter with a roll-off factor of 0.1 is used to implement Nyquist pulse shaping. The generated signal is then loaded onto the DAC that drives the optical modulator. At the receiver end, a wideband coherent receiver of 40 GHz is used to detect the 3 optical carriers. The received signal is digitized by an 80 GSa/s real-time oscilloscope, where the 4 inputs, namely the I and Q in X and Y polarizations, have a bandwidth of 35 GHz each. This is followed by offline processing in MATLAB. Postdetection digital signal processing (DSP) involves the following steps: skew compensation, matched filtering, chromatic dispersion compensation, timing recovery, polarization demultiplexing, frequency offset estimation, carrier phase recovery and frequency domain equalization. Finally, after digital demodulation bits are recovered.

2.1.3.2   Scenario B

The experimental setup shown in Figure 2.6 is a 3×32 Gbaud 16-QAM Nyquist-WDM system with a DSP-enabled coherent receiver. Three tunable lasers with linewidth of 25 kHz and 100 kHz are modulated via a dual-polarization IQ modulator driven by four digital-to-analog converters (DAC). The center and side channels are generated using different DACs to produce uncorrelated signals. The DACs operate at 88 Gsamp/s,
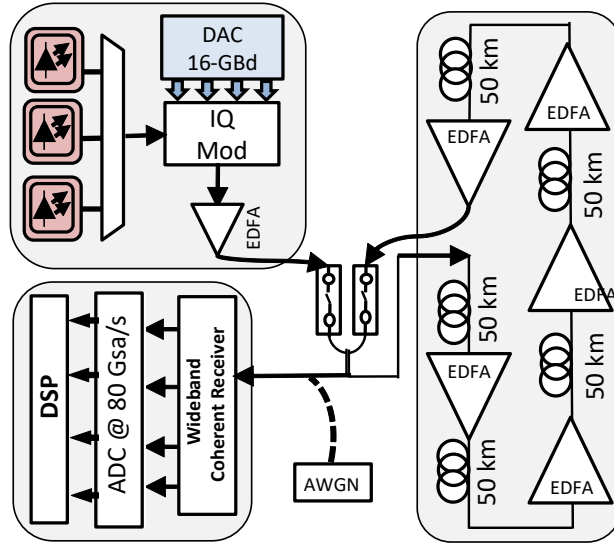
Figure 2.5: Experimental setup of a 16 Gbaud Nyquist-WDM system.
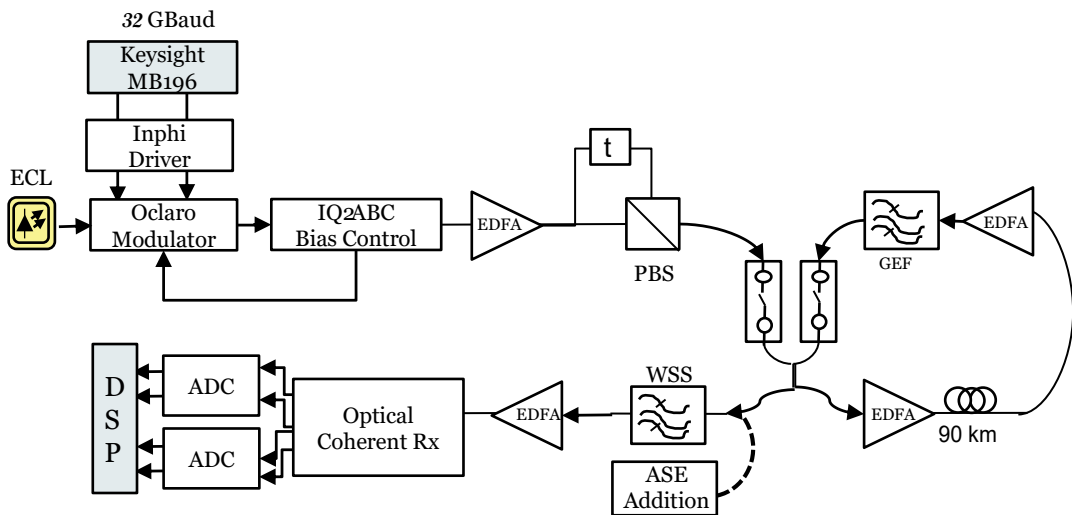
Figure 2.6: Experimental setup of a 32 Gbaud Nyquist-WDM system.

with an electrical bandwidth of 32 GHz, respectively. A random bit sequence is mapped to generate 16-QAM symbols using a root raised cosine filter with a roll-off factor of 0.1. In the back-to-back scenario, optical noise is loaded at the receiver to vary the OSNR. In the scenario of transmission through the fiber, standard single-mode fiber were employed with EDFA's after every 90 km span. At the receiver side, a wideband coherent receiver with an electrical bandwidth of 30 GHz is used to detect the signals. The signals are digitized by an 80 Gsamp/s real-time oscilloscope, followed by offline processing in MATLAB. Post detection DSP implemented the following techniques: skew compensation, matched filtering, chromatic dispersion compensation, timing recovery, polarization demultiplexing, frequency offset estimation, carrier phase recovery and equalization by means of direct-detection least-mean-square (DD-LMS) algorithm. Finally, after digital demodulation bits are recovered.

2.2 Equalization

2.2.1 Least Mean Square Algorithm

The Least-Mean-Square (LMS) Algorithm is an iterative algorithm which finds the coefficients of adaptive filter by an error minimization between training sequence and received signal [60], [61]. It can be seen as follows:

$$y(n) = w^\top(n-1)u(n) \tag{2.3}$$

$$e(n) = d(n) - y(n) \tag{2.4}$$

$$w(n) = w(n-1) + f(u(n), e(n), \mu) \tag{2.5}$$

Weights update function is given by:

$$f(u(n), e(n), \mu) = \mu e(n) u^*(n) \tag{2.6}$$

Where,

n: The current time index.

$w(n)$: weight vector.

$d(n)$: desired signal (training sequence).

$y(n)$: output equalizer signal.

$u(n)$: input equalizer signal.

$u^*(n)$: conjugated of $u(n)$.

e : estimated error.

μ : step size.

2.2.2 Non-Data-Aided Equalizer

The Non-Data-Aided (NDA) equalizer for ICI mitigation is performed in pre-slicing procedure in the DSP and carrier synchronization is not required. The equalization is based on the gradient-descent method in a feed forward FIR filter as the dispersion compensation technique proposed in [62]. The equalization uses the rule of the Constant-Module Algorithm (CMA) to recover the information. QPSK modulation has constant modulus which can be explained as constant amplitude of the symbols for phase modulation signals in the constellation diagram. CMA has been widely used as a blind equalization technique to mitigate channel impairments in telecommunication systems taking advantages of the non-use of training sequences. Blind equalization is also known as a self-recovering equalization, and its objective is to recover the unknown input signal from the unknown channel. The CMA technique can be mathematically described as follow [63]:

$$y(n) = w^H(n)x(n) \tag{2.7}$$

$$e(n) = 1 - |y(n)|^2 \tag{2.8}$$

$$w(n+1) = w(n) + \mu x^*(n)e(n)y(n) \tag{2.9}$$

Where, $x(n)$ is the nth received signal, $w(n)$ is the filter tap weights, $y(n)$ is the received signal at filter output, $e(n)$ is the error estimation, $w(n+1)$ is the weight update equation, μ is the step size parameter, H is the Hermitian function (conjugate transpose) and $(*)$ is the complex conjugate. Error is calculated imposing a constrain on the intensity (2.8) and it is minimized iteratively in function of signal sample n.

2.2.3 Backpropagation

Taking into account that channel characteristics are known, Digital Backpropagation (DBP) is commonly referred as the solution to pre-compensate or post-compensate the deterministic effects in channels at the transmitter or receiver. BP works by using the split-step inverse nonlinear Schrödinger equation (NLSE). The working principle of DBP is straightforward. By means of the channel estimation, in this case, the optical fiber, the channel response can be characterized using a loop back (or other methods). Then, at the receiver side for our applications, the inverse channel response can be applied to the received signal to compensate the optical fiber's impairments. DBP can jointly compensate linear and nonlinear effects at the same time. Launch power in WDM systems can be significantly increased to values beyond of traditional nonlinear limits. As a result, higher OSNR or longer transmission distance can be achieved for same FEC limit obtained without DBP [64], [65], [66], [67].

On the other hand, DBP analysis depends on if PMD is negligible or not. In this work, both cases are exposed as follows.

2.2.3.1 Single Polarization Systems

For systems where polarization mode dispersion (PMD) is negligible o for simplification, signal propagation into the optical fiber can be modeled by a scalar nonlinear Schrödinger equation (NLSE) in the reference polarization as it is described in [65]:

$$\frac{\partial E}{\partial z} = j\gamma|E|^2 E + \left(-j\frac{\beta_2}{2}\frac{\partial}{\partial t^2} - \frac{\alpha}{2}\right)E = (\hat{N} + \hat{D})E \qquad (2.10)$$

where α, β_2 and γ are the loss, group velocity dispersion (GVD) and nonlinear index, respectively.

In the absence of noise, transmitted signal can be calculated from the inverse NLSE [65]:

$$\frac{\partial E}{\partial z} = (\hat{N}^{-1} + \hat{D}^{-1})E \qquad (2.11)$$

2.11 is equivalent of passing the received signal through a fiber with parameters of opposite sign. By using the Split Step Fourier Method (SSFM), the NLSE can be solved numerically as follows [65]:

$$E(t, z+h) = \left(e^{\frac{h}{2}\hat{D}}\right)\left(e^{\int_z^{z+h}\hat{N}(z')dz}\right) \times e^{\frac{h}{2}\hat{D}}E(z,t) \tag{2.12}$$

where h is the step size. Since the nonlinear operator depends on E itself, the integral for $\hat{D}(z)$ is usually approximated by the trapezoidal rule, and an iterative procedure is used to solve Equation 2.12. The accuracy of iterative symmetric SSFM is improved when the number of iterations used to solve Equation 2.12 is increased. Besides, it is improved decreasing the step size. For both cases, the computational requirements are increased.

Nevertheless, a less computational complex algorithm based on a noniterative asymmetric SSFM can be used, where the optical fiber is modeled as a concatenation of nonlinear and linear sections in the m-th channel [67] [68]:

$$E_m(t, z+h) = E_m(z,t)e^{j\gamma h|E_m(t,z)|^2} \tag{2.13}$$

$$\tilde{E}_m(\omega, z+h) = \tilde{E}_m(\omega, z+h) \times e^{-\left(\frac{\alpha}{2}+j\frac{\beta_2}{2}\omega^2\right)h} \tag{2.14}$$

This model is based on the idea that nonlinear effects are strongest at the beginning of a optical fiber link, due to the optical power is higher.

2.2.3.2 Polarization Multiplexed Systems

When polarization effects are taken into account in the signal propagation into optical fiber, instead of representing the non-linear Schrödinger equation (NLSE), the evolution of electrical field into the fiber can be expressed by means of the Manakov equation as follows [64]:

$$\frac{\partial A_x}{\partial z} = -\frac{\alpha}{2}A_x + j\sum_{n>1}\frac{j^n\beta_n}{n!}\frac{\partial^n}{\partial t^n}A_x + j\gamma_m\left(|A_x|^2 + |A_y|^2\right)A_x \tag{2.15}$$

$$\frac{\partial A_y}{\partial z} = -\frac{\alpha}{2}A_y + j\sum_{n>1}\frac{j^n\beta_n}{n!}\frac{\partial^n}{\partial t^n}A_y + j\gamma_m\left(|A_x|^2 + |A_y|^2\right)A_y \tag{2.16}$$

where A_x and A_y are the two polarization components of the total electric field, α is the loss coefficient, β_n is the nth-order dispersion parameter, $\gamma_m = 8/9\gamma$, and γ is the nonlinearity parameter. The Manakov equation is invariant under polarization rotations, and it is written in the x- and y-polarization basis only for convenience [64].

27

2.3 Coding and Clustering

2.3.1 Reed-Solomon FEC

Several FEC techniques have been proposed in optical communications based on electrical communication system such as: Reed-Solomon, BHC, Hamming code, among others [69]. FEC techniques can be roughly classified according to two decisions methods: hard decision and soft-decision. The principal difference between the soft and the hard types of FEC decisions is that hard-decision works at the bit level whilst soft decision operated with a multilevel quantization signal, in other words, information from the physical-layer of the systems is required [70]. Soft-decision FEC ensures better performance and a bit throughput than hard-decision FEC. However, it can be implemented only when a high-speed ADC is used to perform sampling and quantization. Besides, soft-decision algorithm is very complex because it must consider the changes in noise probability distribution caused by channel performance deterioration [71]. For our purpose, classic hard-decision Reed-Solomon FEC code is used, adding a bit-multiplexing stage among carriers after coding the bit sequence. At receiver side, digital equalization is implemented to support the hard-decision performance.

Reed-Solomon (RS) codes are linear no-binary cyclic codes, formed by sequences of m-bits symbols that belong to $(2m)$ extended Galois fields, where m takes values greater than two. A RS code is specified as $RS(n,k)$, where the minimum distance between codewords is $d = n - k = 2t + 1$. Thus, $RS(n,k)$ can correct t symbols. In scenarios where burst errors (in the bit-sequence) can occur more frequently than independent errors, interleaving FEC techniques are proposed for avoiding the inclusion of the overhead in a continuous sequence [72]. In our proposal, the burst errors are avoided due to the distribution of the encoded sequences in different channels. This issue will be further explained in Chapter 4.

2.3.2 k-means algorithm

The clustering is a technique that establishes the relation of a set of elements with respect to a group. The group is also called class. The clustering makes a correlation and classification of a set of data. The k-means algorithm is a well-known clustering technique, having as a main characteristic that it is based on unsupervised learning, where the association of data with the classes is performed through a similarity measure,

for example, the Euclidean distance measure between a data vector and class' centroids [73].

The k-means algorithm involves multiple iterations of clustering [74], [75]. In each iteration each received symbol is assigned to the cluster whose centroid is closest. Mathematically, this involves minimizing the following objective function 2.17:

$$J = \sum_{j=1}^{k} \sum_{i=1}^{n} \left\| x_i^{(j)} - c_j \right\|^2 \tag{2.17}$$

where $x_i(j)$ is the ith received symbol in the jth cluster, c_j is the centroid of the jth cluster, n is the number of symbols in the jth cluster, while k represents the total number of clusters. Usually, the centroids are randomly initialized. For our purpose, k depends on the order of the known m-ary modulation format. The k reference constellation points are used as the initial locations for the centroids in the first iteration, which then changes as the received symbols are assigned to these k clusters.

After the first iteration, the centroids are recalculated based on the clustering in that iteration according to the equation 2.18:

$$c_j = (1/n) \sum_{i=1}^{n} x_i^{(j)} \tag{2.18}$$

Where these recalculated centroids are employed in reassigning the received symbols in the next iteration using the objective function in equation 2.17. These repeated clustering iterations are carried out until the algorithm converges, which occurs when the centroids do not change their spatial locations and therefore no data-symbols are reassigned. In Figure 2.7, an example of clustering based on k-means is shown in a QPSK constellation. Each color represents different clusters. It is shown that the initial centroids are the ideal constellation, because it is expected that the received symbols are not far from that points.

2.4 Summary

In this chapter, a description of Nyquist-WDM systems and a brief explanation of Nyquist concept is presented. Furthermore, the Nyquist-WDM systems modeled in VPITransmissionMaker in co-simulation with Matlab, and two experimental setups implemented in two abroad labs, are depicted.

Received Symbols

*Reference
(Transmitted symbols)

Iteration 1

Iteration 2

Iteration I-th
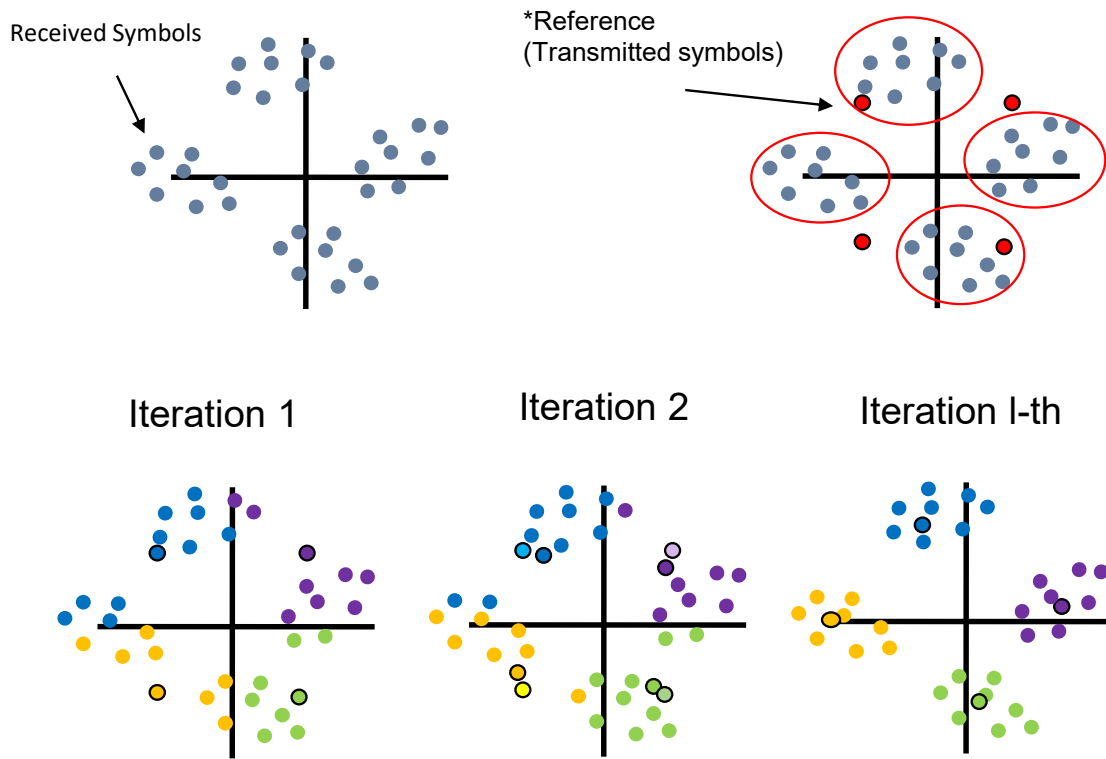
Figure 2.7: Example of Clustering in a QPSK constellation based on k-means.

Additional theoretical background of the important topics of this research, such as equalization, coding and clustering, were presented.

3

Evaluation of ICI Effects

3.1 Introduction

In this chapter, ICI effects are evaluated in the Nyquist-WDM systems presented in the Chapter 2. The ICI is systematically evaluated in terms of BER as function of several system parameters by simulation. Frequency channel spacing is the most important parameter to be modified in the evaluation of ICI impact. It is reduced as close as possible to adjacent channels, to identify the maximum overlapping accepted for a successful demodulation in the scenarios proposed. Moreover, the roll-off factor of the pulse-shaping filter is varied for increasing the channel bandwidth. The ICI characterization is performed in back-to-back (B2B) as well as in transmission distance without optical amplifiers by simulation, and in amplified spans of 50 km and 90 km experimentally.

Moreover, nonlinear impairments of the optical fiber are stimulated by means of high launch power. A comparison between the linear and nonlinear effects are performed for different system parameters, including the digital backpropagation (DBP) algorithm for nonlinear mitigation.

3.2 Methodology for ICI Evaluation

A summary of the parameters used to evaluate the ICI impact as a function of BER are shown in Figure 3.1. When one of those parameter is not under evaluation, the value of such parameter is the typical value shown in Figure 3.1. Our purpose is performed

measuring the impact when channels are overlapped or very close, and the contribution of variations of system's parameters in these cases.

A brief description of the parameter used as variable by simulation is presented as follows and its range of working is shown in Figure 3.1:

- **Roll-Off Factor:** This parameter is varied at transmitter in the pulse-shaping filter. It causes a broadening in the spectrum when is value is higher than zero. It can have values from 0 to 1.

- **Frequency Channel Spacing:** This parameter is varied by using tunable lasers. Frequency (or wavelength) of adjacent channels is modified for the closeness desired. Central laser operates at 193.1 THz and the adjacent ones operate with a deviation from 14 GHz to 50 GHz depending on the specific case.

- **Transmission Distance:** This parameter is modified changing the length of the optical fiber.

- **Laser's Linewidth:** the impact of laser's linewidth is tested when channels are overlapped. Ideal laser would have linewidth equal of zero. Depending on its value, the cost of lasers could be very expensive. That's why its impact is an important issue.

- **Dispersion Factor:** Optical fibers have a value defined by manufactures with the typical value shown in Figure 3.1 of the well-known standard single-mode optical fiber.

- **Mark Probability of PRBS:** This value is modified in the digital transmitter. Even if the probabilistic distribution of PRBS is equal or close of being gaussian, centered in 0.5 (same probability to get "1" or "0" in a bit-sequence), this probability might be different of 0.5 in short time slots. Hence, the interaction of the non-gaussian short bit-sequence might affect the adjacent channels due to the XPM.

- **Launch Power:** Lasers has a defined transmission power. It can be yield at its maximum power, and the launch power may be regulated with an optical amplifier before the optical fiber link. Depending on the power value, the nonlinear effects of the optical fiber could be stimulated.

- **OSNR:** In the experimental setup, the level of optical noise added is varied to watch the ICI impact under different levels of noise.

Parameters	Range	Typical Value
Roll-Off	*0 – 0.5*	*0.1*
Frequency Channel Spacing	28 GHz – 50 GHz @32GBd 15 GHz – 18 GHz @16GBd	30, 32, 35 GHz @32GBd 15.5, 16, 16.5 GHz @16GBd
Transmission Distance	0 km – 250 km	0 km (B2B)
Laser's Linewidth	< 1 kHz – 20 MHz	< 1 kHz
Laser's Wavelength	C-Band	1550 nm
Dispersion Factor	0 – 20 [ps/(nm-km)]	SSMF: 16 [ps/(nm-km)]
Mark Probability of PRBS	0.1 – 0.9	0.5
Launch Power	-4 dBm – 16 dBm	0 dBm
OSNR	14 dB – 37.3 dB	---

Figure 3.1: Summary of parameters used to evaluate the ICI impact.

The ICI impact is presented by means of the calculation of BER versus several system parameters. Firstly, the impact is measured in the central channel of three channel transmission (see section 3.3). Secondly, the impact in the adjacent channels is evaluated in 3.4. It means, the BER of the three channel transmitted is estimated. Additionally, the impact of ICI when one of the adjacent channel of both are modulated with other modulation format (QPSK or 16QAM) is evaluated in Section **??**. Moreover, PRBS's mark probability is varied in Section 3.5 to evaluate the impact of the bit's randomness when channels are very close or overlapped.

Besides, in Section 3.6, power launch is varied with the aim of stimulating the nonlinear effects of the optical fiber. Subsequently, in Section 3.7 the digital backpropagation (DBP) algorithm is implemented at the DSP for the nonlinear mitigation to carry out a comparison with and without the DBP at 16 Gbaud and 32 Gbaud.

3.3 ICI effects as function of system parameters

ICI effects is evaluated in a QPSK transmission for the 3×32 Gbaud system presented in Chapter 2 by a BER estimation as function of frequency carrier spacing, roll-off of the Nyquist filter, laser linewidth, and transmission distance. In Figure 3.2a, a B2B

evaluation of the roll-off impact is done for 3 different frequency carrier spacing of 30 GHz, 32 GHz and 35 GHz. Roll-off values have a high impact in the ICI effects measured in terms of BER due to the excess of the occupied bandwidth. It can be noticed that with 30 GHz of carrier spacing, the impact in terms of BER is very high reaching a BER of 10^{-2} even with a roll-off equal to zero. For a Roll-off variation between 0.1 and 0.2 there is a penalty of 4 decades (double arrow in the plot) in BER, from 10^{-8} to 10^{-4}, respectively. For a carrier spacing of 35 GHz, a better performance is obtained, having a BER of 10^{-12} with a roll-off factor of 0.4. BER vs frequency carrier spacing is showed in the Figure 3.2b for different roll-off factors. For roll-off values between 0 and 0.3, the BER difference is lower than 1 order of magnitude with a carrier spacing of 30.5 GHz (dashed ellipse in the plot), whereas that for a carrier spacing of 31.5 GHz, the BER difference is 4 orders of magnitude (double arrow in the plot). BER values lower 10^{-5} are reached with roll-off factor values up to 0.2 adjusting the frequency carrier spacing.

Figure 3.3a shows BER vs transmission distance for a roll-off of 0.1. For a carrier spacing of 30 GHz the ICI impact is very high regardless of fiber length, reaching BER values close to 10^{-2}. For a carrier spacing of 32 GHz, the BER changes from 10^{-8} in B2B up to 10^{-3}. In this case, until 70 km, the BER is lower than 10^{-7}, whereas that for a carrier spacing of 35 GHz, BER of 10^{-7} is reached at 120 km. Analysis of the laser's linewidth impact in terms of BER is shown in figure 3.3b. The x axis is in logarithmic scale for a comprehensive comparison. It is shown a minimal BER variation between linewidth values from 1 kHz up to 100 kHz. The penalty from 100 kHz to 1 MHz is close to 1 order of magnitude for a roll-off factor of 0.1. For a roll-off equal to 0, it is shown a variation from 10^{-6} to 10^{-3} for linewidth values between 5 MHz up to 10 MHz.

In figure 3.4, BER is estimated as function of the dispersion factor in an uncompensated-link of 10 km. It can be seen that for a dispersion factor higher than 10 $ps/(nm \times km)$, the BER difference between a Nyquist separation (32 GHz) and 35 GHz, is lower than 1 order of magnitude. Higher values than 17 $ps/(nm \times km)$, the impact in BER is very similar. It represents the high impact of uncompensated links.

In table 3.1, some of the results presented in this section are summarized.
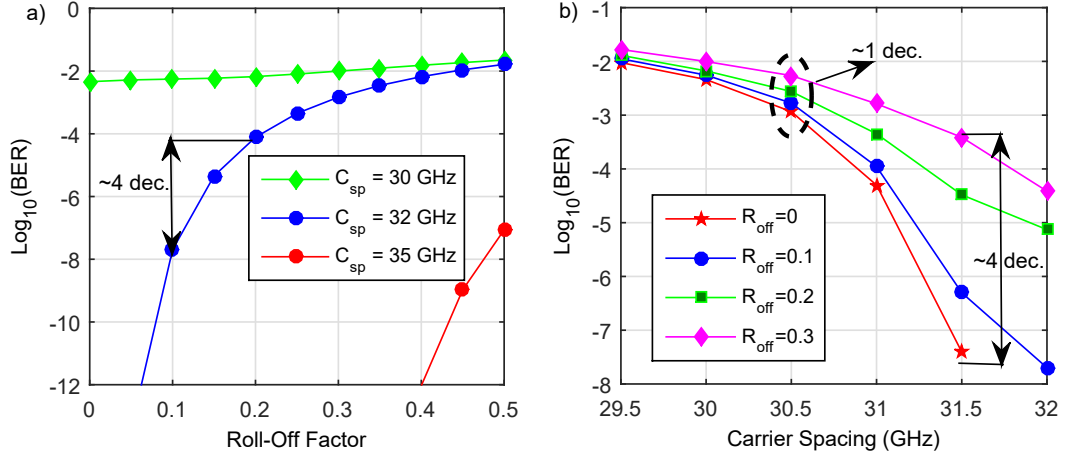
Figure 3.2: a) BER vs Roll-Off Factor, b) BER vs Frequency Carrier Spacing.
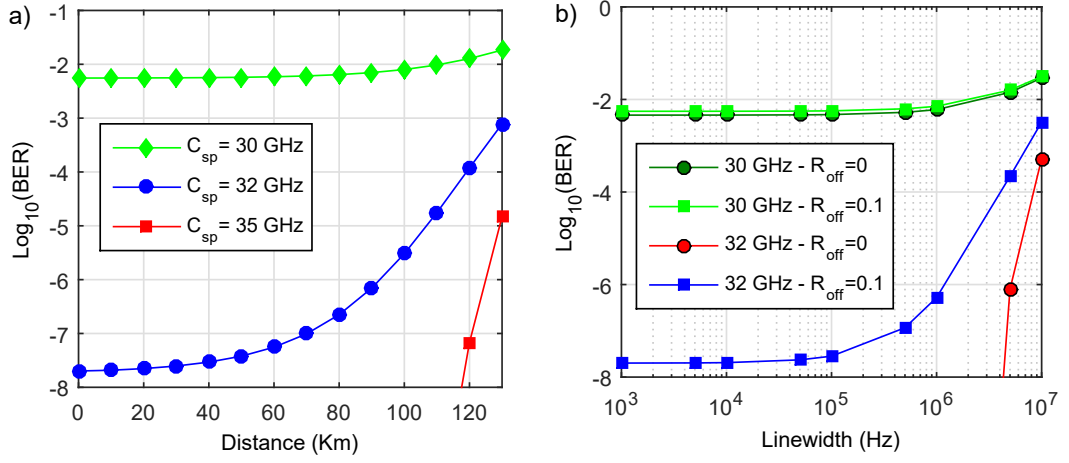
Figure 3.3: a) BER vs Transmission Distance, b) BER vs Laser's Linewidth.

Roll-Off	BER	Carrier Spacing	Distance
0.1 to 0.2	10^{-8} to 10^{-4}	32 GHz	B2B
0 to 0.3	10^{-3} to 10^{-7}	31.5 GHz	B2B
0.1 to 0.4	10^{-8}	32 GHz to 35 GHz	B2B
0.1	10^{-4} to 10^{-7}	32 GHz to 35 GHz	120 km

Table 3.1: Summary of results presented in Section 3.3.
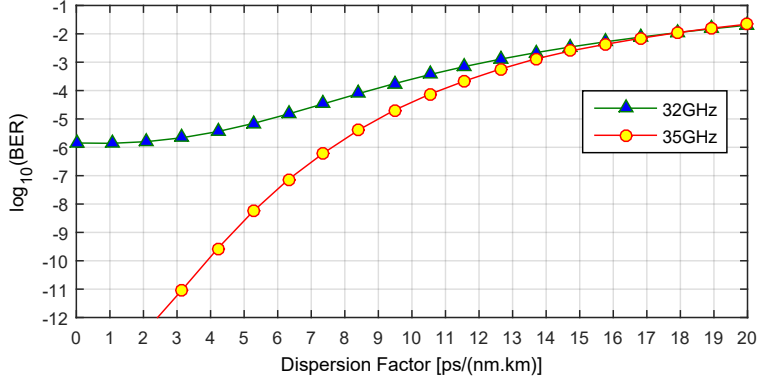
Figure 3.4: a) BER vs Dispersion Factor in 10 km of uncompensated-dispersion link.

3.4 ICI impact in adjacent channels

Figure 3.5 shows BER estimation vs roll-off factor. For a distance of 1 km and channel spacing of 32 GHz (figure 3.5a) is clearly noted that occurs a fast increasing in BER when roll-off factor changes from 0 to 0.1, passing from a BER of 10^{-19} to 10^{-8} for central channel (ch_2). From 0.1 to 0.5 the increasing BER factor is lower, reaching a BER of 10^{-3}. With a channel spacing of 35 GHz (figure 3.5a), the BER has a lower increment in comparison with the previous case, even for a roll-off range from 0 to 0.1, with BER values of 10^{-25} ($R_{off} = 0$) and 10^{-22} ($R_{off} = 0.1$) for central channel. Making a comparison between the best and the worst BER value in figure 3.5a, for a specific roll-off of 0.1, it is obtained a BER difference of 18 orders of magnitude (doble arrow in figure 3.5a). This is a high difference in BER, realizing that there are only 3 GHz of separation between both channel spacing. BER difference among the three channels of 32 GHz is around 9 orders of magnitude (ellipse in figure 3.5a). Figure 3.5b is a 10 km case, also, with channel spacing of 32 GHz and 35 GHz. In both channel spacing, transmission is highly limited in terms of BER and its variation for different roll-off values is lower than 1 order of magnitude for a roll-off of 0.1.

Figure 3.6 shows the BER as function of the channel spacing, for B2B, 1 km and 10 km of uncompensated-dispersion link, with a roll-off of 0.1. At B2B and 1 km, the performance in terms of BER is very similar, BER increases approximately between 4 and 5 orders of magnitude in 2 GHz of spectrum grid difference (32 to 34 GHz). With a channel spacing from 34 to 36 GHz, BER behavior is the same in these three cases

Figure 3.5: BER vs Roll Off factor for a QPSK transmission over a) 1 km and b) 10 km with channel spacing of 32 and 35 GHz.
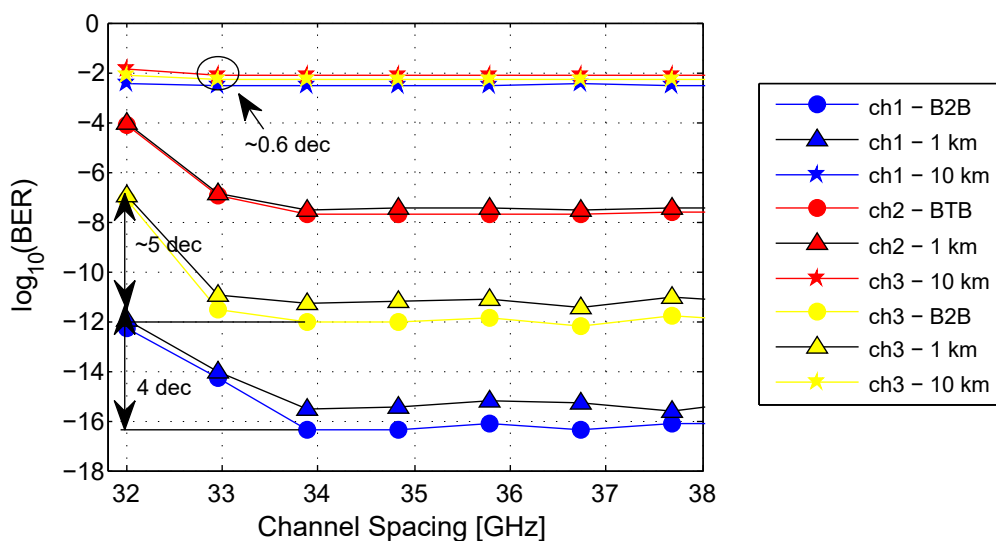
Figure 3.6: BER vs Channel Spacing in QPSK case with roll-off of 0.1 in B2B, 1 km and 10 km.

37
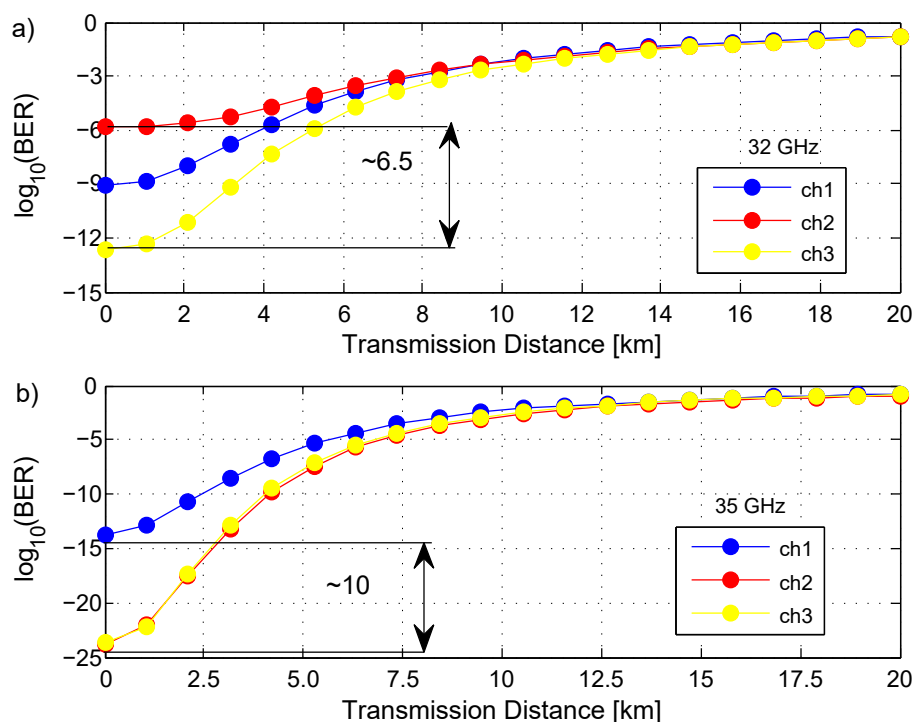
Figure 3.7: BER vs Transmission Distance for uncompensated-dispersion link in QPSK transmission for carrier spacing of a) 32 GHz and b) 35 GHz.
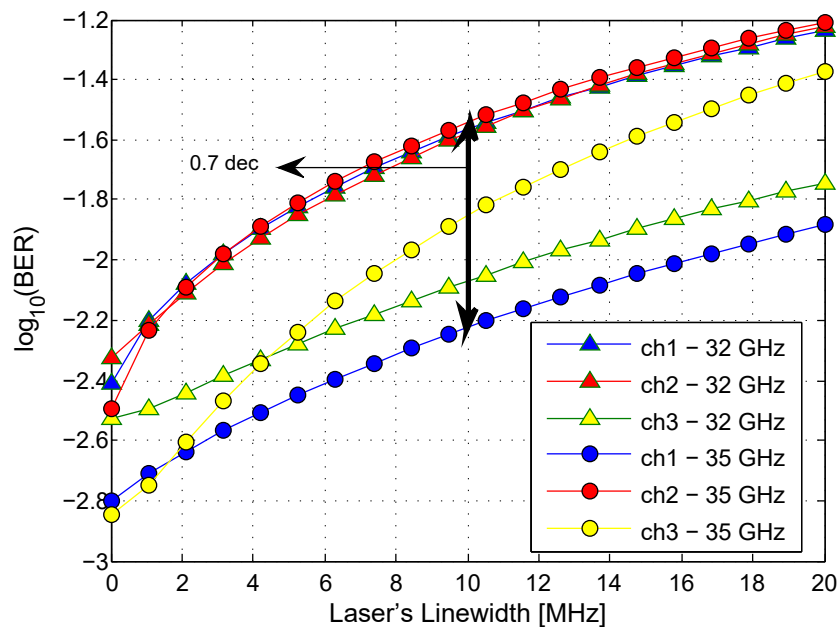
Figure 3.8: BER vs laser's linewidth for QPSK over 10 km of uncompensated-dispersion link.

Roll-Off	BER	Carrier Spacing	Distance
0.1	10^{-6} to 10^{-12}	32 GHz	1 km
0.1	1×10^{-2} to 1.6×10^{-3}	35 GHz	10 km
0.1	1×10^{-2} to 2.5×10^{-3}	33 GHz	B2B
0.1	All channels 10^{-3}	32 GHz	9 km

Table 3.2: Summary of results presented in Section 3.4, difference between central and adjacent channels.

with low variations.

For the two cases of channel spacing (32 and 35 GHz), BER estimation is carried out for different distances from 0 to 20 km. BER increasing behavior is similar between 2 cases (figure 3.7a and 3.7b). A difference of higher than 6 orders of magnitude between ch_2 and ch_3 in B2B is obtained for a channel spacing of 32 GHz (figure 3.7a), and a difference of 10 is obtained for a channel spacing of 35 GHz (figure 3.7b). It is noted that in the second case, ch_1 has a worse BER than ch_2 which is the central channel. Besides, BER values of each channel have significant differences for values lower than 7 km. It was expected that central channel always had the worst BER, but how it is seen in the next subsections, bit probability in a sequence has an important impact in terms of BER. For longer distances than 7 km, BER difference among channels is lower than 1 order of magnitude.

The other parameter evaluated is the laser's linewidth. This parameter increases the delay in the received signal due to the chromatic dispersion effects for long distances. For the evaluation of its effect in channels affected by ICI, the BER is estimated in figure 3.8 for a 10 km transmission. BER values in the worst cases are from -2.8 to -1.2 in log-scale. BER difference among 3 channels and between two different channel spacing are lower than 1 order of magnitude. It confirms that linewidth does not have an important contribution to ICI effects.

In table 3.2, some of the results presented in this section are summarized.

3.5 ICI effects due to the randomness of bit-sequences

Results of section 3.3 clearly show that system parameters have an impact in the ICI effects, measured in terms of BER for a central carrier affected by two adjacent channels.

3. EVALUATION OF ICI EFFECTS

In this section, an analysis about binary sequence impact is carried out, according to the mark probability (MP) of the pseudo-random transmitted binary sequence (PRBS).
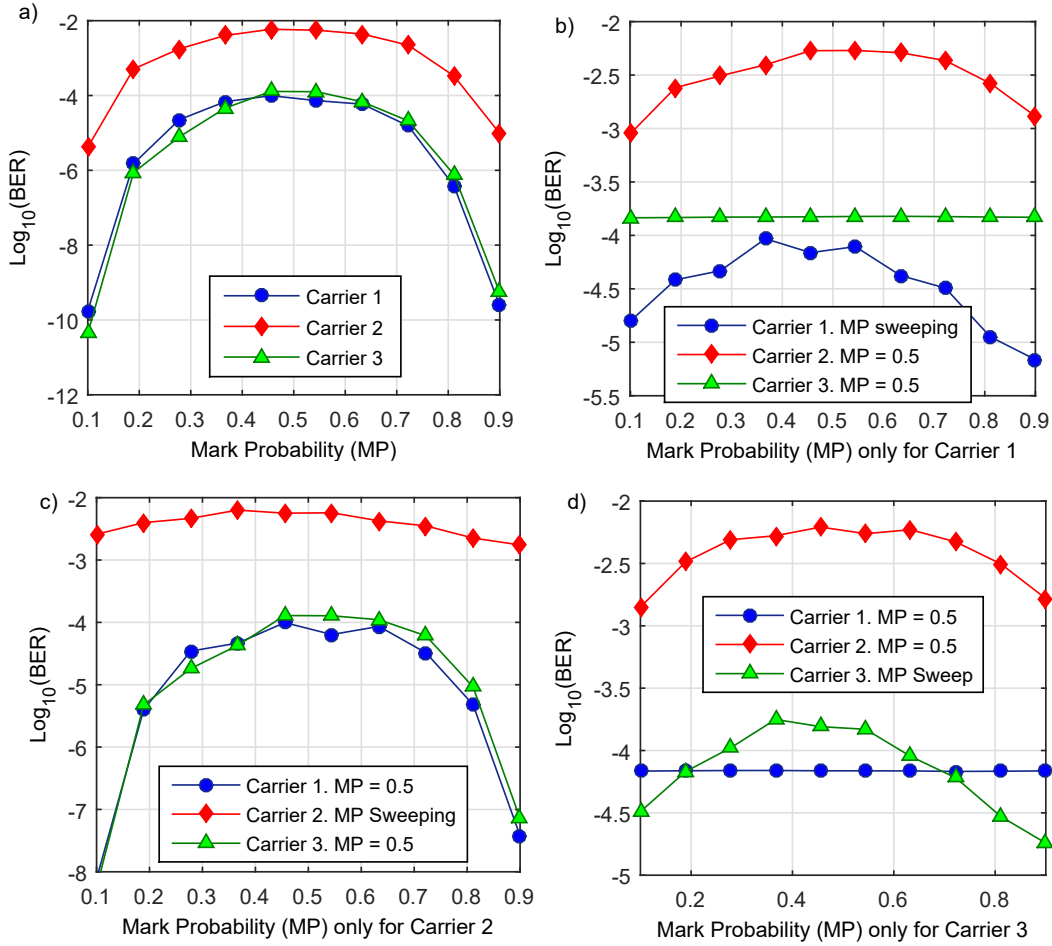
Figure 3.9: BER vs Mark Probability (MP) for a carrier spacing of 30 GHz in B2B.

Figure 3.9 shows BER vs MP curves for QSPK modulation with a roll-off factor of 0.1. The MP of PRBS is the only system parameter that is changing in the 4 plots. Figure 3.9a is obtained for a sweeping in the mark probability factor of transmitter's PRBS. Carrier 1 and Carrier 3 have very similar estimated BER. For these carriers, a minimum log(BER) value is −10 and maximum value is −4. Carrier 2 (central carrier) only reaches a log(BER) of −5 and minimum value of −2. It can be noticed that up to 5 orders of magnitude can vary a carrier performance in terms of log(BER). Figures 3.9b, 3.9c, and 3.9d show the MP variation only for one carrier, keeping the other 2

Figure 3.10: BER vs Mark Probability (MP) for a carrier spacing of 32 GHz for QPSK in a) 1km and b) 10 km of an uncompensated-dispersion link.
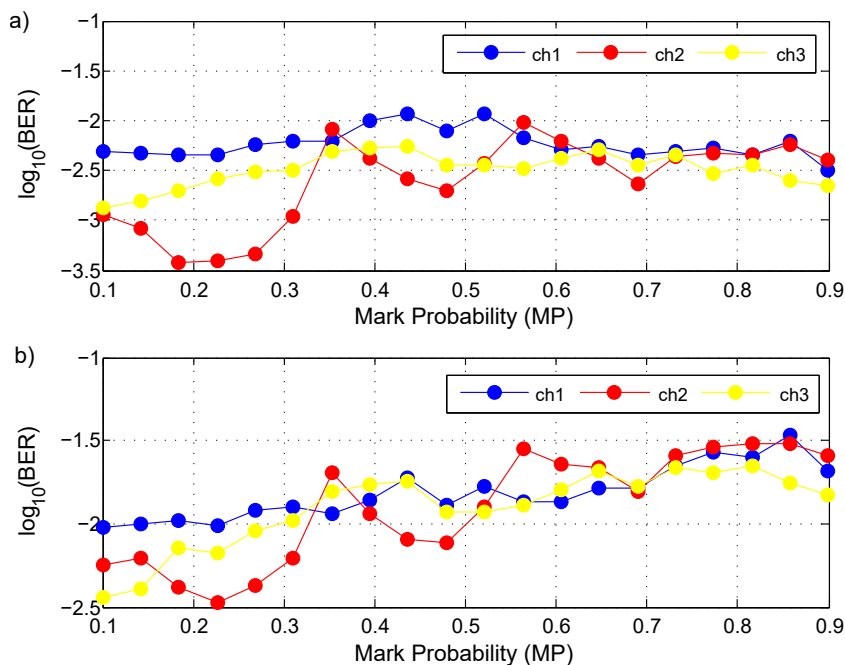
Figure 3.11: BER vs Mark Probability (MP) for a carrier spacing of 32 GHz for 16-QAM in a) 1km and b) 10 km of an uncompensated-dispersion link.
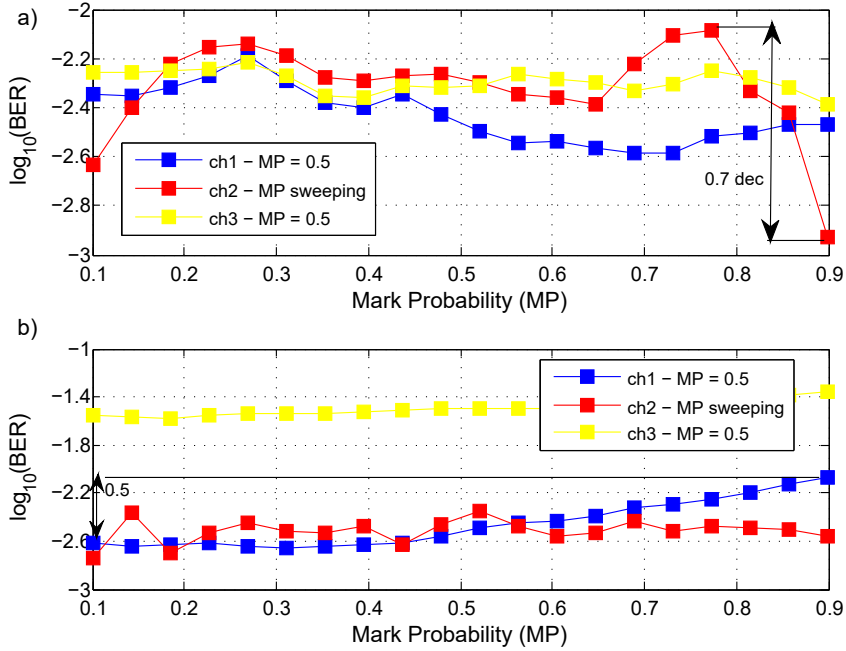
Figure 3.12: BER vs Mark Probability (MP) for a carrier spacing of 32 GHz in 10 km of an uncompensated-dispersion link for a) QPSK and b) 16-QAM.

carriers with a MP equal to 0.5. In figure 3.9b can be observed a log(BER) variation of 1 decade for Carrier 1 case, and how it disturbs the adjacent carrier (Carrier 2 in this case), varying the log(BER) close to 1 decade. Carrier 3 is not affected by the MP variation produced by Carrier 1. When MP of carrier 2 is varying, the BER of both adjacent channels is affected.

Figure 3.10 and figure 3.11 shows BER vs Mark probability curves for QSPK and 16-QAM modulations, respectively, for short transmission of uncompensated-dispersion links. Figure 3.10a is obtained in a transmission of 1 km. Maximum log(BER) value is -5 (ch_2) and minimum value for the same MP is -15 (ch_3). 10 orders of magnitude in BER is a huge difference for a system with fixed parameters. The 10 km case (figure 3.10b), difference among channels is always lower than 1 order of magnitude.

For 16-QAM case (figure 3.11), BER values are similar for 1 km (fig. 3.12a) and 10 km (fig. 3.11b). It means that MP in 16-QAM has penalty higher than the fiber length.

Figure 3.12 shows a particular case, where central channel changes the MP from 0.1 to 0.9, but, adjacent channels (ch_1 and ch_3) have a $MP = 0.5$. However, it is

MP ch1	MP ch2	MP ch3	Carrier Spacing	Distance	BER
0.5	0.5	0.5	30 GHz	B2B	Difference 2 OoM
0.5	0.2	0.5	30 GHz	B2B	Difference 3 OoM
0.4	0.4	0.4	32 GHz	1 km	Difference 4 OoM
0.4	0.4	0.4	32 GHz	10 km	Difference 0.5 OoM

Table 3.3: Summary of results presented in Section 3.5 for QPSK modulation. (OoM: Orders of Magnitude).

clearly noted that log(BER) changes for ch_1 and ch_3 having all parameters fixed in each estimated BER. For 16-QAM curve (figure 3.12b) a pattern is observed, when MP of ch_2 is increasing, log(BER) of ch_1 and ch_3 is incremented in 0.5 decades. Moreover, QPSK case, it does not occur the same pattern as 16-QAM. When MP of ch_2 is increasing, ch_1 and ch_2 have a variation in BER, with a value estimated of 0.3 decades. Maximum BER difference for ch_2 was lower than 1 order of magnitude (0.7) decades in QPSK case.

In table 3.3, some of the results presented in this section are summarized. The BER difference means the difference between the BER of the central channel and the worst BER of the adjacent channel.

3.6 ICI impact due to Linear and Nonlinear Fiber Optic's Effects

For the purpose of this section, in the simulation setup described in Chapter 2, the nonlinear impairments of the optical fiber were stimulated by means of an increasing of the launched power. In Figure 3.13, the BER is estimated as a function of the launch power. It can be noticed how for values higher than 5 dBm, the launched power increase the BER up to 2 orders of magnitude for a channel spacing of 17.6 GHz. For channel spacing of 16 GHz the BER increase up to 1 order of magnitude. For channel spacing of 15.5 GHz, the BER variation is low, due to overlapping penalty is already high (BER higher than 3×10^{-2}).

Figure 3.14 shows BER vs roll-off factor. The difference in terms of BER between linear effects and linear plus nonlinear effects is higher for roll-off values lower than 0.2.
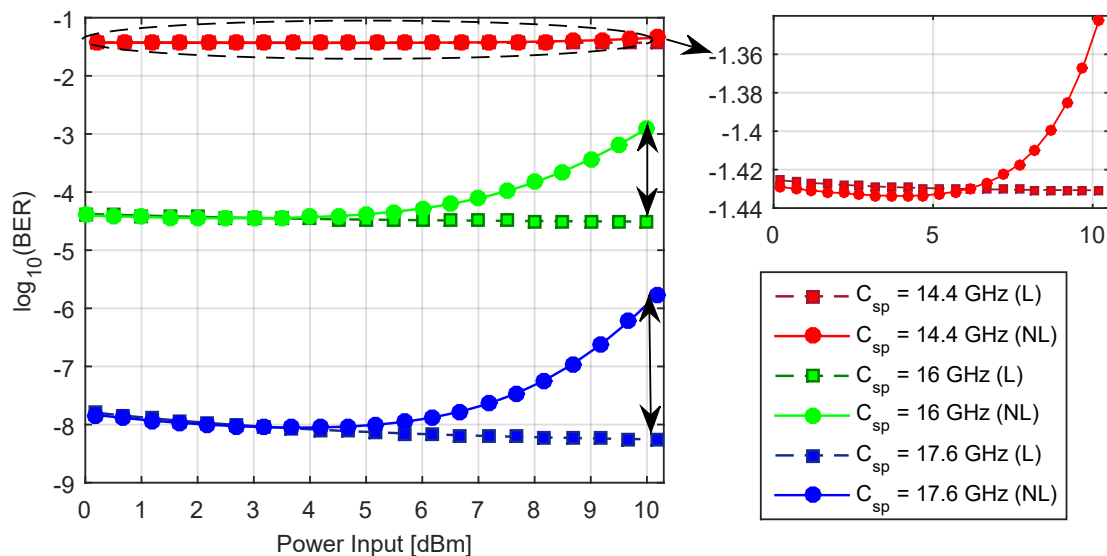
Figure 3.13: BER vs Launched power for different channel spacing in QPSK at 16 Gbaud over a fiber optic-link affected by only linear (L) effects and linear plus nonlinear (NL) effects.
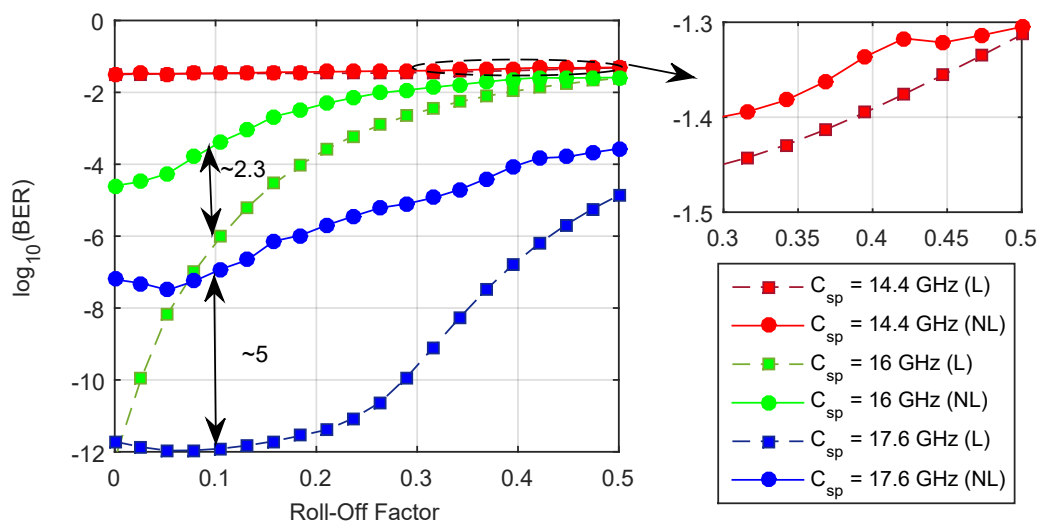
Figure 3.14: BER vs Roll-Off for different channel spacing in QPSK at 16 Gbaud over a fiber optic-link affected by only linear (L) effects and linear plus nonlinear (NL) effects.

Figure 3.15: BER vs Transmission distance for different channel spacing in QPSK at 16 Gbaud over a fiber optic-link affected by only linear (L) effects and linear plus nonlinear (NL) effects.

For a channel spacing of 17.6 GHz, nonlinear impairments have an impact of 6 order of magnitude taking a roll-off of 0.1. Whilst for a channel spacing of 16 GHz, the penalty in BER is close to 2 orders of magnitude. As in the previous case (see Figure 3.13), in Figure 3.14 the ICI impact for overlapped channels is high, showing a low difference in BER (0.1 orders of magnitude) between the lineal and nonlinear case.

Besides, in Figure 3.15 is shown that a BER difference of 3 orders of magnitude between a linear and nonlinear effects in 16 GHz of channel separation is kept from 20 km to 100 km of transmission distance.

In table 3.4, some of the results presented in this section are summarized.

3.7 ICI impact after nonlinear mitigation using Backpropagation Algorithm

3.7.1 Scenario QPSK at 16 Gbaud

The performance is evaluated in sub-Nyquist (15.5 GHz), Nyquist (16 GHz) and quasi-Nyquist (16.5 GHz) channel spacing. Figure 3.16 shows the BER vs launched power. The best performance in the system is obtained for launched powers of 8 dBm in

Carrier Spacing	Launch Power	Distance	BER
16 GHz	10 dBm	90 km	Difference 1.6 OoM
17.6 GHz	10 dBm	90 km	Difference 2.4 OoM
14.4 GHz	10 dBm	50 km	Difference 0.01 OoM
16 GHz	10 dBm	50 km	Difference 2.7 OoM

Table 3.4: Summary of results presented in Section 3.6 for QPSK modulation at 16 Gbaud. Comparison between a linear model and nonlinear model of optical fiber. (OoM: Orders of Magnitude).

all channel spacing under evaluation. Moreover, by using BP, a gain of 11 orders of magnitude is achieved in quasi-Nyquist channel spacing case as it is observed in the vertical double arrow in the plot. In Nyquist channel spacing cases (16 GHz), by using BP, gains up to 2 orders of magnitude are obtained, whereas in sub-Niquist spacing the gains are around 1 order of magnitude.

In figure 3.17, curves of BER vs transmission distance are shown. For sub-Nyquist and Nyquist cases, BP shows a similar improvement of 0.6 and 1 decades, respectively. In quasi-Nyquist case, BP shows a better performance, it can be noticed for a 210 km transmission length, where BP reduces the ICI impact in the BER of 3.5 orders of magnitude.

Figure 3.18 shows the BER vs Roll-off factor curves. Roll Off Factor has a high impact in the ICI effects measured in terms of BER due to the bandwidth broadening in the optical spectrum. For sub-Nyquist channel spacing BP reduces the BER in approximately 2.5 decades for a typical roll-off factor of 0.1. BP can compensate the ICI product due to an increment in the roll-off factor of up to 0.12 for sub-Nyquist and Nyquist cases. In quasi-Nyquist case BP can compensate the ICI due to a roll-off factor increment from 0.35 to 0.45 relaxing the computational complexity of the system.

Figure 3.19 shows the system performance for different values of Laser Linewidth according to a spectral channel Spacing of 15.5, 16.0 and 16.5 GHz. Laser Linewidth lower than 10^4 Hz do not show significant impact on the BER due to the stimulation of phase noise and chromatic dispersion are moderately low. Nevertheless, the linear plus nonlinear effect can be reduced in 4 orders of magnitude in terms of BER by means of the DBP.

Figure 3.16: BER vs Launch power for different channel spacing including nonlinear mitigation in QPSK at 16 Gbaud with (w.) and without (w/o) Backpropagation (BP).

Figure 3.17: BER vs Transmission Distance for different channel spacing including nonlinear mitigation in QPSK at 16 Gbaud with (w.) and without (w/o) Backpropagation (BP).

Figure 3.18: BER vs Roll-Off for different channel spacing including nonlinear mitigation in QPSK at 16 Gbaud with (w.) and without (w/o) Backpropagation (BP).

Figure 3.19: BER vs Laser's linewidth for different channel spacing including nonlinear mitigation in QPSK at 16 Gbaud with (w.) and without (w/o) Backpropagation (BP).

Figure 3.20: BER vs Channel spacing for different launch powers including nonlinear mitigation in QPSK at 16 Gbaud with (w.) and without (w/o) Backpropagation (BP).

Finally, Figure 3.20 shows the curves BER vs Channel Spacing for launch powers of 2, 8, and 14 dBm. The nonlinear ICI degrades the system performance when it is under a launched power higher than 8 dBm as it is observed in the circle marked red line, but when BP is used to compensate this phenomenon, system performance improves significantly, even in sub-Nyquist cases as it can be seen in the 8 dBm curve.

In table 3.5, some of the results presented in this subsection are summarized.

3.7.2 Scenario 16-QAM at 32 Gbaud

According to Figure 3.21, increasing the optical power per channel above 0 dBm has an high impact in the ICI effects measured in terms of BER due to fiber's nonlinearity. However, the digital mitigation of these effects improves the system performance even for Nyquist and sub-Nyquist channel spacing cases. Figure 3.22 shows BER vs span length.

Nevertheless, due to the low phase noise, laser linewidth does not have a significant impact between 0 and 1 MHz, values above this range totally limits the system performance. The mitigation of nonlinear fiber impairments reduce the ICI impact mainly for short distances of span length. For 33 GHz case, it is possible to reduce 1 order of magnitude, reducing the span length 45 km (from 120 km to 75 km). However,

Roll-Off	Carrier Spacing	Launched Power	Distance	BER
0.1	16 GHz	8 dBm	50 km	Difference 2.2 OoM
0.1	15.5 GHz	8 dBm	50 km	Difference 1.8 OoM
0.3	16 GHz	8 dBm	50 km	Difference 1 OoM
0.3	15.5 GHz	8 dBm	50 km	Difference 0.8 OoM
0.1	16 GHz	8 dBm	210 km	Difference 1 OoM
0.1	16.5 GHz	8 dBm	210 km	Difference 3 OoM

Table 3.5: Summary of results presented in Subsection 3.7.1 for QPSK modulation at 16 Gbaud. Comparison using or not using DBP for nonlinear mitigation. (OoM: Orders of Magnitude).
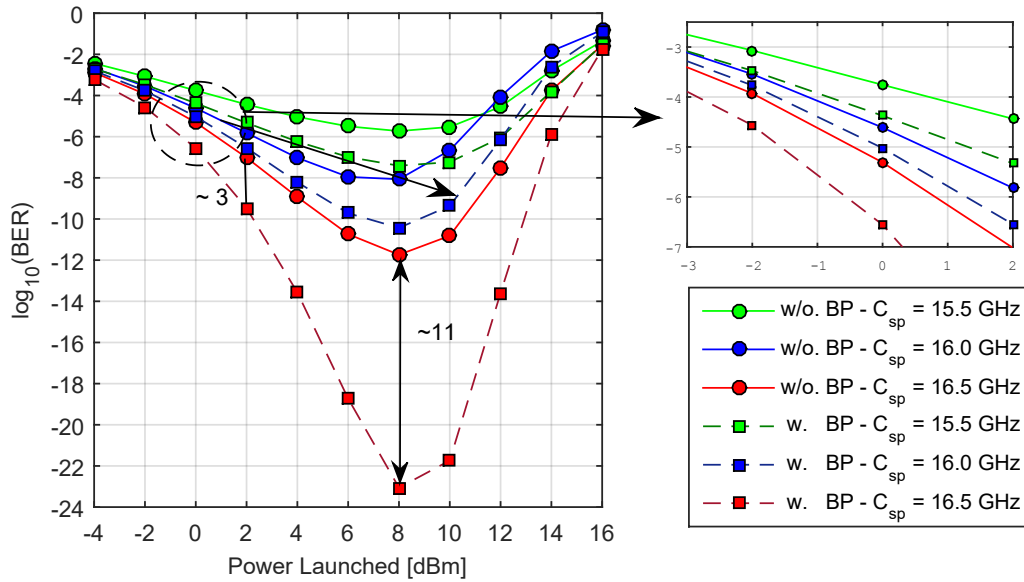

Figure 3.21: BER vs Launch power for different channel spacing including nonlinear mitigation in 16-QAM at 32 Gbaud with (w.) and without (w/o) Backpropagation (BP).
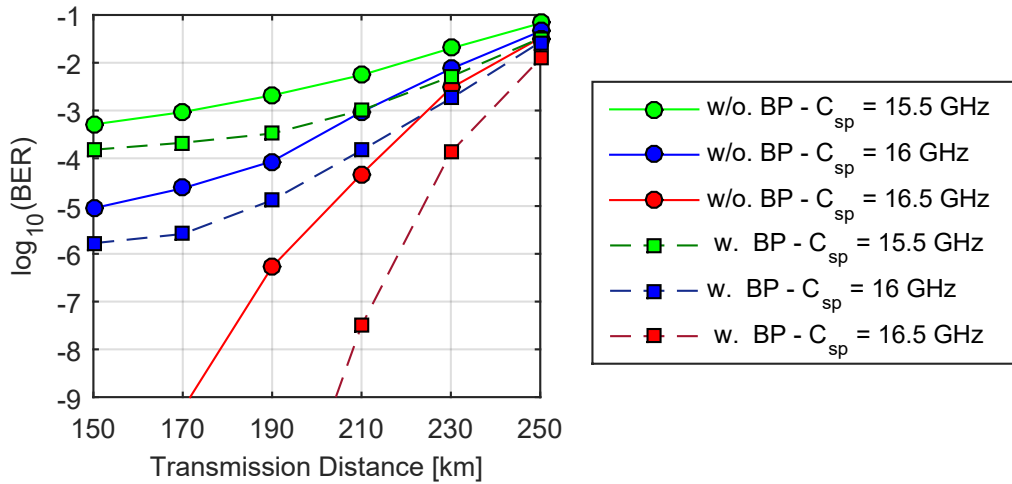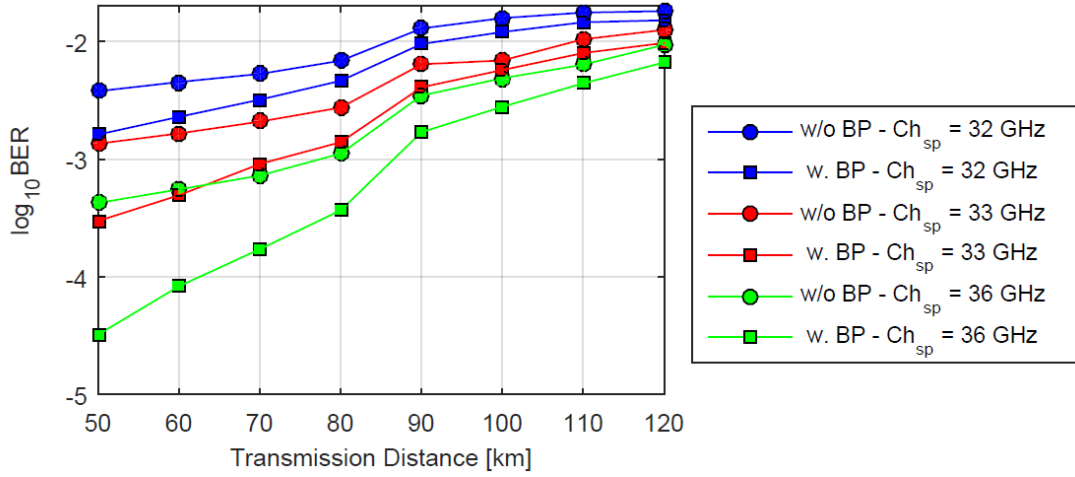
Figure 3.22: BER vs span lenght for different channel spacing including nonlinear mitigation in 16-QAM at 32 Gbaud with (w.) and without (w/o) Backpropagation (BP).
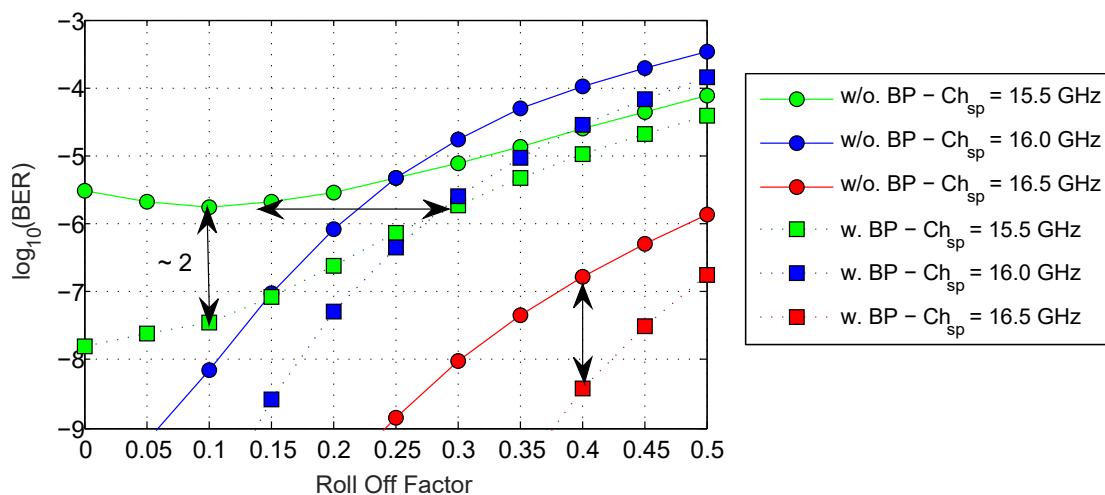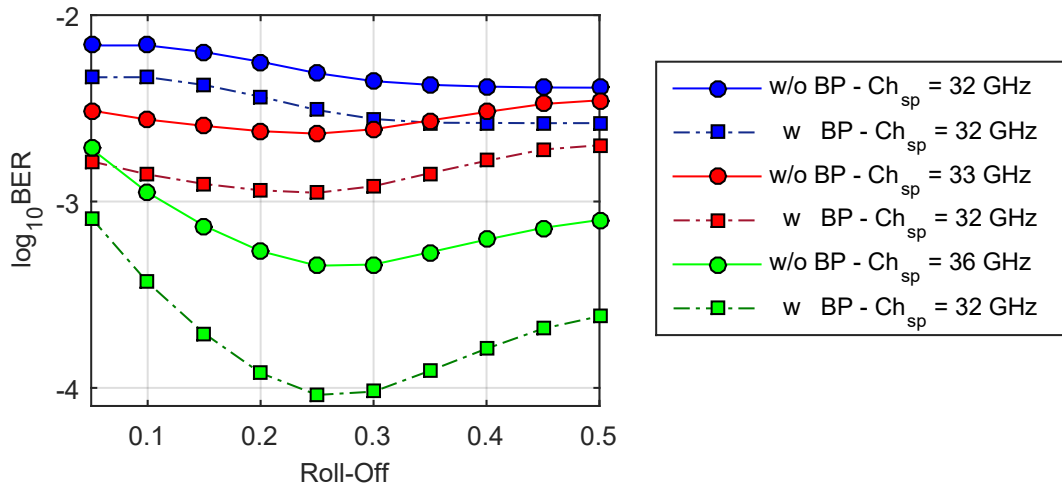

Figure 3.23: BER vs Roll-off for different channel spacing including nonlinear mitigation in 16-QAM at 32 Gbaud with (w.) and without (w/o) Backpropagation (BP).
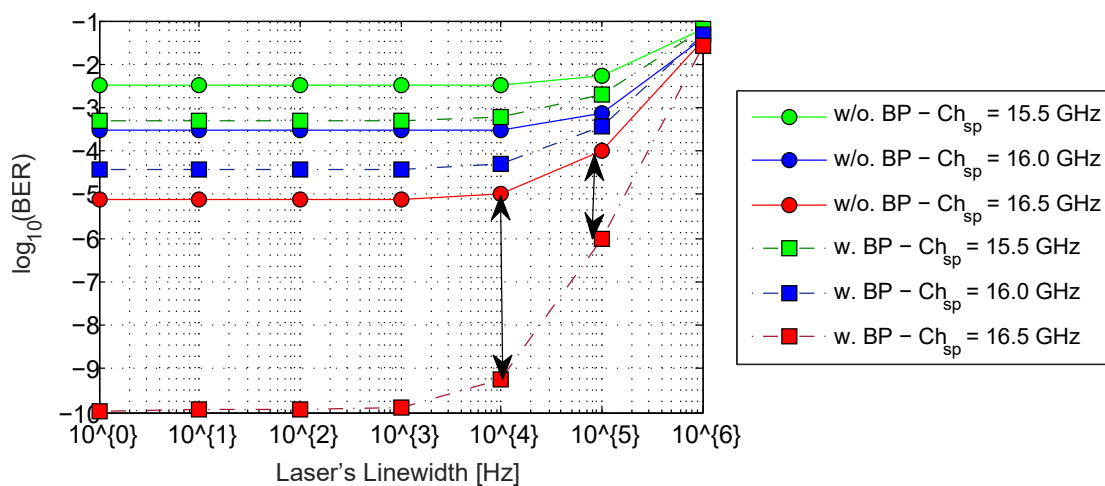
Figure 3.24: BER vs Laser's linewidth for different channel spacing including nonlinear mitigation in 16-QAM at 32 Gbaud with (w.) and without (w/o) Backpropagation (BP).
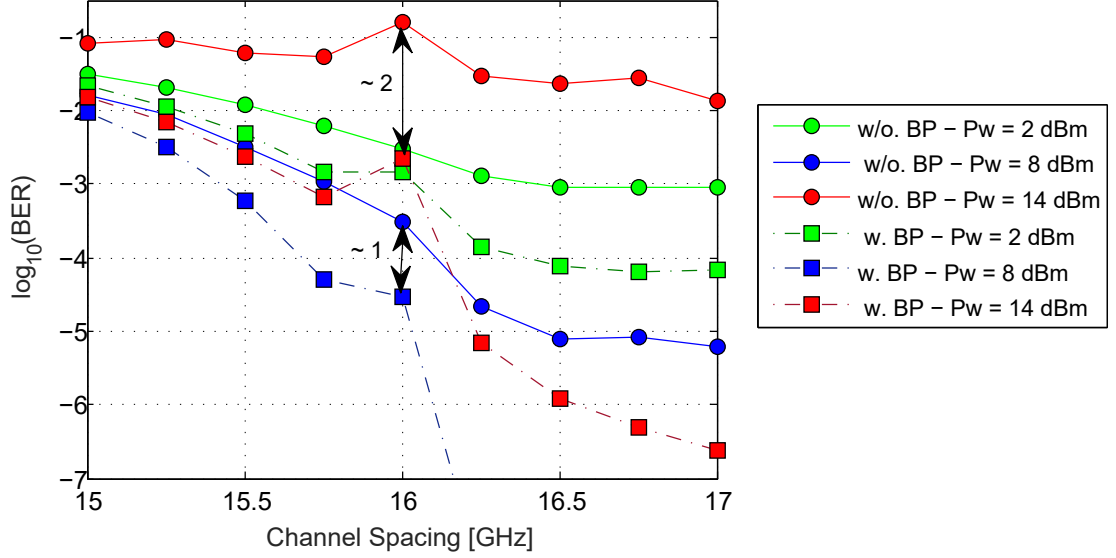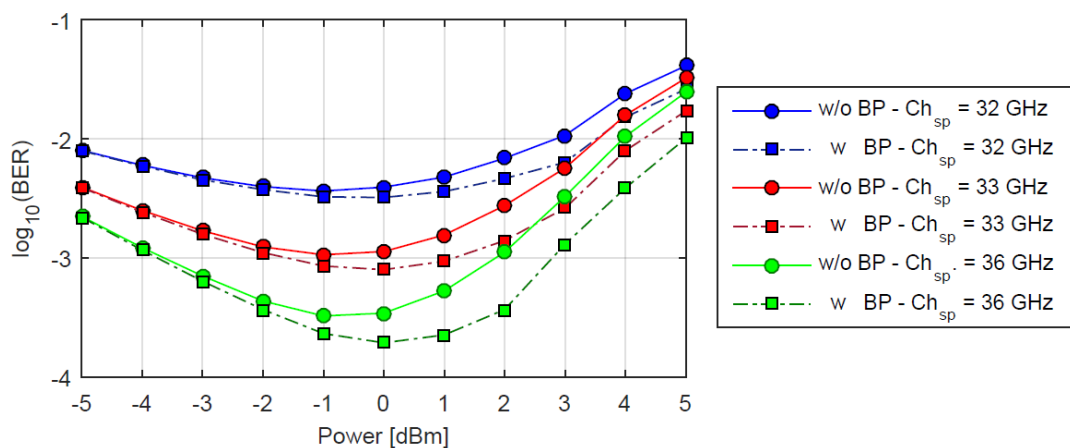

Figure 3.25: BER vs Channel spacing for different launch powers including nonlinear mitigation in 16-QAM at 32 Gbaud with (w.) and without (w/o) Backpropagation (BP).

ICI impact due to spectral overlapping significantly reduces the nonlinear mitigation performance because the noise floor is higher (BER values higher than 10^-3). Besides for 80 km and longer span length, the channel spacing reduction and nonlinear impairments mitigation do not have impact on system performance due to low OSNR received. Nevertheless, a channel spacing reduction from 80 km to 65 km implies a penalization of 15 km in span length, equivalent to a 18% of transmission distance.

Figure 3.23 shows BER vs roll-off factor curves. For channel spacing of 32 GHz (Nyquist) and 33 GHz (sub-Nyquist), variations in roll-off factor do not significantly modify the BER. However, for a channel spacing of 36 GHz, 1 order of magnitude of BER can be reduced with an increment of roll-off factor from 0.1 to 0.3. As Single-Pol QPSK case, laser linewidth values up to 1 MHz do not have a significant impact on the BER. The use of DBP can reduce the impact on BER, especially when channel spacing is increased as it can be seen for the curve of $Ch_{sp} = 36$ GHz.

Figure 3.25 show BER vs channel spacing curves for power per channel of 0.15 and 3 dBm. As can be seen in Figure 3.21, by using a channel power of 0 dBm is obtained the best performance in terms of BER. A channel spacing reduction of 0.5 GHz is possible assuming at a BER limit of 2.7×10^{-2}. A channel spacing reduction of 2.5 GHz increases the BER approximately in 1 order of magnitude when finer nonlinearity is mitigated, for 3 dBm of power per channel.

In table 3.6, some of the results presented in this subsection are summarized.

3.8   ICI as a function of OSNR in experimental setups

Figures 3.26 and 3.27 shows BER vs OSNR is for QPSK and 16-QAM, respectively. Both cases are B2B at 16 Gbaud with a roll-off of 0.1. In Figure 3.26 BER is estimated for five different channel spacing. With a channel bandwidth of 17.6 GHz, there are 2 cases of overlapped channels (14 GHz and 16 GHz). For OSNR values higher than 26 dB, a difference in BER of 4 orders of magnitude is evidenced between the channel spacings of 14 GHz and 16 GHz. Also, a difference in BER of 4 orders of magnitude is obtained (from 10^{-6} to 10^{-10}), between the channel spacings of 16 GHz and 17.6 GHz. for a BER of 1×10^{-6}, a difference in OSNR of 7 dB is noticed between the channel spacings, 16 GHz and 17.6 GHz. For a BER of 4.3×10^{-11}, a difference in OSNR of 10 dB is evidenced between the channel spacing of 17.6 GHz and 21.6 GHz. The impact

Roll-Off	Carrier Spacing	Launch Power	Span Length	BER
0.1	36 GHz	2 dBm	80 km	Difference 0.5 OoM
0.1	33 GHz	2 dBm	80 km	Difference 0.3 OoM
0.1	32 GHz	2 dBm	80 km	Difference 0.15 OoM
0.1	36 GHz	2 dBm	60 km	Difference 0.8 OoM
0.1	33 GHz	2 dBm	60 km	Difference 0.4 OoM
0.1	32 GHz	2 dBm	60 km	Difference 0.2 OoM
0.3	36 GHz	2 dBm	80 km	Difference 0.7 OoM
0.3	33 GHz	2 dBm	80 km	Difference 0.3 OoM
0.3	32 GHz	2 dBm	60 km	Difference 0.2 OoM

Table 3.6: Summary of results presented in Subsection 3.7.2 for 16QAM modulation at 32 Gbaud. Comparison using or not using DBP for nonlinear mitigation. (OoM: Orders of Magnitude).

in BER for a frequency channel separation between 21.6 GHz and 25.6 GHz, is lower than 1 order of magnitude for all OSNR cases evaluated.

In Figure 3.27 BER is estimated for seven different channel spacing, including single channel. With a channel bandwidth of 35.2 GHz, there are 5 cases of overlapped channels: 15, 15.5, 16, 16.5 and 17 GHz. For channel spacing lower than 15.5 GHz, a BER limit of 1×10^{-2} is not reached. Penalty of 3 dB is obtained when channel spacing is going down from 16.5 GHz to 16 GHz at a BER 1×10^{-2}. At a BER of 1×10^{-3}, the OSNR difference bewteen single channel case and 18 GHz case, is 1 dB. For OSNR values higher than 30 dB, a difference in BER of more than 3 orders of maginuted is seen between single channel and ideal Nyquist spacing (16 GHz).

In table 3.7, some of the results presented in this subsection are summarized.

3.9 Summary

In this chapter, the impact of the ICI effects in a $3 \times 16/32$ Gbaud Nyquist-WDM system is investigated. QPSK and 16-QAM modulation formats were alternated between the three optical carriers to study its contribution the ICI effects. ICI characterization in terms of BER was performed as a function of different system parameters variations such as: Roll-off factor, channel spacing, laser linewidth and transmission distance.
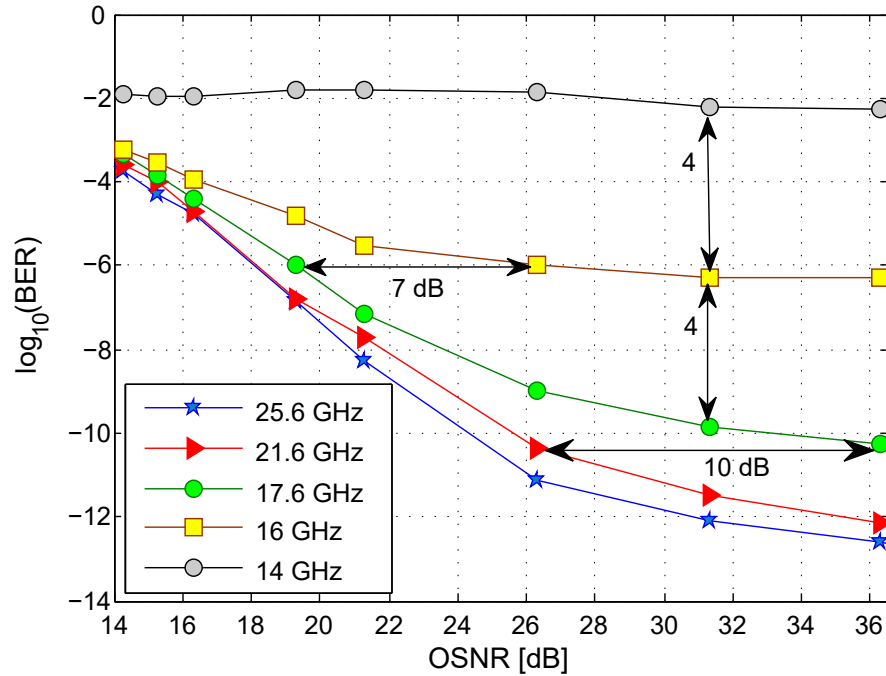
Figure 3.26: BER vs OSNR for different channel spacing at 16 Gbaud in QPSK B2B.
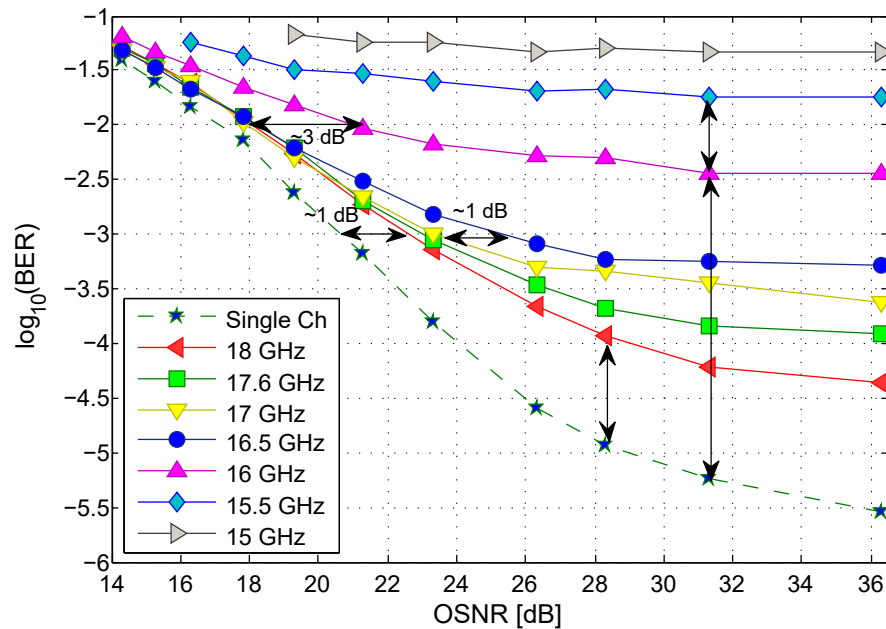
Figure 3.27: BER vs OSNR for different channel spacing at 16 Gbaud in 16-QAM B2B.

3. EVALUATION OF ICI EFFECTS

Mod. Format	Carrier Spacing	OSNR	BER
QPSK	16 GHz	20 dB	10^{-5}
QPSK	17.6 GHz	20 dB	10^{-6}
QPSK	16 GHz	26 dB	10^{-6}
QPSK	17.6 GHz	26 dB	10^{-9}
16QAM	16 GHz	20 dB	1.6×10^{-2}
16QAM	17.6 GHz	20 dB	4×10^{-3}
16QAM	16 GHz	26 dB	4.5×10^{-3}
16QAM	17.6 GHz	26 dB	3.5×10^{-4}

Table 3.7: Summary of experimental results presented in Subsection 3.8 at 16 Gbaud in B2B. (OoM: Orders of Magnitude).

Non-Nyquist spectral shaping of optical carriers presented an important penalty of 8 orders of magnitude (from 1×10^{-17} to 1×10^{-5}) in the BER as a function of the roll-off factor for variation from 0 to 0.1. At 32 Gbaud, according to the presented results, 35 GHz of channel spacing showed a good performance, decreasing the BER in 4 orders of magnitude (from 1×10^{-8} to 1×10^{-4}) compared with a channel separation of 32 GHz (Nyquist concept). In addition, impact of laser's linewidth in BER was close to 1 order of magnitude, from -1.4 to -2.2 in log-scale, for ideal linewidth of 0 MHz and 20 MHz, respectively, when channels are overlapped. Besides, transmission distance has a high impact due to uncompensated-dispersion channel. For 20 km, BER was higher than 10^{-1} for QPSK and 16-QAM even with channel spacing of 35 GHz. On the other hand, we identified a system sensitivity in terms of BER degradation to the mark probability of the PRBS. We observed that the BER difference among channels could reach up to 10 orders of magnitude for QPSK modulation, when the mark probability is not 0.5. For the 16-QAM case, a penalty is higher than in QPSK case, 2 orders of magnitude in BER for B2B cases. It represents a high penalty when the m-ary modulation is doubled. Even if the PRBS in practical implementation is close to 0.5, analysis in short time windows can realize that mark probability changes and it affects the system performance.

Moreover, the use of 8 dBm as the launched Power showed the best performance for sub-Nyquist cases for single-polarization QPSK transmission at 16 Gbaud. The use of DBP algorithm can relax the roll-off factor penalty up to 0.1 in Nyquist channel

spacing cases. Besides, for distances transmission lower than 210 km, BP reduces the BER in more than 3 orders of magnitude for a roll-off factor of 0.1. Finally, the ICI effect when channels are overlapped at low launched power (< 2 dBm) is higher than the ICI effect due to the nonlinear impairments of the optical fiber when channels are not overlapped. The use of DBP algorithm shows good performance for transmission distances up to 50 km per span in an amplified system at 32 Gbaud.

4

Encoded bit-Sequence Distribution among Optical Carriers

4.1 Introduction

Assuming a gridless scenario and the existence of receivers able to coherently detect and jointly process multiple optical carriers, in this chapter a two-steps method is proposed for the mitigation of the intercarrier interference (ICI) in optical multicarrier signal transmission. The method is based on linear equalization and a bit distribution of FEC-coded sequences along the set of optical carriers. This method allows bit error correction in scenarios of non-spectral flatness between the subcarriers composing the superchannel and sub-Nyquist carrier spacing. The concatenation of these two complementary techniques consists of a non-data aided (NDA) equalizer applied to each optical subcarrier, and a hard-decision FEC applied to the sequence of bits distributed along the optical subcarriers regardless prior sub-channel quality assessment as performed in OFDM modulations for the implementation of the bit-loading technique. The technique is validated by simulation in a 3×32 Gbaud single-polarization QPSK Nyquist-WDM system. In the following sections the method is described, including the results by using the NDA equalization as well as the addition of FEC-distributed module.

4.2   Method Description

In our approach, the superchannel is consider as a single entity regardless the number of carriers used. The Figure 5.1a is a layout of a superchannel system (at bit level) of three carriers using FEC coding with an overhead interleaved in time to avoid burst errors. Nevertheless, in multicarrier scenarios where some carriers may be affected more than the adjacent channels, it is possible to find several unrecovered errors. For example, in the figure 1.a, in the central bit-sequence (blue color) the two red frames show that more than the half of the overhead information is damage. Therefore, in our proposed scenario shown in Figure 5.1b, the overhead and the information are equidistributed among all channels (three in this example). Hence, burst errors due to ICI, can be minimized even if a channel has been predominantly more affected. Therefore, the bit-multiplexing acts as a serial to parallel convertor, allowing a frequency interleaving of the FEC overhead. On the other hand, at the receiver side, each optical carrier of the multicarrier signal is demodulated by a coherent receiver and passed through an equalization module to increase the SNR, allowing the improvement of the hard-decision FEC performance. The equalization module used per carrier is a non-data aided (NDA) which mitigates the linear ICI without previous knowledge of the channel statistics neither the adjacent carriers by using the rule of the Constant Modulus Algorithm (CMA) avoiding the use of training sequences. The linear equalization also avoids the use of soft-decision FEC, in spite of it ensures better performance and a bit throughput than hard-decision FEC, only it can be implemented when a high-speed ADC is used to perform sampling and quantization [76]. After equalization, a reverse operation of parallel to serial conversion is performed previous the HD-FEC decoding. All the steps carried out in the simulation process using our proposed method can be summarized as follows:

1. Bit information is coded using Reed-Solomon (RS) FEC based on hard decision. The entire bit-sequence with the overhead is segmented with a specific length. In the simulation setup was implemented the classic RS FEC (255, 239).

2. Coded sequences are distributed bit-to-bit using a bit-multiplexer for creating m sub-channels (serial to parallel conversion).
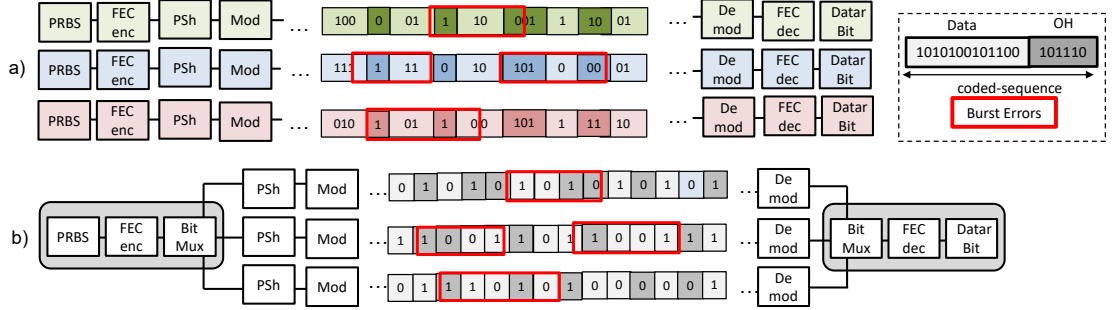
Figure 4.1: Layout of a three carrier superchannel system using FEC encoding : a) classic Nyquist-WDM and b) proposal of encoded sequences distribution. PSh, pulse shaping; Mod, modulation; Demod, demodulation;and OH, overhead.

3. The new m bit-sequences generated after bit-multiplexing are pulse-shaped with root-raised-cosine function.

4. Electrical pulses are mapped to drive an optical IQ modulator for phase modulation.

5. All channels modulated by independent optical carriers are coupled into the optical fiber and received by a multi-coherent optical receiver.

6. In the DSP, the NDA equalization is performed independently for each carrier

7. The signal is demodulated, obtaining one sequence per carrier in the reverse operation of parallel to serial conversion.

8. The m bit-sequences are multiplexed into a single bit sequences obtaining the transmitted sequence.

9. Bit-sequence is decoded, recovering the transmitted data.

The NDA equalization is performed in each carrier after the rectangular electrical filtering at the receiver (see figure 4.2). Due to the ICI can be modeled as a linear channel with time-varying ISI [42], [43],[44], CMA mitigates the linear ICI on a specific carrier, avoiding joint equalizations such as MIMO techniques for ICI mitigation.
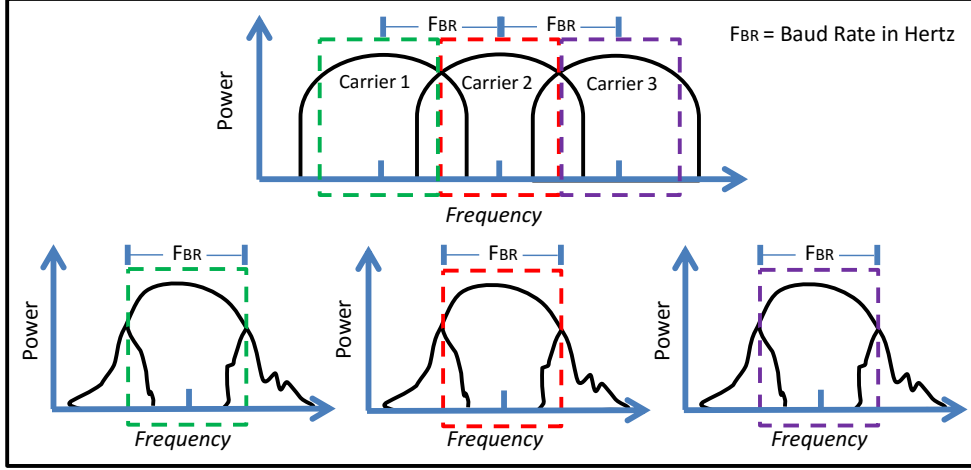
Figure 4.2: Spectrum of 3 channels a) in the transmitter and b) after filtering in the receiver.

4.3 Results and Discussions

4.3.1 Evaluation of the NDA Equalization Performance

Figure 4.3a shows the ICI impact in B2B scenario, with and without CMA equalization (dots and squares in plot, respectively). Mostly, the BER values decrease for all cases according to the increment of the frequency channel spacing. CMA equalization reduces the BER for all roll-off values. For $R_{off} = 0$, with a frequency channel spacing equal to 31.2 GHz, CMA reaches a BER reduction of 1 decade (black double arrow in the plot). In terms of frequency channel spacing, for a $R_{off} = 0$ compared with a $R_{off} = 0.3$, the penalty is 0.8 GHz for a log(BER) of -6 (gray double arrow in the plot) with CMA equalization.

Figure 4.3b shows the log(BER) vs transmission distance for channel spacing frequencies of 30, 31 and 32 GHz. With Nyquist ideal separation (32 GHz), the equalized-curve decreases the log(BER) value more than 1 decade up to 55 km (black double arrow in the plot). For longer distances, the difference in BER between equalized and no-equalized curves is lower than 1 decade, becoming in similar BER values for distances upper than 100 km. CMA improves data transmission even for sub-Nyquist separation (lower than 32 GHz), close to 1 decade (dashed ellipsoidal area in the plot) of the log(BER). The impact in channel spacing between 31 and 32 GHz is high in

terms of BER. It can be seen in a log(BER) a difference of 4 decades between the green curve and the blue curve for even both, equalized and no-equalized case.
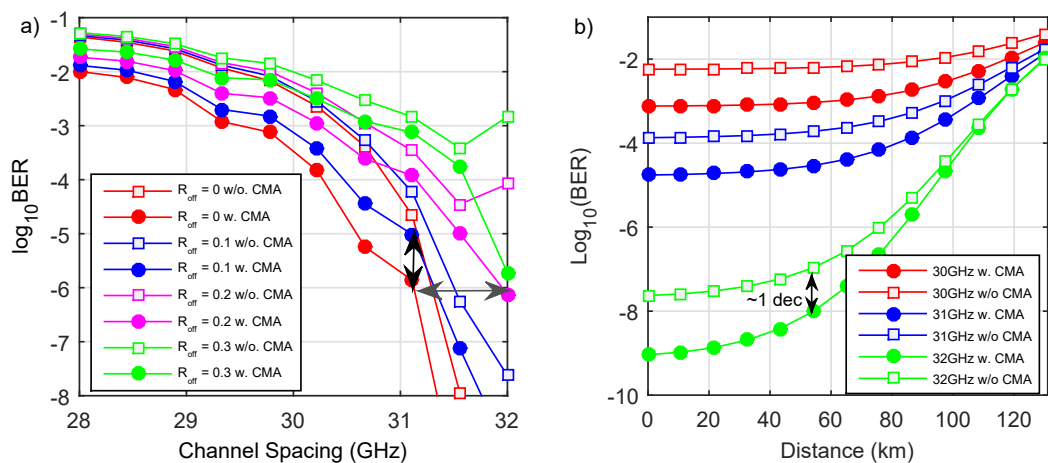
Figure 4.3: a) BER vs Channel spacing for B2B scenario, b) log(BER) vs Transmission Distance with (w) and without (w/o) CMA linear equalization.

In figure 4.4a and 4.4b are plotted dotted lines of BER references for a comprehensive comparison of the obtained results. In figure 4.4a an evaluation of the roll-off impact is performed for distance transmission up to 130 km with ideal Nyquist spacing. The roll-off has a high impact in the ICI effects measured in terms of BER due to the bandwidth broadening in the optical spectrum. The impact of the roll-off can be noticed in 100 km without CMA ICI mitigation (red line), when a BER of 10^{-7} for $R_{off} = 0$, and a BER greater than 10^{-3} for $R_{off} = 0.3$ are achieved. BER reduction by CMA is notorious according R_{off} increases.

Finally, signal demodulation after transmission over 130 km can reach a BER limit of 1.8×10^{-2} without CMA equalization. In the zoomed area of figure 4.4a, it can be seen that the transmission of 130 km with CMA (green dotted line) can present BER limit of 1.0×10^{-2} for roll-off values until 0.22. Moreover, with CMA a transmission of 120 km can reach a BER limit of 1.0×10^{-2} with $R_{off} = 0.3$.

In figure 4.4b, curves of Log(BER) vs frequency channel spacing are shown for different transmission distances. For channel spacing lower than 31.5 GHz, the difference in the BER is greater between the w-CMA and w/o-CMA curves; therefore it can be

affirmed that linear ICI effects are compensated for sub-Nyquist channel spacing using CMA equalization. CMA equalization reduces channel spacing penalty in 1.5 GHz for BER limit of 1.8×10^{-2}. Table 4.1 shows penalty reduction for all cases of figures 4.4a and 4.4b according to the three BER limits. The penalty reduction means the channel spacing value that the equalizer can reduce lower than the baud rate in Hz.
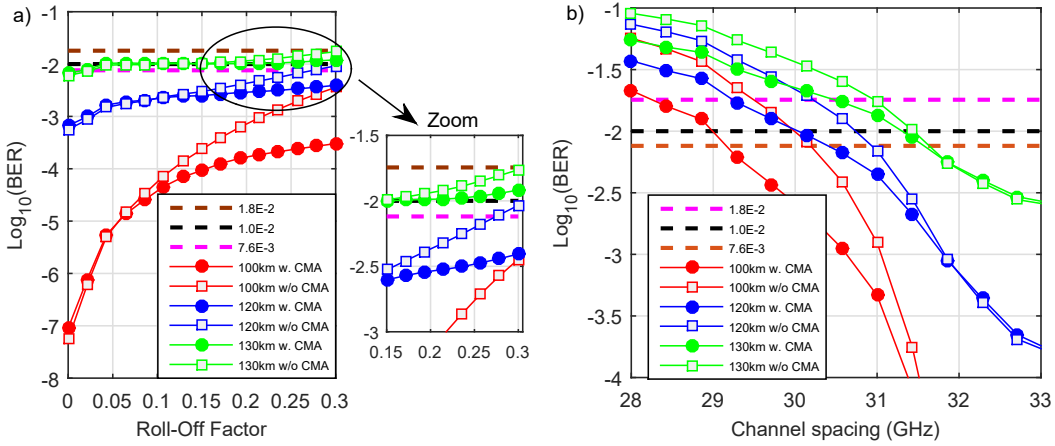
Figure 4.4: a) BER vs roll-off factor for transmission up to 130 km, b) BER vs Channel Spacing Penalty for different transmission distances with $R_{off} = 0$ with (w) and without (w/o) CMA linear equalization.

BER	100 km	120 km	130 km
1.8×10^{-2}	1.5 GHz	0.9 GHz	0.5 GHz
1.0×10^{-2}	1 GHz	0.8 GHz	0.3 GHz
7.6×10^{-2}	1 GHz	0.6 GHz	0.1 GHz

Table 4.1: Penalty reduction in terms of channel spacing using CMA.

4.3.2 Evaluation of the two-stages Method

In the following results, the BER is estimated making a comparison bit-to-bit with a PRBS sequence length of $3 \times (2^{17-1})$. This section shows the BER vs. frequency carrier spacing (Figure 4.5) and the BER vs. roll-off Factor (Figure 4.6) for three transmission cases: *i)* without FEC, *ii)* with FEC and *iii)* with FEC plus CMA equalization.

For a roll-off factor of 0.1 (see figure 4.5a), FEC-distributed can reach a $log_{10}(BER)$ of -4.5 with a carrier spacing of 30 GHz whereas without bit correction reaches a
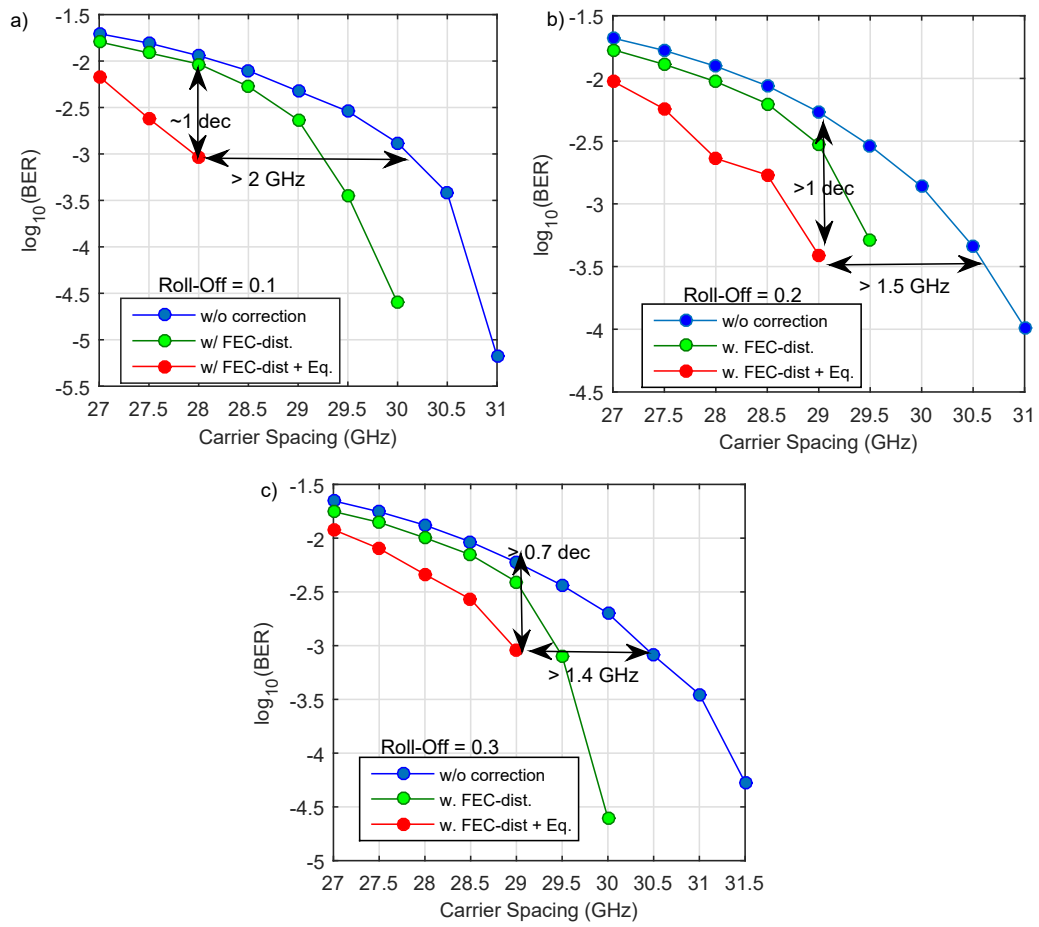
Figure 4.5: BER vs Carrier Spacing for a roll-off of a) 0.1, b) 0.2 and c) 0.3 without (w/o) error correction (blue line), with (w/) FEC-distributed (red line) and with FEC-distributed plus CMA equalization (Eq.).

4. ENCODED BIT-SEQUENCE DISTRIBUTION AMONG OPTICAL CARRIERS
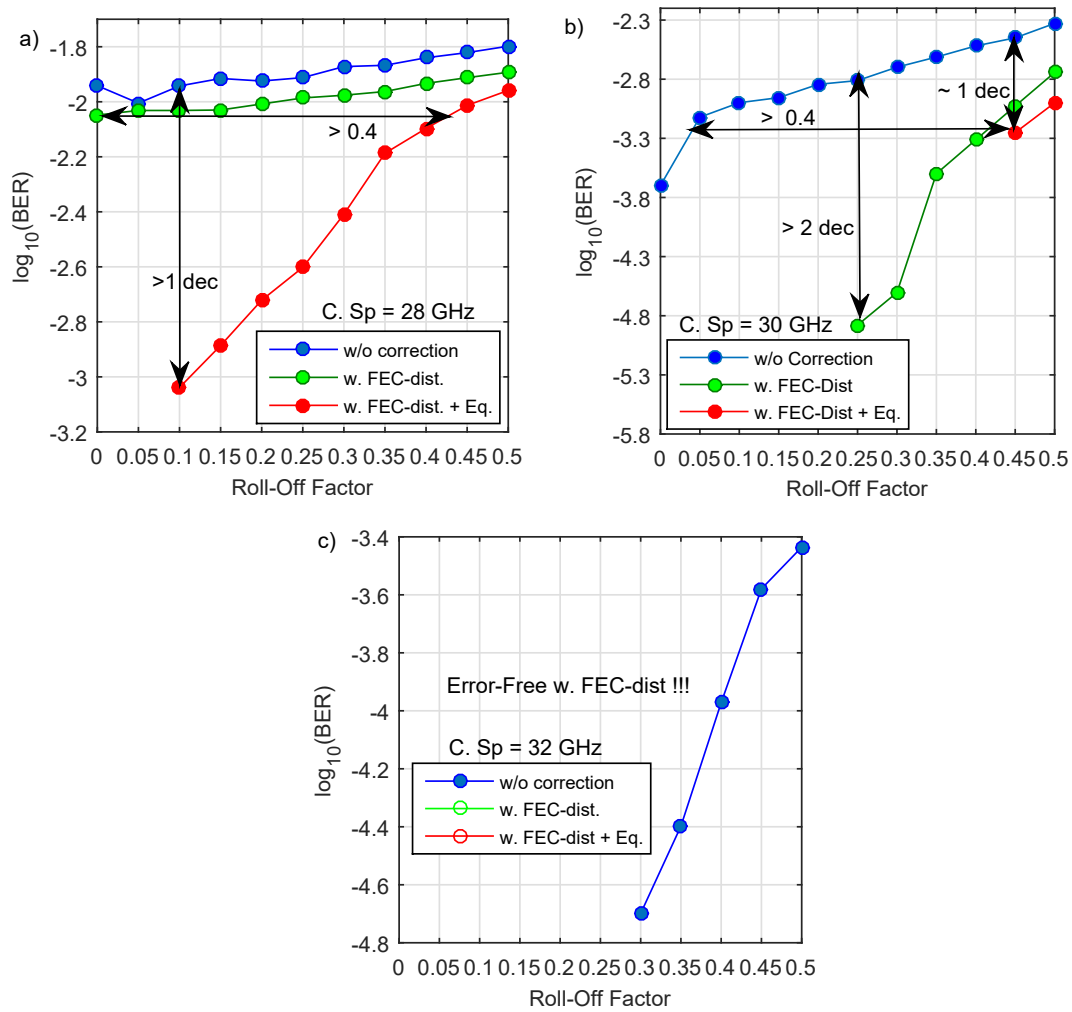
Figure 4.6: BER vs Roll-Off for Carrier Spacing of a) 28 GHz b) 30 GHz and c) 32 GHz without (w/o) error correction (blue line), with (w/) FEC-distributed (red line) and with FEC-distributed plus CMA equalization (Eq.).

BER of 10^{-3}. Adding a CMA equalization module, it can be reached an error-free transmission with a sub-Nyquist carrier spacing of 28.5 GHz, a better performance of 2 GHz compared without equalization module. When roll-off factor increases up, the gain in terms of carrier spacing is reduced. For example, for a roll-off factor of 0.2 and 0.3 (figure 4.5b and 4.5c), the error-free decoding is reached for a carrier spacing of 29.5 GHz.

In figure 4.6a is shown how the narrow spacing of 28 GHz affects the BER even with low roll-off factor, and FEC technique cannot recover the information without the CMA support. For a carrier spacing of 30 GHz in Figure 4.6b is obtained a BER of 10^{-3} for a roll-off Factor of 0.1, 0.45 and 0.5, without FEC, with FEC and with FEC-CMA, respectively. For a Nyquist ideal spacing (32 GHz), error-free is obtained with FEC even without CMA equalization. Figure 4.6c shows the curve without FEC for values of roll-off of 0.3 and 0.5, the estimated BER is -4.7 and -3.5 in log-scale, respectively.

The proposed method was also tested in Rsoft software. The simulation setup was the model of the experimental setup 2, provided by the Georgia Electronic Design Center, which includes all nonlinear models of the whole set of devices. Results are shown in Figure 4.7.

The BER was estimated as a function of the carrier spacing. Figure 4.7a is a B2B case. In this figure is noted that at least in 0.5 GHz of carrier spacing is reduced the penalty by using the two-step method in comparison with only the NDA equalizer. Penalty in OSNR is much higher than the results presented previously in this chapter. It is due to the simulation is more robust in terms of approximation of the experimental setup. Nevertheless, in 34 GHz by means of the proposed method, error-free demodulation is obtained.

On the other hand, Figure 4.7b shows the results obtained for a transmission of 90 km. In this case, a gain of 1 GHz in terms of carrier spacing is obtained when the FEC distribution is performed. Also, error-free transmission is obtained at 34 GHz. It shows that our proposal reduce the ICI impact for a central channel with at least 1.2 GHz of overlapping among both adjacent channels.
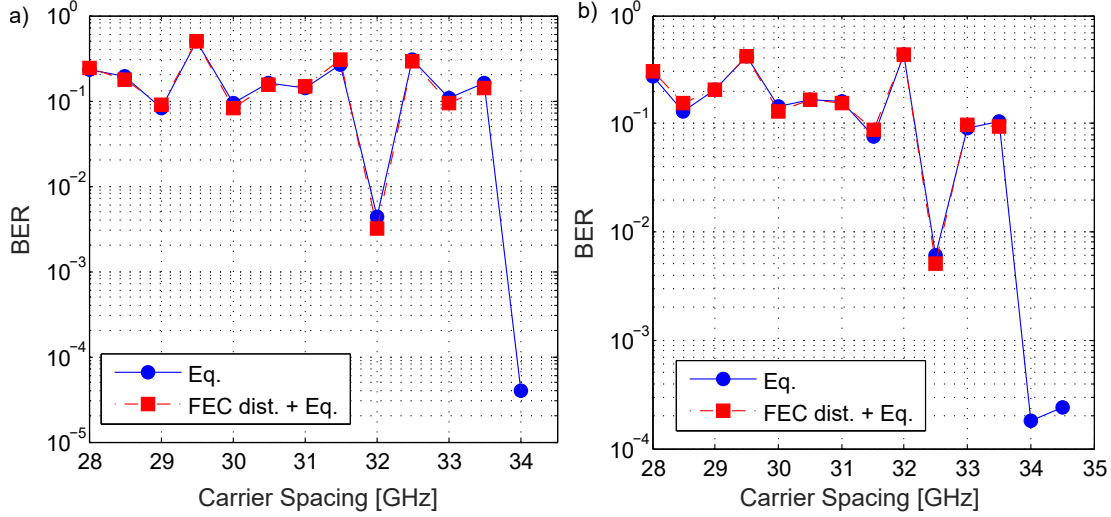
Figure 4.7: BER vs Carrier spacing in a Nyquist-WDM system with only equalization (Eq.) and adding the FEC-distributed technique (FEC-dist + Eq.).

4.4   Summary

The main contribution of our proposed two-steps approach for ICI mitigation can be summarized as follows *i)* the use of non-data aided (NDA) linear equalization based on the constant-modulus-algorithm (CMA) for first step ICI mitigation improves the optical signal to noise ratio per carrier and therefore minimizes the error floor of subsequently implemented error correcting codes, *ii)* carrier independent NDA linear equalization at the physical level for Nyquist pulse shaped signals avoids complex joint multi-carrier processing *iii)*, the implementation of classic hard-decision FEC techniques such as Reed-Solomon code to perform the second ICI mitigation step allows equalization at the bit-data level enabling the application of mature error correcting schemes and *iv)* the modular structure of the proposed two-steps mitigation approach permits system scalability to incorporate advanced linear equalization techniques and error correcting codes. The benefits of the method were evaluated in terms of BER as a function of the carrier frequency spacing and the roll-off factor of the digital pulse-shaping filter in the simulated 3×32 Gbaud single-polarization QPSK Nyquist-WDM system. After the ICI mitigation in a back-to-back scenario, error-free decoding was obtained for a PRBS sequence length of $3 \times (2^{17-1})$ with sub-Nyquist carrier spacing of 28.5 GHz and 30 GHz, for roll-off values of 0.1 and 0.4, respectively.

5

Nonsymmetrical Demodulation enabling ICI Mitigation

5.1 Introduction

In contradistinction of the method presented in Chapter 4, in this Chapter, a nonsymmetrical demodulation (NSD) technique is proposed which enable the minimization of ICI effects. Besides, the NSD technique does not requires a prior information of the optical fiber (as in backpropagation techniques), neither feedback nor information of adjacent channels. Our proposal is an adaptive machine learning-based NSD technique relying on clustering to mitigate time-varying distortions derived from several impairments such as IQ imbalance, bias drift, phase noise, ICI, among others. In this demodulation technique, the k-means algorithm iteratively identifies the cluster centroids in the constellation of the received symbols in short time windows by means of the optimization of decision thresholds for a minimum BER. The effectiveness of both techniques is experimentally verified in a $3 \times 16/32$ Gbaud 16-QAM Nyquist-WDM system over 250 km and 270 km links.

5.2 Method Description based on k-means

In order to improve the BER attainable in the presence of distorted symbols, we replace the conventional (linear and symmetric) demodulation boundaries with nonsymmetrical demodulation (NSD). In the drawing of Figure 5.1a we illustrate a possible worst case of a constellation affected by several impairments, including IQ imbalance and phase

5. NONSYMMETRICAL DEMODULATION ENABLING ICI MITIGATION
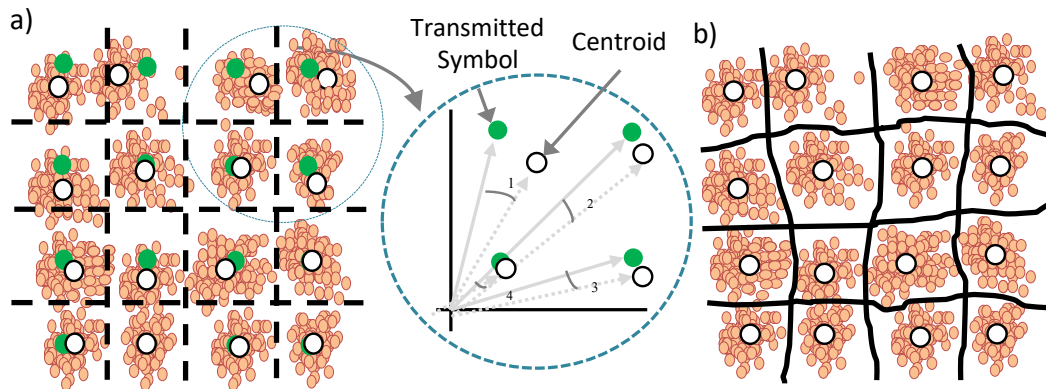
Figure 5.1: Example of a distorted 16QAM constellation diagram. a) Comparison of the transmitted symbols with estimated centroids. b) Thresholds for nonsymmetrical demodulation.
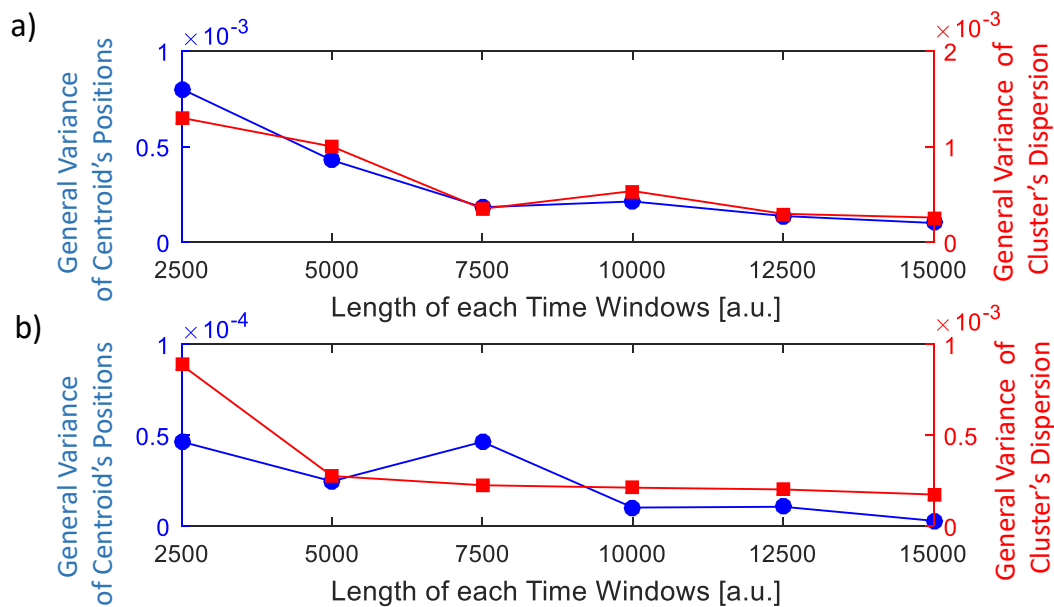
Figure 5.2: General variance of centroids and general variance of cluster's dispersion for a) single channel and b) WDM affected by ICI at 16 Gbaud estimated in 10 TWs of different length in terms of symbol. Centroids: blue dot markers). Cluster's dispersion (red square markers).

Figure 5.3: a) Cluster of received symbols at two sequential time windows, and b) its centroid variation (blue dot markers) and its variance (brown square markers) for 10 time windows. (TW=N circle markers and TW=N+1 square markers).
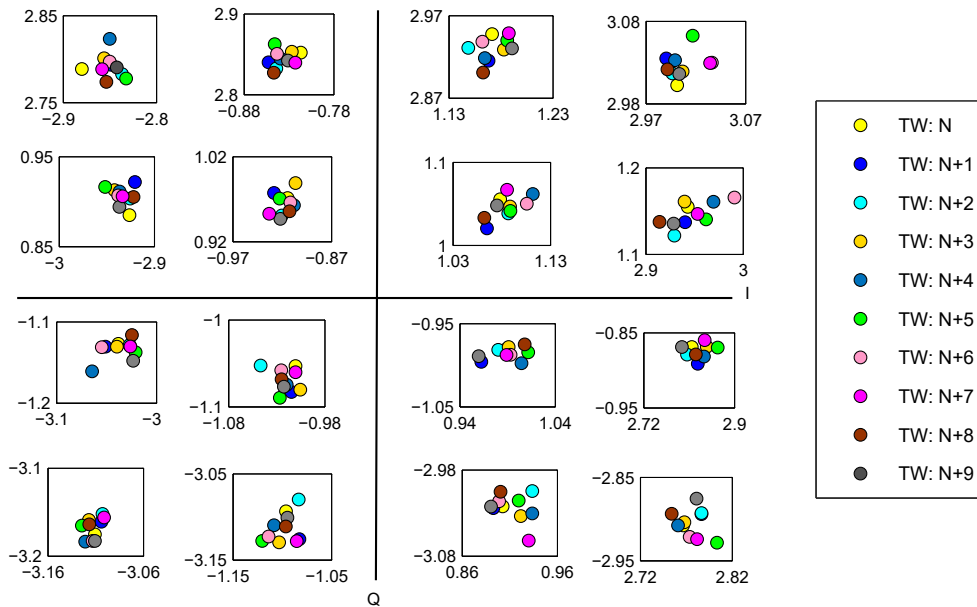
Figure 5.4: Received symbols zoomed in two random clusters of a 16-QAM constellation at 16 Gbaud with a channel spacing of 16 GHz.

71
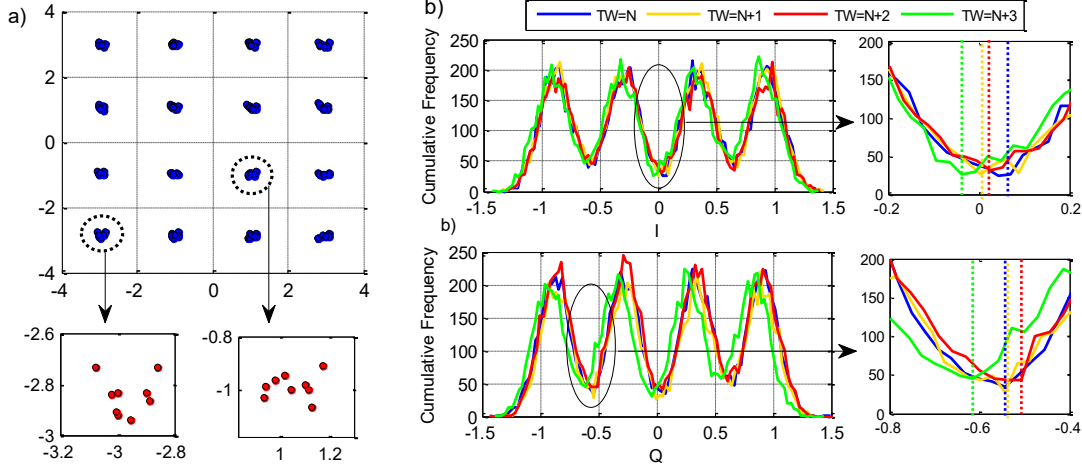
Figure 5.5: Qualitative analysis of the deviation of symbols locations in a 16QAM transmission at 32 Gbaud , represented as: a) Centroids estimated in different TWs of 10k symbols, and b) Histograms calculated from one symbol of the constellation diagram.

noise. Our technique combines short temporal windowing with the k-means clustering algorithm for dynamic estimation of the nonsymmetrical thresholds, as seen in Figure 5.1b. The short temporal windows (TW) that we employ are indexed, where the Nth frame is TW=N. The nonsymmetrical thresholds were computed independently for each symbol frame, because it was observed that the centroid distortions varied from frame to frame and were typically not correlated. The choice of the length of the TW is a balance between computational complexity (keep it short) and stability (centroid moves too much at very short TWs, keep it longer). After 10k symbols, the centroid stability is good (variance is low), as we show as follows:

Variance of centroid's position and variance of cluster's dispersion was calculated in 10 consecutive TWs. This calculus was done in two steps: In the first one, the variance of centroid's positions and cluster's dispersions were calculated in each TW. In the second one, general variances of centroids and clusters were calculated based on the 10 TWs variances obtained in the first step. In Figure 5.2 we show the general variance of centroid's positions (blue circle markers) and the general variance of cluster's dispersion (red square markers). The Figure 5.2a is for single channel case, and Figure 5.2b is for WDM when three channels are overlapped. It can be noticed how for TWs lower than 7500 symbols for single channel and 10000 symbols for multichannel, the variance curves are not stable. With the intention of using the shortest TWs possible without

incurring in convergence errors, 10k symbols was chosen as length of each TWs in our analysis. For clarification, the period of each TW depends on the baud rate, in this work, 16 Gbaud or 32 Gbaud.

In Figure 5.3a, received symbols of a 16-QAM constellation are shown for one specific cluster (ideally centered in -1+j) in 2 different TWs. Figure 5.3b shows how the cluster's centroid (circle markers) and the cluster's variance (square markers) changes with time. The detail of the centroid motion is depicted in Figure 5.4 for 10 different sequential TWs. The figure zooms in on each centroid of the 16-QAM constellation with each box representing 6.6% of the standard decision boundary.

In Figure 5.5a, centroids of a constellation affected by interchannel interference are plotted for 10 TWs. A deviation from the ideal constellation can be noticed in each TW. In Figure 5.5b, two histograms of a specific cluster (I and Q components) of a 32 Gbaud transmission are shown. The cumulative frequencies (y axis), represent the number of symbols in such region. A shift in the thresholds can be seen in the histograms' valley zone for different TWs.

The k-means algorithm involves multiple iterations of clustering. In each iteration each received symbol is assigned to the cluster whose centroid is closest. The reference constellation points are used as the initial locations for the centroids in the first iteration. The repeated clustering iterations are carried out until the algorithm converges, which occurs when the centroids do not change their spatial locations and therefore no data-symbols are reassigned. The re-initialization between time windows adds computational complexity in comparison with classic k-means (only initialized once), but it is added only to track the time-varying distortions avoiding the use of past time windows in the decision of new centroids. However, the mode value is around 4 iterations per time window for convergence, being a small value due to the time-varying effects are not large, seen in a Euclidean scale. It means that the computational complexity of this algorithm is low thanks to the number of clusters and the dimension is fixed.

5.3 Results and Discussions

5.3.1 Performance Evaluation in Scenario A

Figure 5.6 shows BER performance vs. OSNR for a 16 GBd B2B link. This link incorporated a source laser with linewidth $100kHz$ and no automatic bias control on

the modulator. It is noticed that even without optical fiber transmission and modest baud rate, a gain of nearly 0.2 dB can be achieved for single channel operation at a BER of 1×10^{-2}. For multicarrier links, Figure 5.7 shows different carrier spacing cases. The gain increases up to 0.56 dB when the spectral channel separation is 18 GHz (see Figure 5.7a), and 0.43 dB for a channel spacing of 17.6 GHz (see Figure 5.7b). From Figures 5.7c to 5.7f, multicarrier scenarios for channels overlapped are shown. For channel spacing of 17, a gain up to 1.4 dB is obtained at a BER of 1×10^{-2} for a channel spacing of 16 GHz. It shows the ability of the NSD to minimize the interchannel interference effects due to overlapping. For transmission of 250 km and a received signal with OSNR > 30 dB. Figure 5.8 shows the improvement in BER using NSD for 3 different carrier spacing compared to the single channel case, enabling near Nyquist channel spacing with single channel performance.
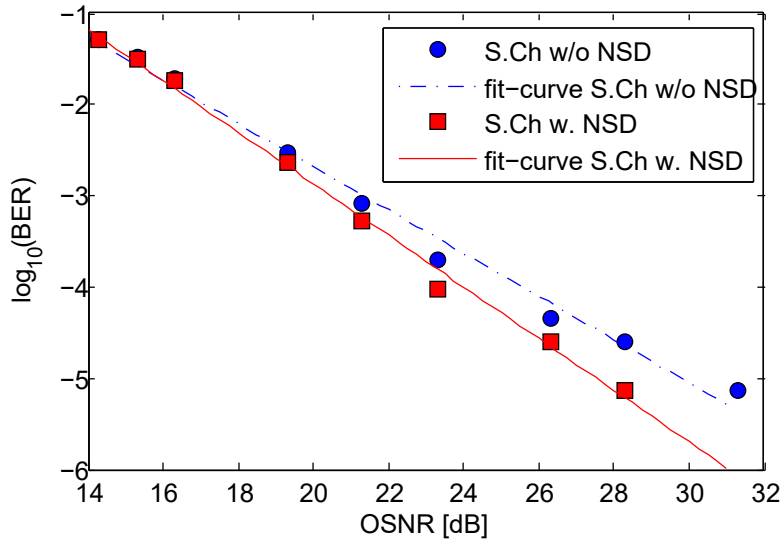
Figure 5.6: BER vs OSNR for single channel at 16 Gbaud in B2B with (w.) and (w/o) NSD.

5.3.2 Performance Evaluation in Scenario B

The BER is calculated by error counting in 600000 bits (15 TWs of 10k symbols each one). Figure 5.9a shows two B2B cases. The single channel case presents a gain of 0.4 dB, and the multichannel case (carrier spacing of 34 GHz) shows 0.2 dB benefit at BER of 1×10^{-2}. Figure 5.9b and 5.9c show the BER vs OSNR performance at 32 Gbaud
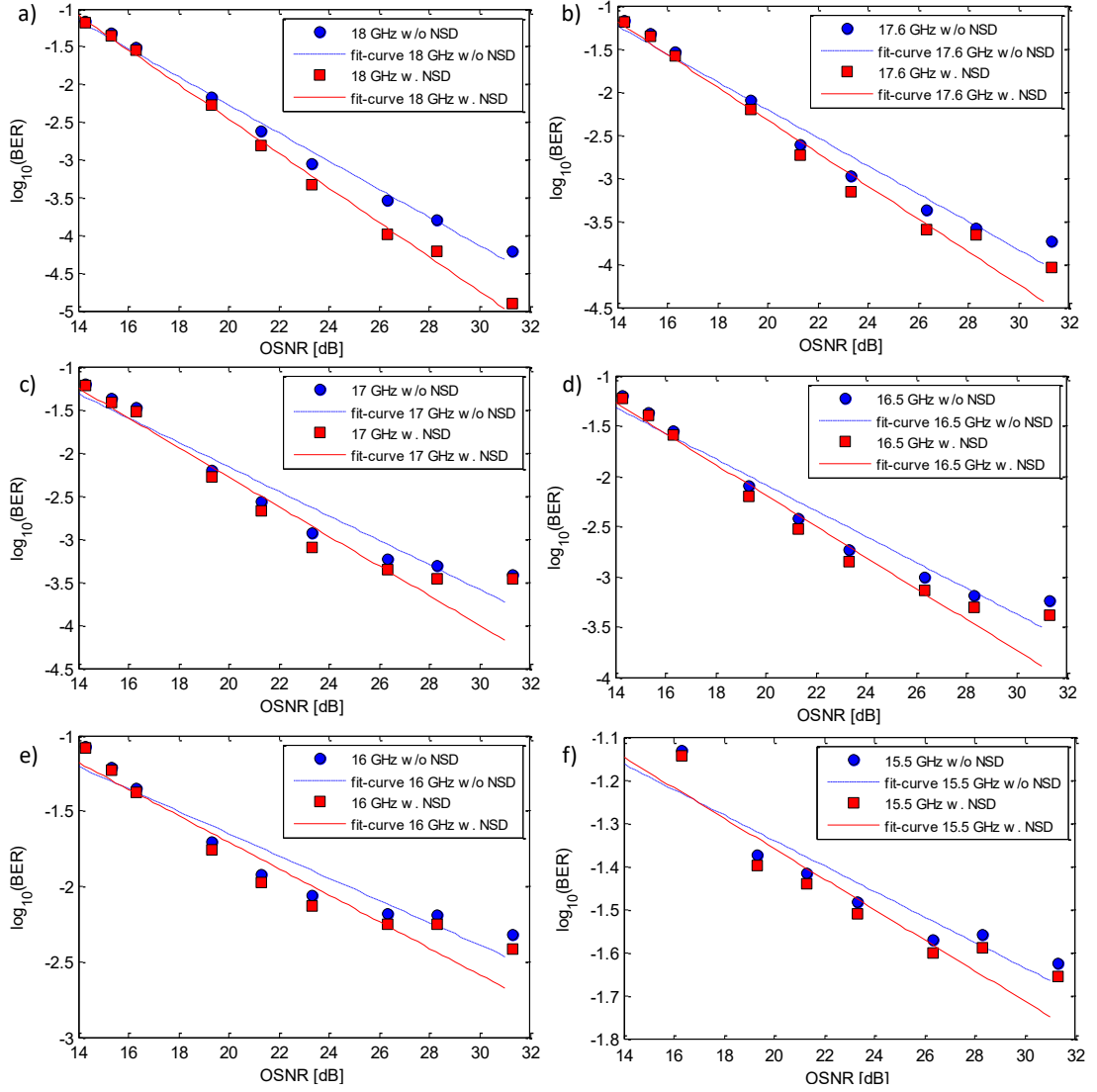
Figure 5.7: BER vs OSNR for different carrier spacings at 16 Gbaud in B2B a) 18 GHz, b) 17.6 GHz, c) 17 GHz, d) 16.5 GHz, e) 16 GHz and f) 15.5 GHz with (w.) and (w/o) NSD.

5. NONSYMMETRICAL DEMODULATION ENABLING ICI MITIGATION
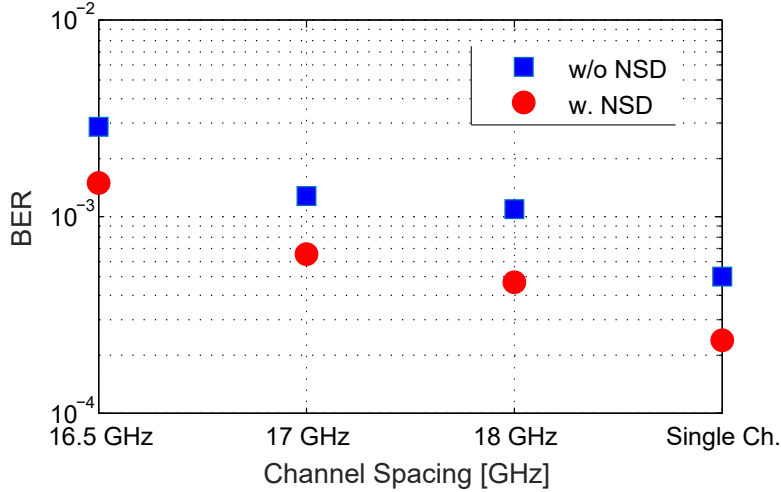
Figure 5.8: BER vs OSNR at 16 Gbaud over 250 km of optical fiber with an OSNR ¿ 30 dB with (w.) and (w/o) NSD.

for 90 km transmission for 2 different launch powers: 0 and 9 dBm. In Figure 5.9b, a single channel case using narrow linewidth laser (< 25 KHz) was used. Nonetheless an improvement of 1 dB is achieved for a BER of 1×10^{-3} for both launch powers. For a BER 1×10^{-2}, the gain is lower but still useful, 0.3 dB. We note that 9 dBm launch power exhibits a penalty of up 2 dB due to nonlinear effects. Similar improvements are observed in Figure 5.9c for the same launch powers (0 and 9 dBm) in a transmission of three overlapped channels (carrier spacing of 34 GHz).

Figures 5.10 and 5.11 show BER performance vs OSNR for multichannel transmission over 270 km with a launch power of 9 dBm, for twelve different frequency carrier spacings. Figure 5.10a shows a WDM standard transmission (carrier separation of 50 GHz), a gain of 0.35 dB and 1 dB by using NSD is observed at 1×10^{-2} and 1×10^{-3}, respectively. For a carrier spacing of 37.5 GHz, the gain is 0.28 dB at 1×10^{-2} and 0.6 dB at 2×10^{-3}. Figure 5.10c shows, a near Nyquist spacing case of 36 GHz, the improvement in BER using NSD is 0.28 dB. For overlapped channels, nine cases are presented. At BER limit of 1×10^{-2}, the gains are between 0.27 dB and 0.5 dB using NSD for a carrier spacing between 33 GHz and 35 GHz (see also Figure 5.11). It is noticed that even with a reduced carrier spacing (< 32 GHz), a gain of nearly 0.6 dB can be achieved at a BER higher than of 10^{-2}. However, due to the ICI, a BER of 1×10^{-2} is not achieved with OSNR values lower than 31 dB.
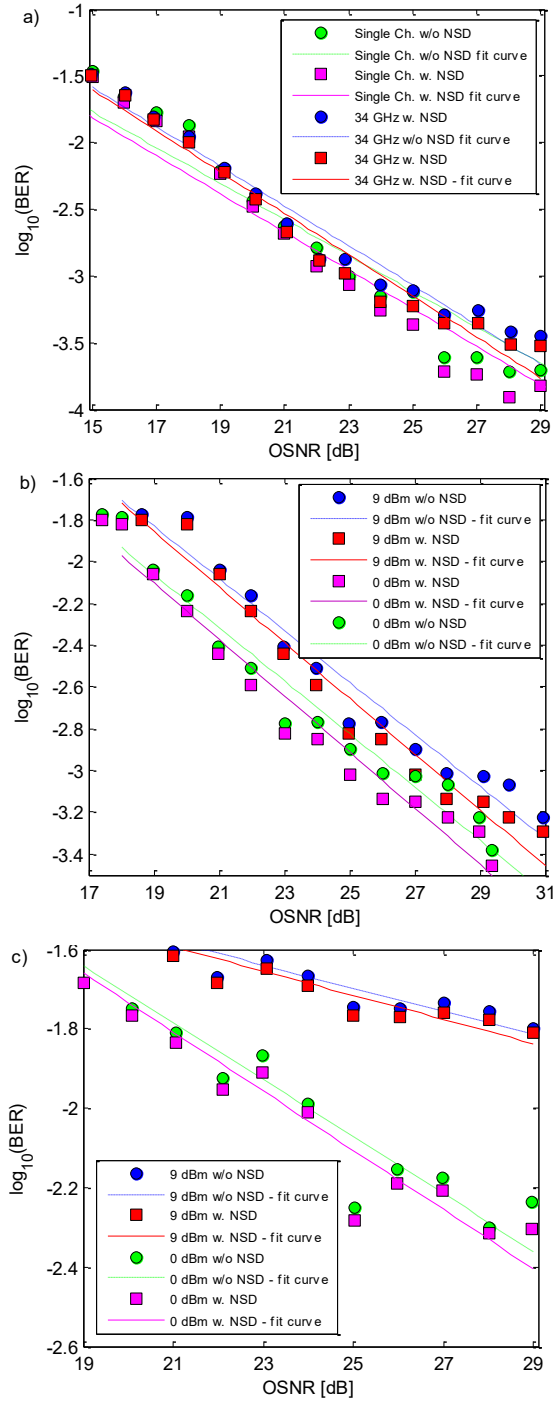
Figure 5.9: BER vs OSNR at 32 Gbaud in a) Back-to-Back, and for 2 launched powers over 90 km: b) in single channel and c) for a carrier spacing of 34 GHz.
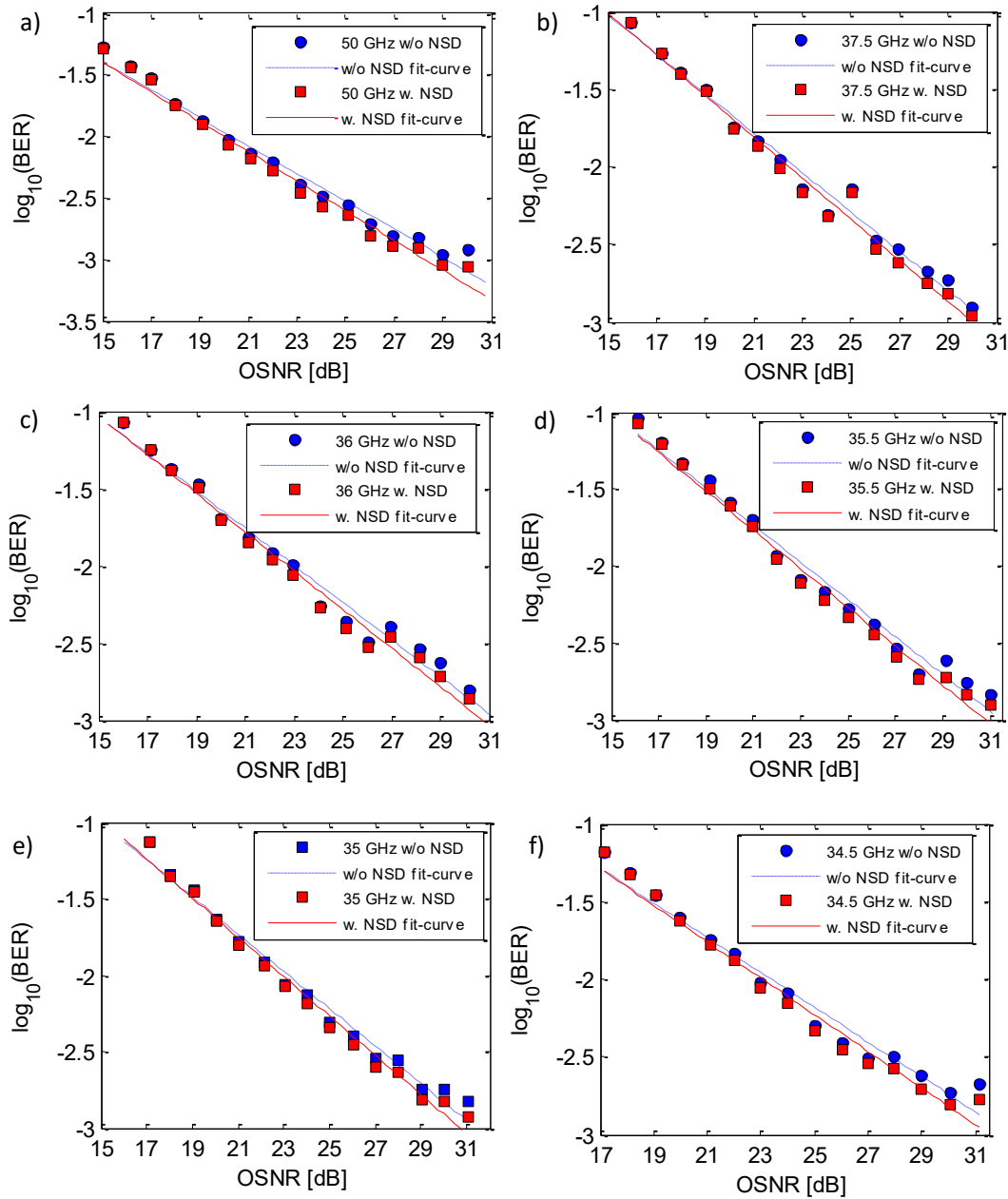
Figure 5.10: BER vs OSNR for multichannel transmission over 270 km at 32 Gbaud for different carrier spacings. (first part) a) 50 GHz, b) 37.5 GHz, c) 36 GHz, d) 35.5 GHz, e) 35 GHz and f) 34.5 GHz, with (w.) and (w/o) NSD.
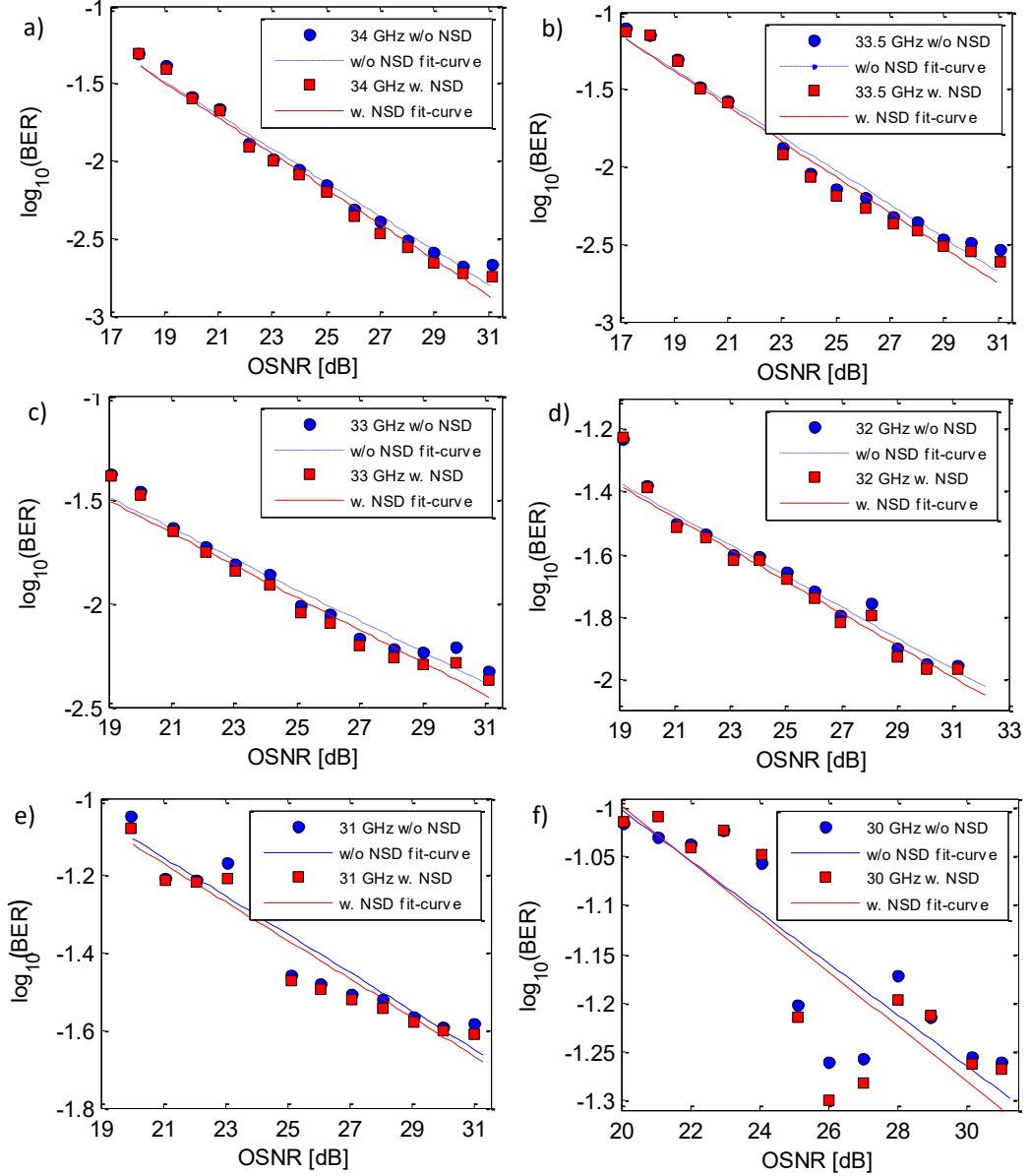
Figure 5.11: BER vs OSNR for multichannel transmission over 270 km at 32 Gbaud for different carrier spacings. (second part) a) 34 GHz, b) 33.5 GHz, c) 33 GHz d) 32 GHz, e) 31 GHz, and f) 30 GHz with (w.) and (w/o) NSD.

5.4 Summary

A machine learning-based nonsymmetrical demodulation technique for a DSP-enabled receiver was experimentally demonstrated. With the aim of enabling the mitigation of time-varying distortions including ICI. Employing short time windows for demodulation further enables inline optical monitoring, which is a valuable diagnostic tool for future terabit optical communication systems. Moreover, even if the gain is modest with the analyzed setups, in uncontrolled scenarios higher gains are expected due to the the proposed technique is transparent to the specific source of nonlinearity, which makes it simple yet robust.

6

Conclusions and Future Work

6.1 Conclusions

Nyquist-WDM, a promising solution for increasing the capacity in optical networks, was the technology chosen to be analyzed in this thesis, envisioning its feasible of being developed in gridless scenarios in a near future. The aim of these study is of avoiding the use of guard bands in Nyquist-WDM systems. Furthermore, the spectral separation between adjacent modulated carriers was reduced as much as possible, even under the baud rate in Hz (sub-Nyquist separation), driving to interchannel interference (ICI) due to the spectral overlapping.

In this thesis, the impact in terms of BER of the ICI effects was analyzed in a $3 \times 16/32$ Gbaud QPSK/16-QAM Nyquist-WDM. A systemic evaluation of the ICI effects has been given in Chapter 3 with the consideration of linear and nonlinear impairments, and variations of system parameters, such as: frequency channel spacing, roll-off factor of the pulse-shaping filter, OSNR, transmission distance, launch powers, among others.

It was shown that a roll-off factor of 0.3 induces an important penalty in terms of BER, when it is compared to an ideal roll-off value of 0, by approximately 3 orders of magnitude in a B2B scenario using QPSK. Besides, no signal demodulation is successfully achieved for roll-off factors greater than 0.1 for sub-Nyquist carrier spacing (less than the baud rate in Hz).

Additionally, we identified degradations of the system performance, in terms of BER, for variations of the mark probability (MP) of the PRBS. Even if the MP of

commercial system is close to 0.5 (gaussian distribution), in short time slots this parameter could have some variations, affecting the adjacent channels when there are overlapping.

Besides, the ICI impact due to the overlapping of modulated carriers, even without nonlinear stimulation, is higher in terms of BER, than the nonlinear impact for standard fixed-grid WDM transmission. Hence, the BP algorithm was implemented in the DSP, for nonlinear mitigation due to the high launch power. The use of BP algorithm could relax the roll-off factor penalty up to 0.1 in Nyquist channel spacing cases. Thus, a BP equalizer may improve the multicarrier spectral efficiency by allowing acceptable levels of interchannel interference in nonlinear scenarios affected by high launch power. However, its computational complexity could be very high.

Thereby, we proposed a method for the minimization of ICI effects to be implemented in gridless Nyquist-WDM systems. The proposed method takes advantages of the distribution among optical carriers of encoded sequences supported in the receiver side by the NDA equalization applied per carrier. It was shown how the NDA equalization supports a hard-decision FEC technique for the proper ICI mitigation without using joint signal processing. The effectiveness of the proposed method to improve the spectral efficiency by the ICI mitigation was confirmed through numerical simulations in a 3×32 Gbaud single-polarization QPSK Nyquist-WDM system. For a measured BER in $3 \times (2^{17-1})$ bits, error-free decoding for frequency carrier spacing values greater than 28.5 GHz and roll-off factor of 0.1, is proven. Also, an error-free decoding is achieved for roll-off factor as great as 0.4 in sub-Nyquist spacing regime of 30 GHz. For a BER limit of $1x10^{-3}$ the method reduces the carrier spacing penalty in 2, 1.5, and 1.4 GHz for roll-off factor values of 0.1, 0.2 and 0.3, respectively. In addition, the system may be relaxed in terms of hardware requirements for signal generation, because of greater roll-off factor implies shorter RCC filter length and less required electronic resources. Thus, this novel method may lead to the design of hybrid ICI mitigation techniques exploiting the advantages of signal equalization at both levels, the physical level for any digital and analog pulse shaping and the bit-data level and its ability to incorporate advanced correcting codes. Furthermore, by using this technique the spectral efficiency may be increased

On the other hand, we proposed and experimentally demonstrated a machine learning-based nonsymmetrical demodulation technique for a DSP-enabled WDM receiver, with

the aim of enabling the mitigation of time-varying distortions, including the ICI. The major sources of time-varying distortions were laser phase noise, IQ imbalance drifting and interchannel interference. Experimental results for a 3×16 Gbaud 16-QAM system at different channel spacings and OSNR values showed that the proposed technique can improve the system performance for channel spacings greater than 16 GHz, when employing a roll off factor of 0.1. Furthermore, it was experimentally shown that the time-varying nature of the non-linearity results in BER variation between various time windows. Hence, for the first time we successfully demonstrated the use of k-means algorithm based detection in conjunction with time windowing in order to optimally overcome time varying channel nonlinearity in a Nyquist-WDM system. The proposed technique is transparent to the specific source of nonlinearity, which makes it simple yet robust. Additionally, experimental results at 32 Gbaud showed that our nonsymmetrical demodulation technique outperforms in terms of BER the conventional QAM demodulation technique, adapting the k-means algorithm each time window with a length of 10k symbols. We also demonstrated that the OSNR requirement can be reduced by 1 dB for signals affected by interchannel interference. Employing short time windows for demodulation further enables inline optical monitoring, which is a valuable diagnostic tool for future terabit optical communication systems.

6.2   Future Work

Further characterization of the ICI impact after wavelength conversion, and when wavelengths are added and dropped several times in transit nodes are currently being planned in joint with dynamic bandwidth allocation. In figure 6.1, a test in Rsoft Software is performed, similar to the scenario modeled in VPITransmissionMaker presented in Chapter 2. ASE noise is added in B2B and a transmission link of 90 km. The BER variation is calculated as a function of the noise spectral density for the central channel, simulating a dramatic damage of an specific wavelength (central one in this case) in a multicarrier transmission using the proposed method. It could emulate a wavelength which has been added or dropped several times in a network with transit nodes, being highly affected by reduction of OSNR.

Besides, the design or use of different FEC codes for the distribution among optical carriers in superchannels, could form part of future work and its implementation in
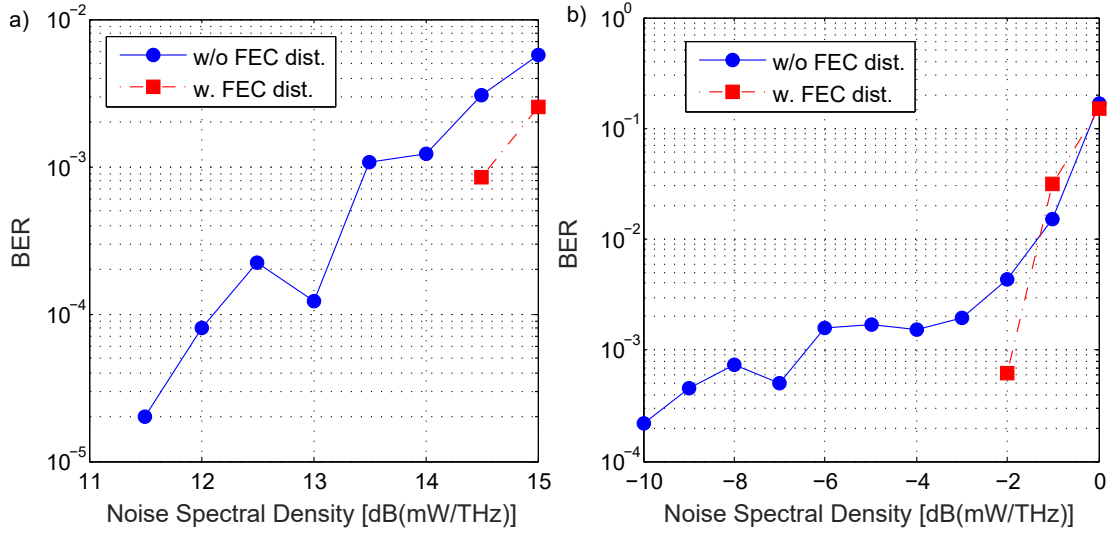
Figure 6.1: BER vs Noise Spectral Density in a) B2B and b) 90 km Transmission.

coherently detected systems. Additionally, for the encoded bit-sequence distribution technique proposed, synchronism among the carriers has been assumed. However, for implementation, the synchronistic is a challenging issue which is required for bit redistribution at the receiver side, for the whole set of carriers used.

On the other hand, the proposed machine learning-based NSD method may also allow simplification of the standard demodulation blocks in particular the equalizer. For preliminaries studies, we noted that the receiver's equalizer is relaxed in terms of number of taps when NSD is applied. For example, Figure 6.2a shows the BER estimation as a function of the number of taps of a DD-LMS equalizer in the scenario B presented in Chapter 2. Regardless the number of taps, the performance in terms of BER by using NSD is always better than without NSD. For example, a BER of 5×10^{-3} is obtained with 61 taps without NSD and with 41 taps with NSD. Figure 6.2b shows BER vs OSNR for a channel spacing of 34 GHz. For three different number of taps, by means of NSD, the BER is reduced in all cases. According to this results, a complexity computational's study would be an interesting line of research in NSD applications.

Moreover, higher order modulation formats may be applied for increasing the capacity in flexible and gridless networks. Preliminary result for 64-QAM generation is
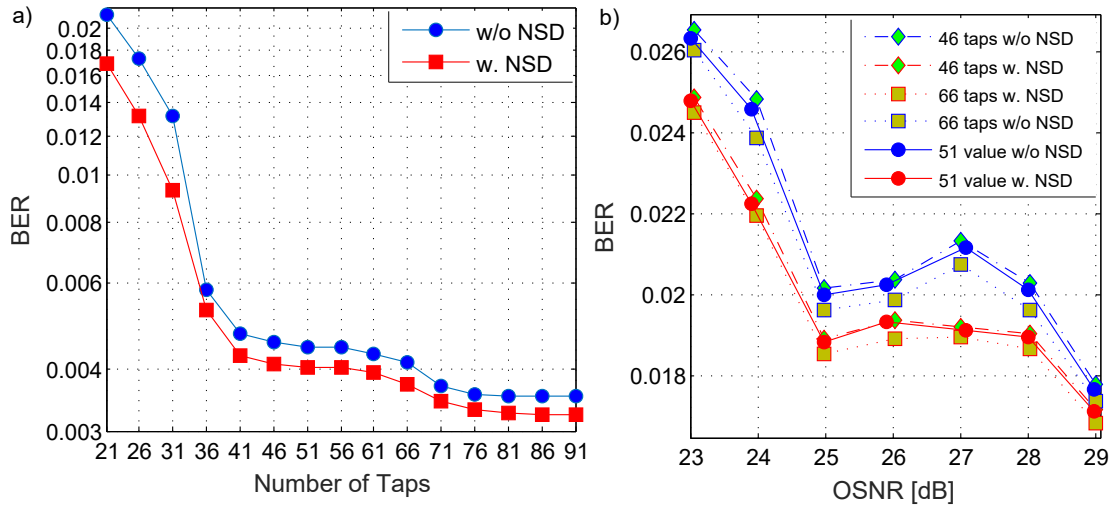
Figure 6.2: a) BER vs Equalizer's Number of taps for a channel spacing of 35.6 GHz, b) BER vs OSNR for a channel spacing of 34 GHz with (w) NSD and without (w/o) NSD.
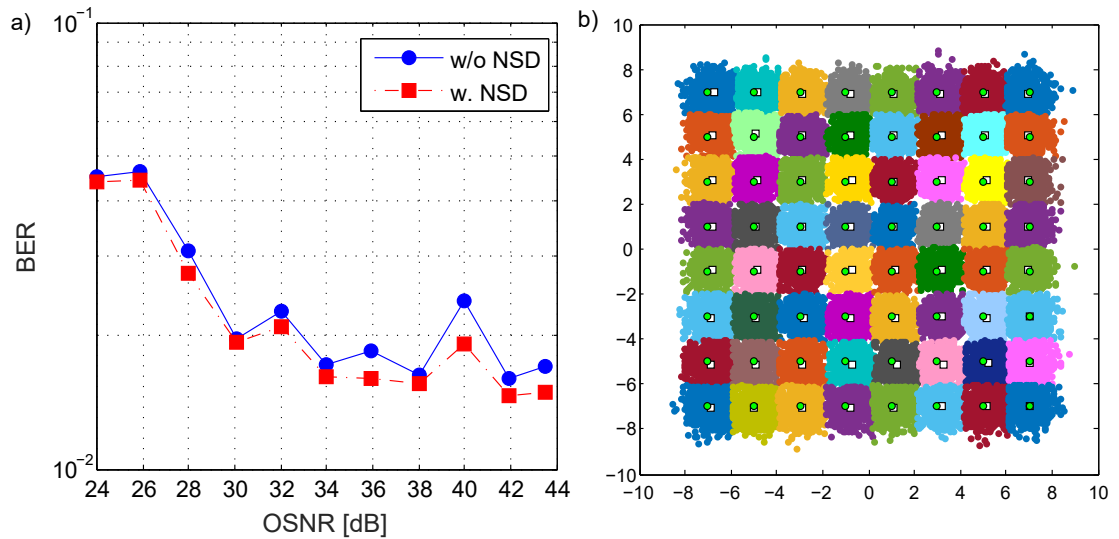
Figure 6.3: 64-QAM Nyquist-shaping Generation in B2B. a) BER vs OSNR with (w) NSD and without (w/o) NSD, b) Constellation diagram for a OSNR of 44 dB.

shown in Figure 6.3b for B2B. NSD method is applied. It can bee seen as each symbol y plotted in different colors. White square markers are the reference (ideal) constellation, and the centroids are represented as green dot markers. A centroid deviation is noticed. Figure 6.3a shows BER vs OSNR. BER is improved for all OSNR values. Indeed, the NSD method can be applied for any QAM format. A research about non-conventional modulation formats would be a potential future work supported by NSD.

Additionally, future work would be focused on the further investigation of non-symmetrical demodulations approaches. A goal would be the use of distances unlike Euclidean distance in the constellation diagram, allowing more robustness to face non-linear and noisy scenarios.

Appendix A

PRBS correlated among channels

A 5×32 Gbaud Nyquist-WDM system with coherent detection was modeled in VPI-TransmissionMaker (VPI) software. ICI effects according to the channel spacing and the BER were evaluated when the whole set of channels use the same PRBS. Additionally, equalization based on the Least-Mean-Square (LMS) was implemented at the receiver side.

A.1   ICI Analysis

Tables A.1 and A.2 show the EVM and BER for transmission of 1 km and 3 km respectively. These values measure the distortion of the signal received. EVM values are similar in the 5 channels, as well as, BER values. It can be verified with their standard deviation (σ) . For 1 km $EVM = 0.014$ and $log(BER) = 0.015$, for 3 km $EVM = 0.0097$ and $log(BER) = 0.0054$. The following information is the result from only one channel, assuming the similar performance of the other channels, how we can demonstrate at the end of the section.

	Ch1	Ch2	Ch3	Ch4	Ch5
EVM	11.424	11.443	11.436	11.444	11.462
Log(BER)	-3.262	-3.253	-3.257	-3.258	-3.245

Table A.1: EVM and BER estimation for a 16-QAM transmission with a channel spacing penalty of 1 GHz and roll-off of 0.15 in 1 km.

	Ch1	Ch2	Ch3	Ch4	Ch5
EVM	14.211	14.208	14.205	14.226	14.2242
Log(BER)	-2.340	-2.341	-2.342	-2.337	-2.338

Table A.2: EVM and BER estimation for a 16-QAM transmission with a channel spacing penalty of 1 GHz and roll-off of 0.15 in 3 km.
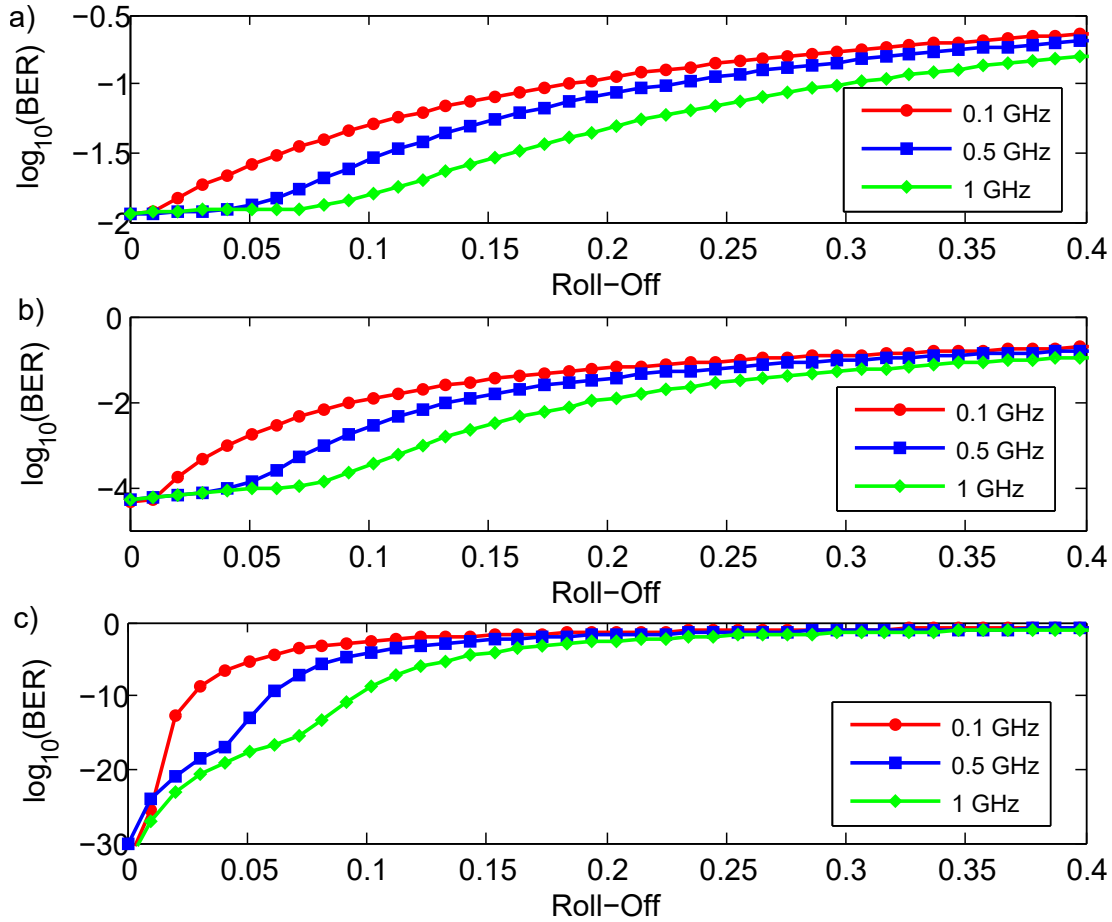
Figure A.1: BER vs Roll Off factor for different channel spacing penalty in a) 5 km, b) 3 km and c) B2B.
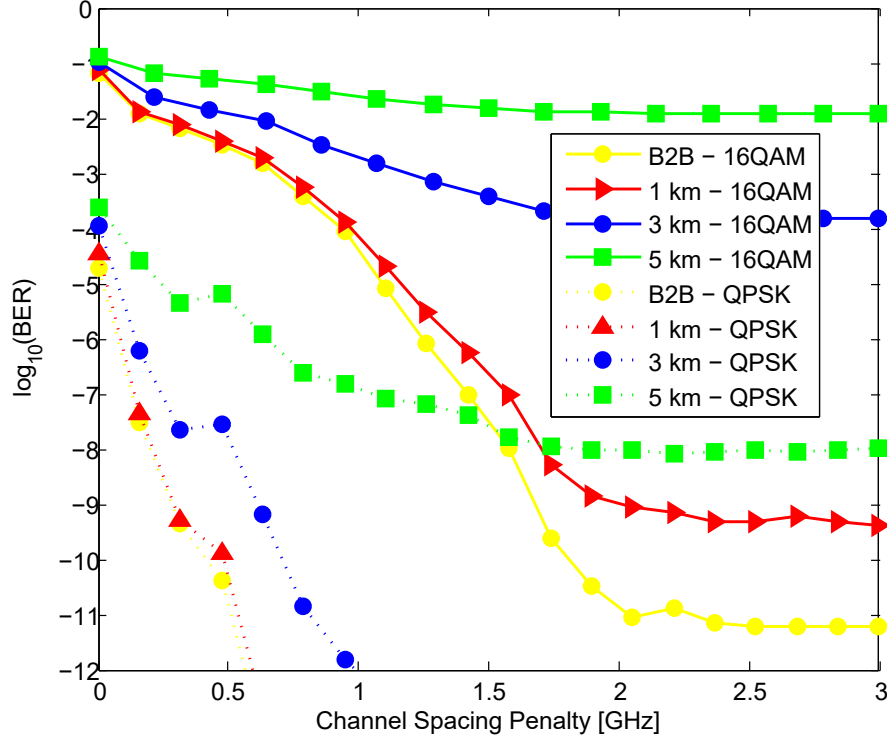
Figure A.2: BER vs channel spacing penalty for different transmission distances for QPSK and 16-QAM Modulation at 32 Gbaud with roll-off of 0.15.

In figure A.1, an evaluation of the roll-off impact is done for 3 different channel spacing penalties of 0.1, 0.5 and 1 GHz in a 32 Gbaud 16-QAM transmission. Roll-off value has a high impact in the ICI effects measured in terms of BER. It can be noticed in figure A.1c, that even in B2B, roll-off factor with a value change from 0 to 0.1 represents a log(BER) increase from -30 to -10, for a channel spacing penalty of 1 GHz. Nevertheless, with an ideal Nyquist-optical pulse, optical fiber impairments even in short distance considerably affect the BER. For $R_{off} = 0$ the log(BER) is -4 in 3 km (figure A.1b.) and -2 in a 5 km transmission, while, in B2B case, log(BER) is equal to -30.

Besides of roll-off factor, optical fiber length and channel spacing penalty increase the ICI effects. In figure A.2, BER vs. channel spacing penalty for different transmission distances, with 16-QAM and QPSK modulation for a $R_{off} = 0.15$ is shown. QPSK is more tolerant to the ICI effects than 16QAM at the same symbol rate. QPSK reaches log(BER) of -12 for a 1 GHz channel spacing penalty in 3 km; however, in

Channel Spacing Penalty	[%]EVM Before LMS	%EVM After LMS
0 GHz	21.82	5.41
0.4 GHz	16.35	5.49
0.7 GHz	14.52	4.59
1 GHz	12.78	3.84
1.5 GHz	11.12	3.37
1.8 GHz	9.72	2.99
2 GHz	8.47	2.78

Table A.3: Measured EVM in 16-QAM transmission over 3 km of uncompensated-dispersion link, before and after LMS equalization.

16-QAM, the log(BER) is -2 for the same case. Depending on the distance, BER can increase considerably. For example, in 16-QAM transmission, log(BER) increases from -9 to -4 in only 2 km, having a log(BER) of -2 for 5 km distance. Channel spacing penalty variation from 1 to 2 GHz, decreases the log(BER) from -4 to -9, in a 1 km transmission. For 5 km, the BER variation is minimum for different channel spacing penalty, reaching only a log(BER) of -2 in 3 GHz.

A.2 ICI impact after LMS equalization

In figure A.3, constellation diagrams are showed, for a 3 km transmission with different channel spacing penalty, before LMS and after LMS equalization. In each constellation obtained before LMS equalization of figure A.3, when channel spacing penalty increases, symbol dispersion in each of the constellations decreases. After LMS, each constellation qualitatively presents similar dispersion symbols for different channel spacing penalty. For the constellation diagram shown in figure A.3, EVM is calculated (see table A.3). Measured EVM in the constellations is reduced after LMS equalization. Maximum value of EVM before LMS equalization is 21.82%, and after LMS its value is 5.41%. It means a reduction of the ICI effects impact.

Figure A.4 shows BER vs. channel spacing penalty. LMS reduces the log(BER) from -1 to -11 for an ideal Nyquist spacing. In B2B, by using LMS equalization a log(BER) of -10 can be obtained for a channel spacing penalty of 0. The same performance is obtained without LMS but with a channel spacing penalty of 3 GHz.
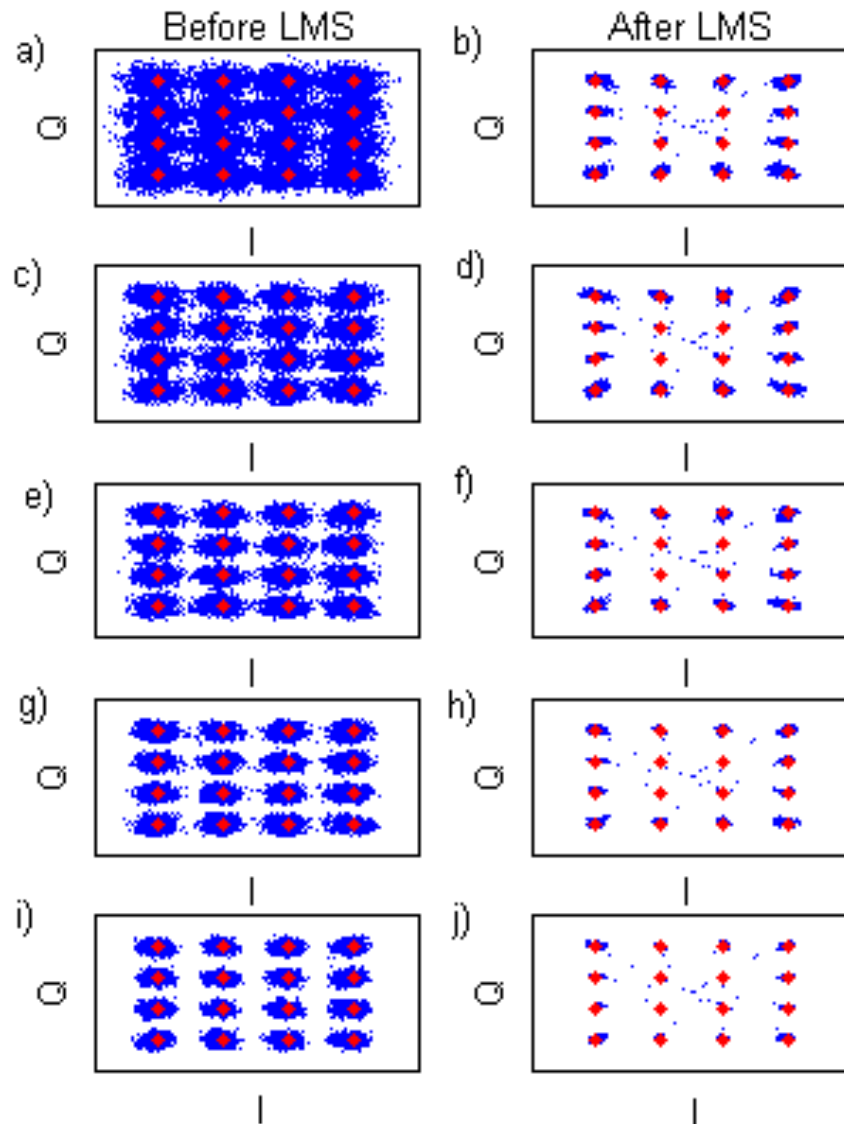
Figure A.3: 16QAM Constellation Diagram obtained in a transmission over an uncompensated-dispersion optical fiber.

A. PRBS CORRELATED AMONG CHANNELS

Figure A.5 shows the BER values with regard to the channel number, for 4 transmission cases, before LMS (green dots) and after LMS (blue dots) equalization. At the beginning of this section was analyzed that BER variation among channels is minimum before LMS processing. After channel equalization, the log(BER) also has a small variation among channels. The penalty of the channel location is minimum with regard to transmission parameters. The BER can have minimum variations according to the training sequence, and the parameters used to adapt the coefficients by the LMS algorithm.
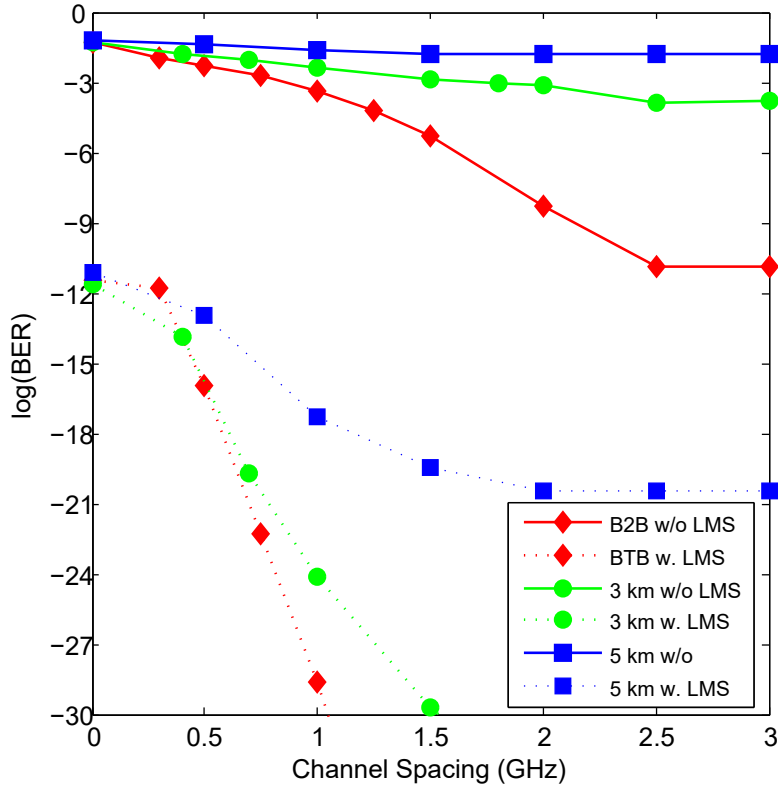
Figure A.4: BER vs Channel spacing penalty in a transmission over an uncompensated-dispersion optical fiber with (w.) and without (w/o) LMS equalization.
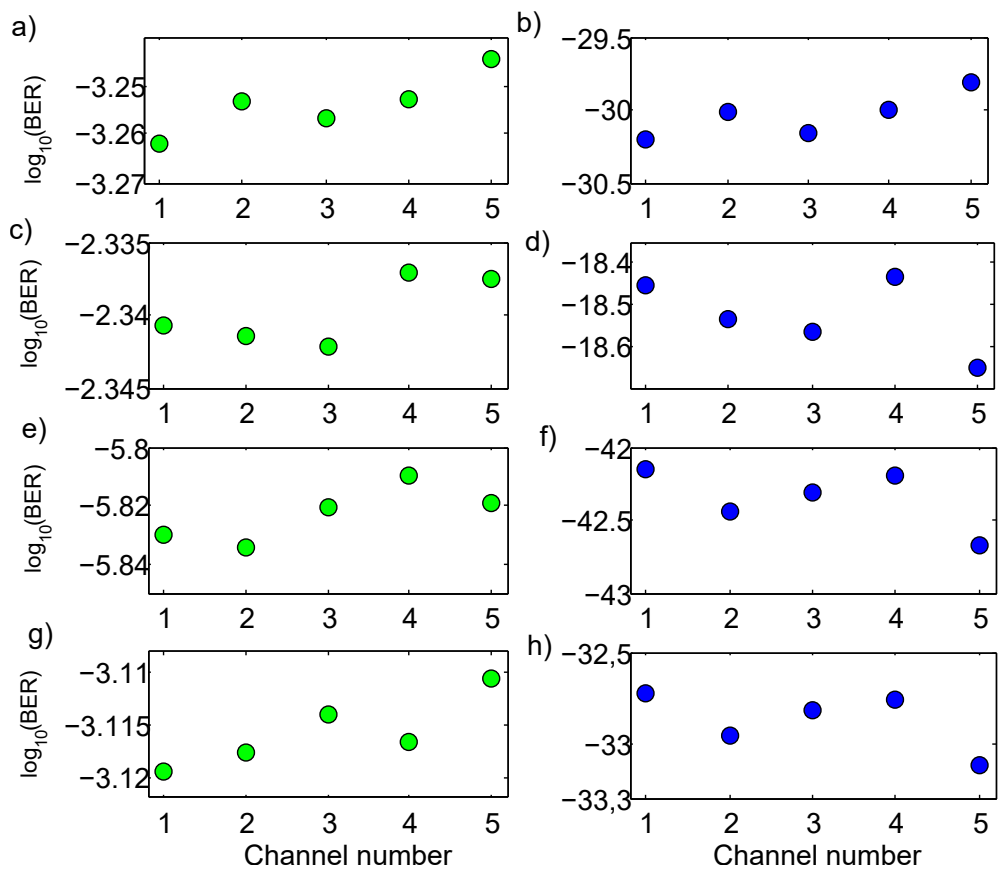
Figure A.5: BER obtained in each channel before and after LMS equalization.

A. PRBS CORRELATED AMONG CHANNELS

Appendix B

Impact of modulation format in adjacent channel

In a multi-carrier system, each carrier of 32 Gbaud can be modulated with different modulation format. In this subsection is analyzed the impact, in terms of BER, of introducing a 16-QAM channel next to a QPSK channel (or viceversa), as it is shown in figure B.1. Cases from 1 to 6 of figure B.1 are analyzed in terms of BER as a function of the transmission distance in figure B.2, and cases from 7 to 12 are analyzed in figure B.3.

Cases 1 and 2 of figure B.1 are represented in the results obtained in figures B.2a and B.2b. Both cases should show the same results, but estimated BER has a difference of 3 orders of magnitude in one of its channel at B2B. Besides, adding a third channel has not a representative impact. For example, figure B.2e shows better perfomance for QPSK channels with a 16-QAM in the middle, than figure B.2b with only two channels QPSK. Figures B.2c and B.2d show a 16QAM channel case with a BER greater than 10^{-2}, while the two QPSK channels have different BER value. For example, in figure B.2c, BER values in log-scale of -8 and -13 for 0 km are obtained in QPSK, and in figure B.2.d both QPSK channels have the same BER value in B2B 10^{-8}. Figure B.2f shows three channels QPSK, with a BER difference among channels for B2B of 9 orders of magnitude.

Figures B.3a and B.3b shows the performance of two channels 16QAM transmitted in different wavelengths over a optical link without compensation of chromatic dispersion. That's why the BER is not the same in both plots. In Figures B.3c, central

B. IMPACT OF MODULATION FORMAT IN ADJACENT CHANNEL
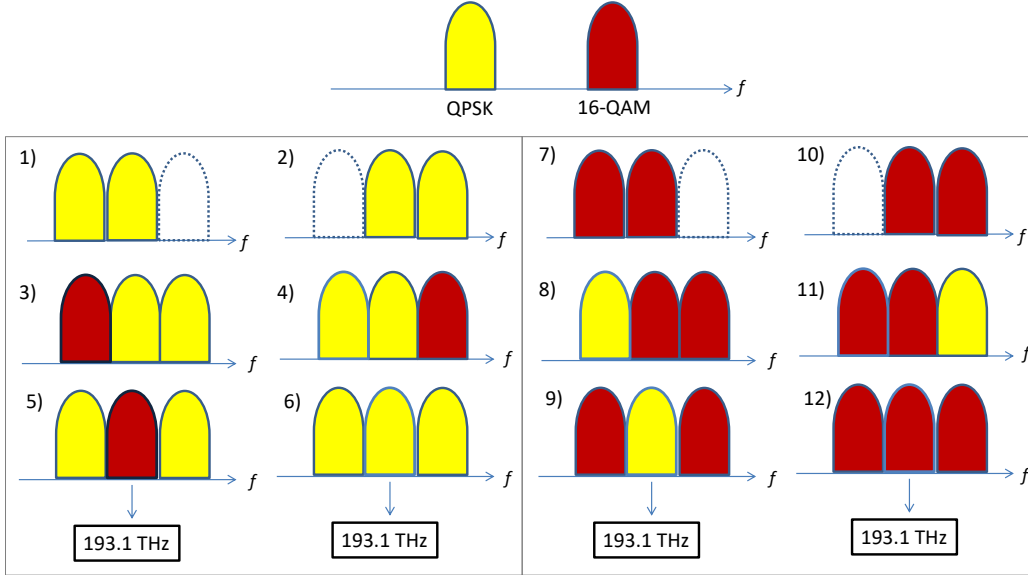
Figure B.1: Spectra of three channel transmission with QPSK and 16-QAM modulation format.

channel is QPSK modulated and adjacent channels are 16QAM. Even if the central channel is always most affected by ICI, 16QAM has a lower performance in the adjacent channels, around 3 orders of magnitude at 4 km of an uncompensated link. in cases of Figures B.3d and B.3e, QPSK as an adjacent channel has the same performance of 16QAM channels after 10 km. It means chromatic dispersion has a very high impact in comparison with ICI.

In table B.1, some of the results presented in this section are summarized.

NoC QPSK	NoC 16QAM	Central one	Distance	BER
2	0	QPSK	9 km	10^{-3}
2	1	16QAM	4 km	Difference: 3 OoM.
0	2	16QAM	16 km	10^{-2}
1	2	QPSK	4 km	Difference: 4 OoM

Table B.1: Summary of results presented in this appendix for cases with carrier spacing of 32 GHz.(OoM: Orders of Magnitude; NoC: Number of Channels).
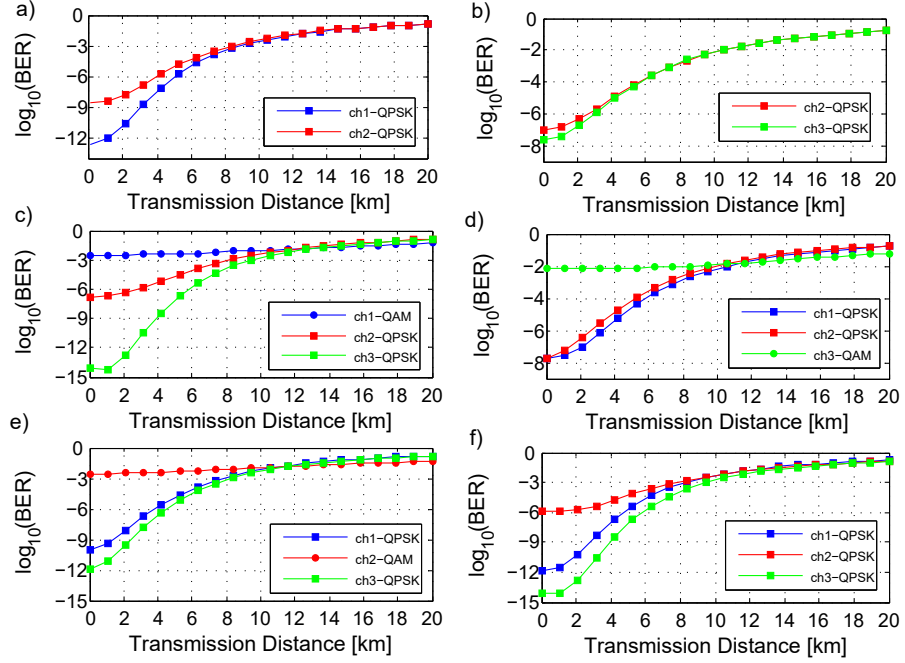
Figure B.2: BER vs Transmission Distance in a uncompensated-dispersion link for different modulation formats with a channel spacing of 32 GHz.
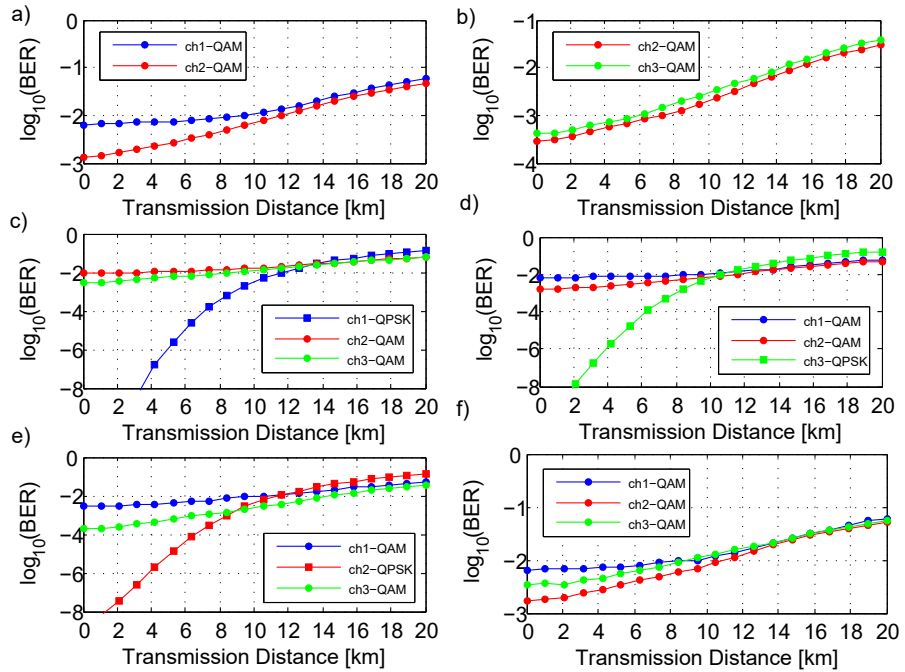
Figure B.3: BER vs Transmission Distance in a uncompensated-dispersion link for different modulation formats with a channel spacing of 32 GHz.

B. IMPACT OF MODULATION FORMAT IN ADJACENT CHANNEL

Bibliography

[1] N. CVIJETIC, M. CVIJETIC, M. F. HUANG, E. IP, Y. K. HUANG, AND T. WANG. **Terabit Optical Access Networks Based on WDM-OFDMA-PON**. *Journal of Lightwave Technology*, **30**(4):493–503, Feb 2012. 1

[2] W. WEI, C. WANG, AND J. YU. **Cognitive optical networks: key drivers, enabling techniques, and adaptive bandwidth services**. *IEEE Communications Magazine*, **50**(1):106–113, January 2012. 1

[3] J. FICKERS, A. GHAZISAEIDI, M. SALSI, G. CHARLET, F. HORLIN, P. EMPLIT, AND S. BIGO. **Design rules for pulse shaping in PDM-QPSK and PDM-16QAM Nyquist-WDM coherent optical transmission systems**. In *2012 38th European Conference and Exhibition on Optical Communications*, pages 1–3, Sept 2012. 2

[4] F. CUGINI, G. MELONI, F. PAOLUCCI, N. SAMBO, M. SECONDINI, L. GERARDI, L. POTI, AND P. CASTOLDI. **Demonstration of Flexible Optical Network Based on Path Computation Element**. *Journal of Lightwave Technology*, **30**(5):727–733, March 2012. 2

[5] A. ROSA, C. CAVDAR, S. CARVALHO, J. COSTA, AND L. WOSINSKA. **Spectrum allocation policy modeling for elastic optical networks**. In *High Capacity Optical Networks and Emerging/Enabling Technologies*, pages 242–246, Dec 2012. 2

[6] TOMKOS I., PALKOPOULOU E., AND ANGELOU M. **A survey of recent developments on flexible/elastic optical networking**. *14th International Conference on Transparent Optical Networks (ICTON)*, pages 1–6, 2012. 2, 6, 7

[7] G. Shen and Q. Yang. **From coarse grid to mini-grid to gridless: How much can gridless help contentionless?** In *2011 Optical Fiber Communication Conference and Exposition and the National Fiber Optic Engineers Conference*, pages 1–3, March 2011. 2

[8] S. Zhang and B. Mukherjee. **Energy-efficient dynamic provisioning for spectrum elastic optical networks**. In *2012 IEEE International Conference on Communications (ICC)*, pages 3031–3035, June 2012. 2

[9] M. Angelou, K. Christodoulopoulos, D. Klonidis, A. Klekamp, F. Buchali, E. Varvarigos, and I. Tomkos. **Spectrum, cost and energy efficiency in fixed-grid and flex-grid networks**. In *OFC/NFOEC*, pages 1–3, March 2012. 2, 4, 6

[10] N. Sambo et al. **Next generation sliceable bandwidth variable transponders**. *IEEE Communications Magazine*, **53**:163–171, 2015. 3, 5

[11] Gerstel O., Jinno M., Lord A., and Yoo S.J.B. **Elastic optical networking: a new dawn for the optical layer?** *IEEE Communications Magazine*, **50**:12–20, 2012. 3

[12] V. López et al. **Finding the target cost for sliceable bandwidth variable transponders**. *IEEE/OSA Journal of Optical Communications and Networking*, **6**:476–485, 2014. 3, 4

[13] Hui Wang et al. **Multicarrier Group Detection in Receiver-Side Duobinary-Shaped WDM Superchannel Systems**. *IEEE/OSA Journal of Optical Communications and Networking*, **24**:1206–1208, 2012. 3

[14] Jinno M. et al. **Elastic and adaptive optical networks: possible adoption scenarios and future standardization aspects**. *IEEE Communications Magazine*, **49**:164–172, 2012. 3

[15] P. P. Biswas, A. Singh, and D. Chadha. **Energy efficient design for Green optical core network**. In *2013 National Conference on Communications (NCC)*, pages 1–5, Feb 2013. 3

[16] G. Zhang, M. De Leenheer, A. Morea, and B. Mukherjee. **A Survey on OFDM-Based Elastic Core Optical Networking**. *IEEE Communications Surveys Tutorials*, **15**(1):65–87, First 2013. 4

[17] J. X. Cai, C. R. Davidson, A. Lucero, H. Zhang, D. G. Foursa, O. V. Sinkin, W. W. Patterson, A. N. Pilipetskii, G. Mohs, and N. S. Bergano. **20 Tbit/s Transmission Over 6860 km With Sub-Nyquist Channel Spacing**. *Journal of Lightwave Technology*, **30**(4):651–657, Feb 2012. 4

[18] R. Cigliutti, A. Nespola, D. Zeolla, G. Bosco, A. Carena, V. Curri, F. Forghieri, Y. Yamamoto, T. Sasaki, and P. Poggiolini. **Ultra-long-haul transmission of 16 x 112 Gb/s spectrally-engineered DAC-generated Nyquist-WDM PM-16QAM channels with 1.05x(symbol-rate) frequency spacing**. In *OFC/NFOEC*, pages 1–3, March 2012. 4

[19] Z. Dong, H. C. Chien, Z. Jia, and X. Li. **Joint Digital Preequalization for Spectrally Efficient Super Nyquist-WDM Signal**. *Journal of Lightwave Technology*, **31**(20):3237–3242, Oct 2013. 4, 6

[20] Z. Jia, J. Yu, H. C. Chien, Z. Dong, and D. Di Huo. **Field Transmission of 100 G and Beyond: Multiple Baud Rates and Mixed Line Rates Using Nyquist-WDM Technology**. *Journal of Lightwave Technology*, **30**(24):3793–3804, Dec 2012. 5

[21] H. C. Chien, J. Yu, Z. Jia, Z. Dong, and X. Xiao. **Performance Assessment of Noise-Suppressed Nyquist-WDM for Terabit Superchannel Transmission**. *Journal of Lightwave Technology*, **30**(24):3965–3971, Dec 2012. 5

[22] R. Borkowski, A. Caballero, D. Klonidis, C. Kachris, A. Francescon, I. d. Miguel, R. J. Durn, D. Zibar, I. Tomkos, and I. T. Monroy. **Advanced modulation formats in cognitive optical networks: EU project CHRON demonstration**. In *OFC 2014*, pages 1–3, March 2014. 5

[23] T. J. Xia, G. A. Wellbrock, Ming-Fang Huang, Shaoliang Zhang, Yue-Kai Huang, Do il Chang, S. Burtsev, W. Pelouch, E. Zak, H. de Pedro, W. Szeto, and H. Fevrier. **Transmission of 400G PM-16QAM channels**

over long-haul distance with commercial all-distributed Raman ampli-
fication system and aged standard SMF in field. In *OFC 2014*, pages 1–3,
March 2014. 5

[24] T. Richter, C. Schmidt-Langhorst, R. Elschner, T. Kato, S. Watan-
abe, and C. Schubert. **Distributed generation of a 400-Gb/s Nyquist
16QAM dense superchannel by fiber-frequency conversion**. In *OFC 2014*,
pages 1–3, March 2014. 5

[25] X. Liu, S. Chandrasekhar, and P. J. Winzer. **Digital Signal Process-
ing Techniques Enabling Multi-Tb/s Superchannel Transmission: An
overview of recent advances in DSP-enabled superchannels**. *IEEE Signal
Processing Magazine*, **31**(2):16–24, March 2014. 5

[26] P. Zhu, J. Li, Y. Chen, Y. Xu, N. Zhang, B. Guo, Z. Chen, and Y. He.
**Demonstration of 1-to-13 PDM-8QAM SCFDM superchannel multicas-
ting in HNLF**. In *OFC 2014*, pages 1–3, March 2014. 6

[27] X. Liu and S. Chandrasekhar. **Superchannel for next-generation optical
networks**. In *OFC 2014*, pages 1–33, March 2014. 6

[28] Y. Lu, Y. Fang, B. Wu, K. Wang, W. Wan, F. Yu, L. Li, X. Shi, and
Q. Xiong. **Experimental comparison of 32-Gbaud Electrical-OFDM and
Nyquist-WDM transmission with 64GSa/s DAC**. In *39th European Con-
ference and Exhibition on Optical Communication (ECOC 2013)*, pages 1–3, Sept
2013. 6

[29] X. Liu, S. Chandrasekhar, P. J. Winzer, R. W. Tkach, and A. R.
Chraplyvy. **406.6-Gb/s PDM-BPSK superchannel transmission over
12,800-km TWRS fiber via nonlinear noise squeezing**. In *2013 Optical
Fiber Communication Conference and Exposition and the National Fiber Optic
Engineers Conference (OFC/NFOEC)*, pages 1–3, March 2013. 6

[30] J. D. Reis, M. Garrich, D. M. Pataca, J. C. M. Diniz, V. N. Rozental,
L. H. H. Carvalho, E. C. Magalhes, U. Moura, N. G. Gonzalez, J. R. F.
Oliveira, and J. C. R. F. Oliveira. **Flexible optical transmission systems**

for future networking. In *2014 16th International Telecommunications Network Strategy and Planning Symposium (Networks)*, pages 1–6, Sept 2014. 6

[31] TELECOMMUNICATION STANDARDIZATION SECTOR OF ITU. **Spectral grids for WDM applications: DWDM frequency grid**. Recommendation G.694.1, International Telecommunication Union (ITU-T), Feb 2012. 6

[32] A. MALIK, W. WAUFORD, Z. PAN, N. K. GOEL, S. HAND, AND M. MITCHELL. **Implications of super-channels on colorless, directionless and contentionless (CDC) ROADM architectures**. In *OFC 2014*, pages 1–3, March 2014. 6

[33] D. RAFIQUE, A. NAPOLI, S. CALABRO, AND B. SPINNLER. **Digital Preemphasis in Optical Communication Systems: On the DAC Requirements for Terabit Transmission Applications**. *Journal of Lightwave Technology*, **32**(19):3247–3256, Oct 2014. 7

[34] D. WANG, M. ZHANG, M. FU, Z. CAI, Z. LI, H. HAN, Y. CUI, AND B. LUO. **Nonlinearity Mitigation Using a Machine Learning Detector Based on k -Nearest Neighbors**. *IEEE Photonics Technology Letters*, **28**(19):2102–2105, Oct 2016. 7

[35] ZHU C. ET AL. **Nyquist-WDM With Low-Complexity Joint Matched Filtering and Adaptive Equalization**. *IEEE Photonics Technology Letters*, **26**:2323–2326, 2014. 8

[36] ZHU C. ET AL. **1.15 Tb/s Nyquist PDM 16-QAM transmission with joint matched filtering and frequency-domain equalization**. *Optical Fiber Communications Conference and Exhibition (OFC), San Francisco (CA)*, pages 1–3, 2014. 8

[37] MINGCHIA WU AND W. I. WAY. **Fiber nonlinearity limitations in ultra-dense WDM systems**. *Journal of Lightwave Technology*, **22**(6):1483–1498, June 2004. 8

[38] AGRAWAL. *Nonlinear Fiber Optics*. Optics and Photonics, 3 edition, 2001. 8

[39] M.S. Ferrerira. *Nonlinear effects in optical fibers.* 8

[40] R. J. Essiambre et al. **Capacity Limits of Optical Fiber Networks**. *Journal of Lightwave Technology*, **28**:662–701, 2010. 9

[41] M. Shtaif et al. **Nonlinear interference noise in fibre-optic communications**. *16th International Conference on Transparent Optical Networks (ICTON)*, pages 1–3, 2014. 9

[42] M. Shtaif et al. **Nonlinear interference noise in WDM systems and approaches for its cancelation**. *European Conference on Optical Communication (ECOC), Cannes*, pages 1–3, 2014. 9, 61

[43] R. Dar et al. **Inter-Channel Nonlinear Interference Noise in WDM Systems: Modeling and Mitigation**. *Journal of Lightwave Technology*, **33**:1044–1053, 2015. 9, 61

[44] R. Dar et al. **Mitigation of inter-channel nonlinear interference in WDM systems**. *European Conference on Optical Communication (ECOC), Cannes*, pages 1–3, 2014. 9, 61

[45] G. Colavolpe et al. **Robust Multilevel Coherent Optical Systems With Linear Processing at the Receiver**. *Journal of Lightwave Technology*, **27**:2357–2369, 2009. 9

[46] M. Selmi et al. **Block-Wise Digital Signal Processing for PolMux QAM/PSK Optical Coherent Systems**. *Journal of Lightwave Technology*, **29**:3070–3082, 2011. 9

[47] C. Liu et al. **Joint digital signal processing for superchannel coherent optical systems: Joint CD compensation for joint ICI cancellation**. *European Conference on Optical Communication (ECOC), Amsterdam*, pages 1–3, 2012. 9, 10

[48] M. Xiang et al. **Linewidth-Tolerant Joint Digital Signal Processing for 16QAM Nyquist WDM Superchannel**. *IEEE Photonics Technology Letters*, **27**:129–132, 2015. 9, 10

[49] T. Koike-Akino et al. **Han-Kobayashi and Dirty-Paper Coding for Superchannel Optical Communications**. *Journal of Lightwave Technology*, **33**:1292–1299, 2015. 10

[50] M. Sato et al. **Frequency Diversity MIMO Detection for DP- QAM Transmission**. *Journal of Lightwave Technology*, **33**:1388–1394, 2015. 10

[51] G. Colavolpe et al. **Time-Frequency Packing for High-Capacity Coherent Optical Links**. *IEEE Transactions on Communications*, **62**:2986–2995, 2014. 10

[52] T. Foggi et al. **Spectral Efficiency Optimization in Flexi-Grid Long-Haul Optical Systems**. *Journal of Lightwave Technology*, **33**:2735–2742, 2015. 10

[53] Amirhossein Mohajerin Ariaei, morteza ziyadi, Yinwen Cao, ahmed almaiman, Fatemeh Alishahi, Ahmad Fallahpour, Changjing Bao, Peicheng Liao, Bishara Shamee, Joseph Touch, Moshe Tur, Carsten Langrock, Martin Fejer, and Alan Willner. **Demonstration of Tunable Mitigation of Interchannel Interference of Spectrally Overlapped 16-QAM/QPSK Data Channels using Wave Mixing of Delayed Copies**. In *Optical Fiber Communication Conference*, page Th3J.5. Optical Society of America, 2017. 10

[54] K. Nosu, H. Toba, and K. Iwashita. **Optical FDM transmission technique**. *Journal of Lightwave Technology*, **5**(9):1301–1308, Sep 1987. 17

[55] T. Ono and Y. Yano. **Key technologies for terabit/second WDM systems with high spectral efficiency of over 1 bit/s/Hz**. *IEEE Journal of Quantum Electronics*, **34**(11):2080–2088, Nov 1998. 17

[56] TELECOMMUNICATION STANDARDIZATION SECTOR OF ITU. **Transmission characteristics of optical components and subsystems**. Recommendation G.671.1, International Telecommunication Union (ITU-T), Feb 2001. 17

[57] G. Khanna, T. Rahman, E. d. Man, E. Riccardi, A. Pagano, A. Chiado Piat, B. Spinnler, S. Calabro, D. Rafique, U. Feiste, H. d. Waardt, B. Sommerkorn-Krombholz, T. Drenksi, M. Bohn, A. Napoli, and N. Hanik. **Comparison of Single Carrier 200G 4QAM, 8QAM and 16QAM in a WDM Field Trial Demonstration over 612 km SSMF**. In *ECOC 2016; 42nd European Conference on Optical Communication*, pages 1–3, Sept 2016. 17

[58] G. Bosco, A. Carena, V. Curri, P. Poggiolini, and F. Forghieri. **Performance Limits of Nyquist-WDM and CO-OFDM in High-Speed PM-QPSK Systems**. *IEEE Photonics Technology Letters*, **22**(15):1129–1131, Aug 2010. 18

[59] N. S. Alagha and P. Kabal. **Generalized raised-cosine filters**. *IEEE Transactions on Communications*, **47**(7):989–997, Jul 1999. 18

[60] A. D. Poularikas and Z. M. Ramadan. *Adaptive Filtering Primer with MATLAB*. Taylor and Francis Group, 2006. 24

[61] Paulo S. Ramirez. *Adaptive Filtering: Algorithms and Practical Implementation*. Springer, 2 edition, 2002. 24

[62] Seb J. Savory. **Digital filters for coherent optical receivers**. *Opt. Express*, **16**(2):804–817, Jan 2008. 25

[63] Marco Mussolin. **Digital signal processing algorithms for high-speed coherent transmission in optical fibers**. *Master Thesis, Universit degli studi di Padova*, 2010. 25

[64] F. Yaman and G. Li. **Nonlinear Impairment Compensation for Polarization-Division Multiplexed WDM Transmission Using Digital Backward Propagation**. *IEEE Photonics Journal*, **2**(5):816–832, Oct 2010. 26, 27

[65] E. Ip and J. M. Kahn. **Compensation of Dispersion and Nonlinear Impairments Using Digital Backpropagation**. *Journal of Lightwave Technology*, **26**(20):3416–3425, Oct 2008. 26

[66] G. Gao, J. Zhang, and W. Gu. **Analytical Evaluation of Practical DBP-Based Intra-Channel Nonlinearity Compensators**. *IEEE Photonics Technology Letters*, **25**(8):717–720, April 2013. 26

[67] Eduardo F. Mateo, Fatih Yaman, and Guifang Li. **Efficient compensation of inter-channel nonlinear effects via digital backward propagation in WDM optical transmission**. *Opt. Express*, **18**(14):15144–15154, Jul 2010. 26, 27

[68] R. Deiterding, R. Glowinski, H. Oliver, and S. Poole. **A Reliable Split-Step Fourier Method for the Propagation Equation of Ultra-Fast Pulses in Single-Mode Optical Fibers**. *Journal of Lightwave Technology*, **31**(12):2008–2017, June 2013. 27

[69] T. Mizuochi. **Next Generation FEC for Optical Communication**. In *OFC/NFOEC 2008 - 2008 Conference on Optical Fiber Communication/National Fiber Optic Engineers Conference*, pages 1–33, Feb 2008. 28

[70] A. Tychopoulos, O. Koufopavlou, and I. Tomkos. **FEC in optical communications - A tutorial overview on the evolution of architectures and the future prospects of outband and inband FEC for optical communications**. *IEEE Circuits and Devices Magazine*, **22**(6):79–86, Nov 2006. 28

[71] F. Chang, K. Onohara, and T. Mizuochi. **Forward error correction for 100 G transport networks**. *IEEE Communications Magazine*, **48**(3):S48–S55, March 2010. 28

[72] F. Casu, J. Cabrera, F. Jaureguizar, and N. Garca. **Inter-packet symbol approach to Reed-Solomon FEC codes for RTP-multimedia stream protection**. In *2011 IEEE Symposium on Computers and Communications (ISCC)*, pages 49–54, June 2011. 28

[73] Javier Fernando Botía Valderrama. *Methodology for predicting and/or compensating the behavior of optical frequency comb*. PhD thesis, Universidad de Antioquia, Faculty of Engineering, 2016. 29

[74] S. Lloyd. **Least squares quantization in PCM**. *IEEE Transactions on Information Theory*, **28**(2):129–137, March 1982. 29

[75] Junjie Wu. *Advances in K-Means Clustering, A Data Mining Thinking.* Springer, China, 1 edition, 2012. 29

[76] F. Chang et al. **Forward error correction for 100 G transport networks**. *IEEE Communications Magazine*, **48**:48–55, 2010. 60